TRANSPORT PROPERTIES OF SOME SEMICONDUCTING III-V COMPOUNDS AND ALLOYS

par

Marcel J. Aubin

Thèse présentée en vue de l'obtention

du grade de Ph.D.

Département de Physique

Faculté des Sciences Pures et Appliquées

Université d'Ottawa

Ottawa, Canada

© Marcel J. Aubin 1969

ABSTRACT

The electron effective mass m_0^* at the bottom of the (000) conduction band of $InAs_xSb_{1-x}$ and $In_{1-x}Ga_xSb$ alloys was determined by magnetothermoelectric measurements at room temperature. The variation of m_0^* with x exhibited a parabolic behavior for both alloy systems with m_0^* dipping to a minimum of .010 m at $x \sim .3$ in the $InAs_xSb_{1-x}$ system. It was shown that optical phonons dominate the scattering in these alloys and that alloy scattering is negligible.

The magnetic field dependence of the Hall coefficient of GaAs at room temperature was found to agree with the theoretical predictions based on an energy dependent relaxation time and yielded a scattering parameter of $\sim .40$. This agreed with the results of magnetothermoelectric power measurements. The magnetoresistivity was found to be slightly greater than predicted. This was interpreted as the effects of inhomogeneities and or impurity levels.

Magnetoresistivity measurements of InSb alloyed with In_2Te_3 and In_2Se_3 at 4.2^oK showed the <111> conduction band minimum to be .43 eV above the (000) band minimum in pure InSb. As the Te or Se content was increased, the band separation ΔE was found to decrease at a rate of .07 eV/at. % Te and .20 eV/at. % Se.

STATEMENT OF ORIGINALITY

The author claims originality for the following phases of his work.

1) The determination of the effective mass m_0^* and scattering parameter s of $InAs_xSb_{1-x}$ and $In_{1-x}Ga_xSb$ alloys. These results were obtained from magnetothermoelectric power measurements. Simultaneous optical measurements by other workers in the same laboratory yielded m_0^* values with the same alloys.

2) The derivation of a formulation of the Kane model which allows the determination of the conduction band Fermi level from the magnetothermoelectric power when the effective mass is unknown. This formulation is valid for all energies as long as $m_0^* \ll m$.

3) The determination of s in GaAs by magnetothermoelectric, Hall and magnetoresistance measurements.

4) The use of magnetoresistance to obtain the separation ΔE of the (000) and <111> conduction band minima in degenerate InSb as well as the observation of a change of ΔE with Te and Se content.

5) A consistent use of numerical integration whenever the band structure was involved thus eliminating the need for certain approximations. Most workers, even recently, tend to assume degenerate or non degenerate conditions, constant effective mass, one type of scattering, etc. Rather than comparing data with predicted values assuming a certain value of s, the author calculated specific values of s. This applies to magnetothermoelectric, Hall and magnetoresistance measurements.

REMERCIEMENTS

Je voudrais remercier mon épouse Françoise ainsi que mes parents pour leur encouragement durant ces années d'études exigeantes. Je veux remercier aussi (Monsieur) le docteur John C. Woolley pour son intérêt et sa disponibilité constante durant ce projet. Les conseils de mon prédécesseur (Monsieur) le docteur H.B. Harland et la collaboration de mes collègues MM. W.M. Coderre, C.C.Y. Kwan, E.H. van Tongerloo et plusieurs autres m'ont apporté une aide incalculable.

Je tiens à souligner mon appréciation au Conseil National de Recherches et à la province d'Ontario pour leur support financier ainsi qu'au personnel de l'atelier du département de physique et du Centre de Calcul pour leur souci de rendre service.

TABLE OF CONTENTS

LIST OF FIGURES

LIST OF TABLES

CHAPTER I

INTRODUCTION

1. CONTEXT OF THE PROBLEM.

The discovery of the semiconducting properties of III-V compounds by Welker (52W, 53W, 54W) considerably broadened the horizons of semiconductor research, hitherto limited to germanium and silicon. Initially, most of the compound work centered on InSb, first of all because single crystals were easy to prepare and secondly, because its unusually high mobility made it both interesting and easy to study experimentally.

Eventually, interest spread to other compounds such as GaAs, GaP, GaSb, InAs and to alloys of these compounds. In several cases (55F, 56Wa, 59A) two of these compounds molten together will exhibit complete solubility for any composition. Furthermore, the energy gap and effective mass values generally vary smoothly through the alloy system from one compound to the other. This not only provides a tool to resolve ambiguous results for the compounds as will be seen later, but also makes available material of any energy gap from 0.10 to 2.3 eV at room temperature. Thus it is possible for one to produce devices for any wavelength in this range.

Interest in the energy band structure of these compounds and alloys has led to a considerable number of publications, many of which are summarized in Madelung's book (64M) and in the series by Willardson and Beer (66W). At the Physics Department of the University of Ottawa, a group of workers, headed by Dr. J. Woolley, investigated experimentally certain parameters related to the band structure of III-V semiconducting compounds and alloys. One member of this group was the author. It will become evident that the results of different workers in the group were complimentary in the sense that one had to use another's result to complete one's analysis.

2. BAND THEORY

The Drude-Lorentz theory provided a useful model to explain the behavior of metals. It assumed that in metals, a large number of electrons were free and obeyed Maxwell-Boltzmann statistics when in thermal equilibrium. Such an explanation was consistent with the Wiedemann and Franz law which states that the ratio of electrical to thermal conductivities is a constant for many metals. However, the predicted electronic component of the specific heat disagreed with experimental results until Sommerfeld decided to use Fermi-Dirac statistics rather than the classical Maxwell-Boltzmann statistics. These developments were only partially satisfactory, however, since they did not explain the difference between metals and non-metals.

With the advent of quantum mechanics came Bloch's theorem (known previously to mathematicians as Floquet's theorem). Here we consider the motion of a single electron in a perfectly periodic potential which has the periodicity of the lattice. The Bloch theorem is obtained by solving Schrödinger's equation for the wave functions of a single electron in a perfectly periodic potential. These are given by

$$\psi_{\underline{k}}(\underline{r}) = \exp(i\,\underline{k}.\underline{r})\, u_{\underline{k}}(\underline{r}) \qquad (1,1)$$

where $u(\underline{r})$ is a periodic function with the periodicity of the lattice. The form of these wave functions is that of a plane wave with wave vector $\underline{k}$. The application of these results by Wilson (31W, 31Wa) led to the concepts of allowed energy bands and forbidden energy gaps and finally explained the different behaviors of metals, semiconductors and insulators. A semiconductor could then be described as having a "small" but finite forbidden energy gap at normal temperatures. Similarly, the forbidden energy gap of an insulator is "large" and that of a metal is zero or negative. These results are now well known and are summarized in a number of standard texts e.g. Semiconductors (59S).

The energy E of an electron in a semiconductor is a function of the wave vector $\underline{k}$ and the form of this dependence constitutes the band structure. If E is plotted as a function of $\underline{k}$ for different directions in $\underline{k}$ space, it will be found that the extrema in the

conduction and valence bands usually occur in special directions of high symmetry such as the <100> and <111> as well as at the (000) or Γ point. Thus, graphs of E versus $\underline{k}$ are usually drawn for these directions with $\underline{k}$ varying in the face-centered cubic lattice from $\underline{k} = (0,0,0)$ to $\underline{k} = \frac{2\pi}{a}(\frac{1}{2}, \frac{1}{2}, \frac{1}{2})$ and $\underline{k} = \frac{2\pi}{a}(1,0,0)$ at the first Brillouin zone boundary. Here, the parameter 'a' is the lattice constant. Figure (1,1) illustrates the band structure of InSb.

It should be realized that if the <100> minima occur at the edge of the Brillouin zone in a face-centered cubic lattice, there will be three equivalent minima. Should the minima occur inside the zone (as is the case for Si) the number of equivalent minima is six. Similarly, in the <111> directions, four or eight equivalent minima may occur.

To satisfy the equations of motion of carriers, the reciprocal of the effective mass is defined as the second order tensor,

$$\left(\frac{1}{\underline{\underline{m}}^*}\right) = \frac{1}{\hbar^2} \nabla_{\underline{k}} (\nabla_{\underline{k}} E)$$

whose elements are

$$\left(\frac{1}{m^*}\right)_{\alpha\beta} = \frac{1}{\hbar^2} \frac{\partial^2 E}{\partial k_\alpha \partial k_\beta}$$

where $\hbar$ is Planck's constant divided by 2π. The tensor nature of the effective mass is necessary because the curvature of the $E(\underline{k})$ relation is not necessarily the same along all possible directions in $\underline{k}$ space and a different effective mass may be required for each possible direction. In a crystal which has cubic symmetry however, the constant energy surfaces near an extremum in $\underline{k}$ space may be approximated by ellipsoids of revolution about the direction along which the extremum is oriented. In this case, the off-diagonal elements of the effective mass tensor are zero and one is left with three components, $m_{11} = m_L$, the longitudinal effective mass and $m_{22} = m_{33} = m_T$, the transverse effective mass. When the extremum is centered on the Γ point, the constant energy surfaces are spherical and we may write $m_{11} = m_{22} = m_{33}$. Under these circumstances, the "band curvature" effective mass defined above reduces to

$$\frac{1}{m^*} = \frac{1}{\hbar^2} \frac{\partial^2 E}{\partial k^2} \qquad (1,2)$$

Also found useful by many authors is the "cyclotron effective mass" defined by

$$\frac{1}{m^*} = \frac{1}{\hbar^2 k} \frac{\partial E}{\partial k} \qquad (1,3)$$

If the energy E is proportional to k^2, the two definitions become identical. We then say that the band is parabolic. When the constant energy surfaces are ellipsoids of revolution rather than spheres, $m_T \neq m_L$ but one may define the "density of states" effective mass:

$$m^* = (m_L m_T^2)^{1/3} \qquad (1,4)$$

Several experimental methods have been used to determine effective masses, among them, magnetothermoelectric power, Faraday rotation, cyclotron resonance and magneto-optical absorption.

3. REVIEW OF THE LITERATURE

A) BAND CALCULATIONS

The theoretical prediction of band structures encounters serious difficulties. The crystal potential is not known accurately and the complexity of the computations forces one to resort to approximations. This leads to a picture of the band structure which is only qualitatively correct.

The development of the $\underline{k}.\underline{p}$ method by Seitz (40S), Shockley (50Sa) and Dresselhaus et al (55D) brought forth a quantitative picture by combining the symmetry properties of the crystal with a judicious use of empirical results. With the aid of perturbation theory, one can determine the band structure near important points of symmetry in $\underline{k}$ space since only a few adjustable parameters are involved and these can be determined from experimental data. The application of the $\underline{k}.\underline{p}$ method to the Γ point by Kane (57K) has proved to be particularly useful and is referred to as the Kane model. A brief outline will now

be given. Consider first the Schrödinger equation for an electron in a periodic potential $V(\underline{r})$:

$$\left[\frac{p^2}{2m} + V(\underline{r}) + \frac{\hbar}{4m^2c^2}\,(\nabla V \times \underline{p})\cdot\underline{\sigma}\right]\psi_{\underline{k}} = E_{\underline{k}}\,\psi_{\underline{k}}$$

where $\underline{p}$ and $\underline{\sigma}$ are the momentum and spin operators respectively. Using the Bloch functions given by equation (1,1), the expression for the lattice periodic function $u_{\underline{k}}(\underline{r})$ can be written as follows:

$$(H_0 + H_1 + H_2 + H_3)\,u_{\underline{k}} = E'_{\underline{k}}\,u_{\underline{k}}$$

where $H_0 = \frac{p^2}{2m} + V(\underline{r})$ $\qquad H_1 = \frac{\hbar}{m}\,\underline{k}\cdot\underline{p}$

$$H_2 = \frac{\hbar}{4m^2c^2}\,(\nabla V \times \underline{p})\cdot\underline{\sigma}$$

$$H_3 = \frac{\hbar^2}{4m^2c^2}\,(\nabla V \times \underline{k})\cdot\underline{\sigma} \qquad E'_{\underline{k}} = E_{\underline{k}} - \frac{\hbar^2 k^2}{2m}$$

Here, H_0 is the Hamiltonian of the unperturbed problem while H_1 is the spin-independent perturbation and $H_2 + H_3$ is the spin-dependent perturbation. The functions corresponding to the conduction band have the symmetry properties of s functions under the operations of the tetrahedral group and are doubly degenerate including spin. The valence band functions have the symmetry properties of p functions

and are thus six fold degenerate when spin is included. Kane restricts himself to these eight wave functions, thus considering one conduction band and three valence bands while neglecting the effect of higher and lower bands. First order perturbation theory leads to an 8 x 8 secular determinant whose solution gives

$$E' \left[E' (E' - E_0) (E' + \Delta) - k^2 P^2 (E' + \frac{2}{3} \Delta) \right] = 0 \qquad (1,5)$$

where P is a matrix element. The four eigenvalues for $\underline{k} = 0$ are

$$E_1 = E_0$$
$$E_2 = E_3 = 0$$
$$E_4 = -\Delta$$

Since the energy is measured from the top of the valence band, we may identify E_1 as the bottom of the conduction band, which is separated from the valence band by the forbidden gap E_0, E_2 and E_3 as the top of the valence bands of the heavy and light holes, and E_4 as the third valence band split off by the spin orbit interaction by an amount Δ. Equation (1,5) will be developed further in Chapter II.

B) BAND STRUCTURE OF III-V SEMICONDUCTING COMPOUNDS

The III-V semiconducting compounds to be considered in this thesis crystallize in the zinc blende structure, which is a face-centered cubic lattice but which may also be considered as two inter-

penetrating face-centered cubic sublattices with one sublattice containing group III atoms and the other group V atoms. It therefore has a lower symmetry than the diamond lattice of Ge and Si which is identical except that its two sublattices contain the same type of atom. This leads to the fact that the diamond lattice has a centre of symmetry but that the zinc blende lattice has none.

Part of the band structure of InSb is shown in Figure (1,1). It will be noted that the lowest minimum in the conduction band occurs at the Γ point and that the highest maximum of the valence band occurs at or near the Γ point. The spin degeneracy of the V_1 band is lifted even at $\underline{k} \simeq 0$ except in the [100] direction, while that of the V_2 band lifted everywhere except in the [100] and [111] directions. The V_3 band is split off by the spin orbit splitting Δ.

Several other III-V semiconducting compounds have a band structure similar to that of InSb but the latter has one of the smallest if not the smallest fundamental energy gap. This causes the (000) conduction band to deviate considerably from parabolicity, because of the influence of other bands. By comparison, GaAs has a much larger fundamental gap and a nearly parabolic conduction band.

A few parameters related to the conduction bands of five semiconducting compounds are listed in Table (1,1). One peculiarity of

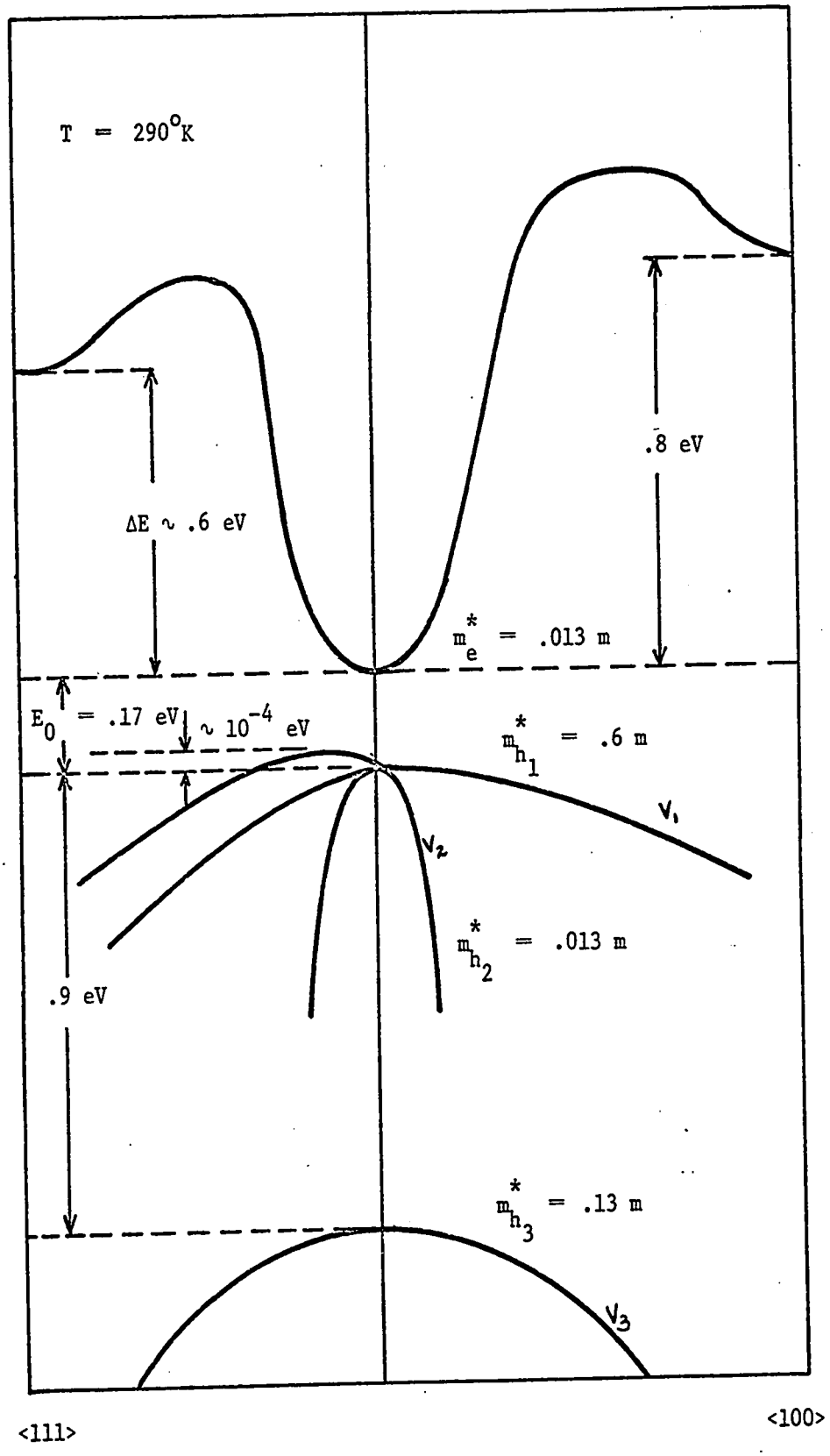

FIGURE (1,1) BAND STRUCTURE OF InSb

TABLE (1,1) CONDUCTION BAND PARAMETERS OF SOME III-V COMPOUNDS

COMPOUND	E_0 (eV)	Δ_{111} (eV)	Δ_{100} (eV)	m_0^*/m	m_{111}^*/m	m_{100}^*/m
InSb	.22 (64H) .17 (64M)	.35 - .56 (66F), 0^oK .62 (67K), 0^oK	.8 (64H)	.014 (64H) .013 (59M), 77^oK .013 (57K), 0^oK		
InAs	.43 (64H)	1.1 (64H) .70 (68K), 4.2^oK	1.2 (64H)	.022 (64H)		
GaSb	.82 (66Wa), 0^oK .80 (64H)	.08 (64H) .078 (69V), 4.2^oK	.70 (66Wa), 0^oK	.047 (64H)	.43 (66H) .23 (69V)	
InP	1.34 (66C) 1.40 (64H)	.7 (64H)	.4 (64H)	.067 (64H)		
GaAs	1.44 (66T) 1.38 (66S)	.48 (64H)	.33 (64H) .36 (60E), 0^oK	.068 (64H) .072 (60E)		1.2 (60E)

E_0 is the direct gap at $k = 0$

Δ_{111} and Δ_{100} are the heights of the <111> and <100> minima above the (000) minimum.

m_0^*, m_{111}^* and m_{100}^* are electron effective masses in the (000), <111> and <100> bands.

All data from (64H) are for 77^oK while others are for 295^oK unless indicated otherwise.

GaSb is that the second highest conduction band, the <111> , is only 0.08 eV above the (000) conduction band minimum. The <111> band is the second lowest for three of the four compounds while for GaAs, the <100> band is the second lowest.

C) ALLOY SEMICONDUCTORS

The alloy produced from two III-V semiconducting compounds is usually itself a semiconductor. The alloys to be considered here, have either the group III or group V atom in common and are found to be pseudo-binary.

Several of these alloys form a solid solution throughout the alloy range (55F, 56Wa, 59A). In producing them, however, one must take care to obtain a single phase equilibrium condition (69C). Should non-equilibrium conditions be present as indicated by the presence of two or more phases, the results of measurements will be ambiguous and misleading.

All the pseudo-binary systems to be considered here are disordered alloys. This means that in the $In_{1-x}Ga_x Sb$ system, the In and Ga atoms are randomly distributed on the available lattice sites. The potential seen by an electron in disordered alloy is given by

$$V_{alloy}(\underline{r}) = V_p(\underline{r}) + V_{np}(\underline{r})$$

where V_p is the periodic part, representing the ideal crystal, giving the average alloy potential over all possible random arrangements of atoms on the lattice and V_{np} is the non-periodic part, representing the effects of disorder, giving the deviation from the average.

Parmenter (55P, 55Pa) was the first to apply the "virtual crystal" model to alloy semiconductors. While first order perturbation theory does not affect the conduction and valence bands, higher order perturbation theory tends to smear the edges of the allowed bands into the forbidden bands, but to a limited extent. This justifies the application of the band structure concept, including the Kane model, to alloy semiconductors. Of course, perturbation theory may be applied only if the effects of disorder V_{np} is small. The fact that these alloys form at all shows that this must be the case.

Another important consequence of the virtual crystal model is that certain physical parameters should vary linearly with composition. Such a variation of the lattice constant (Vegard's law) was found to hold quite well for several III-V compounds (56Wa, 57W). The energy gap on the other hand deviates from linearity and seems to follow a parabolic behavior (59W, 61W, 63W). If x is the mole fraction of compound 1, and (1-x) the mole fraction of compound 2, then the deviation from linearity due to the aperiodic component of the crystal potential is found (63C) to be proportional to $x(1-x)$. The total crystal potential

may then be expressed as

$$V = d + ex + fx(1-x)$$

where d, e and f are constants. The first two terms describe the linear behavior mentioned above while the third term can be attributed to second order perturbation effects of the aperiodic component of the crystal potential. Realizing that these effects should appear in the properties of the alloys, Thompson and Woolley (67T) attempted to fit the measured variation of the fundamental energy gap E_0 for five III-V alloys to an equation of the form

$$E_0 = A + Bx + Cx^2$$

The constant A is the direct gap of the first compound while that of the second compound is A + B + C. In all cases, the experimental data fitted the above equation very well. It was also found that the parabolic term C varied inversely as the square root of the mean energy gap E_m of the two compounds, i.e.

$$C = a E_m^{-\frac{1}{2}}$$

where $a = 0.3\ eV^{3/2}$ for all III-V alloys investigated.

Cardona (63Ca) derived expressions for the effective masses of the conduction and valence bands in terms of transitional energies which may be obtained from reflectance measurements. The results agreed quite well with experimental determination of effective masses of the compounds and led Woolley and Thompson (64W) to apply the analysis to predict values of m^* in III-V alloys. It was assumed that P^2, the square of the

matrix element was constant and equal to 23 eV but it was found later (68V) that for the $InAs_xSb_{1-x}$ alloys, P^2 decreased to 18 eV at about $x = 0.4$. Nevertheless, the effective mass determinations at the time indicated that the results were reasonable.

D) SCATTERING MECHANISMS

An important quantum mechanical result is that in a perfectly periodic lattice, there would be no scattering of the charge carriers, giving rise to an infinite mobility. In practice of course, there are always deviations from periodicity due to lattice vibrations (phonons), impurities, dislocations, etc. and the mobility is limited by one or more scattering mechanisms. These in turn depend on the material, the temperature and the amount of doping.

The mobility is given by the expression $\mu = \frac{e\tau}{m^*}$ where e is the electronic charge and τ is the relaxation time. The latter depends on a number of factors such as the quality of the specimen, the carrier concentration and the temperature as well as on the material itself. In a specimen of arbitrary band shape and spherical constant energy surfaces, the relaxation time varies with the energy E and wave vector $\underline{k}$ of the electrons in the following manner (62Z):

$$\tau = t\, k^{2s-1} \frac{\partial E}{\partial k} \qquad (1,6)$$

where t is a function of temperature and s is a parameter whose value depends on the scattering mechanism involved. In the case of a parabolic band, equation (1,6) reduces to the more familiar form

$$\tau = c\, E^{s} \qquad (1,7)$$

Here, however, we are concerned with III-V semiconducting compounds and alloys whose conduction bands are markedly nonparabolic and a Kane band is assumed.

The scattering mechanisms which may be significant in III-V compounds and alloys will now be reviewed briefly. Others, such as neutral impurity scattering (50E), dislocation scattering (54R), intervalley scattering (55H), electron-electron and electron-hole scattering (59Sc) are not important for these materials under the experimental conditions involved in this thesis and will not be dealt with.

a) Acoustic phonons

i) Deformation potential scattering

The first step in deriving transport equations is usually the setting up of the Boltzmann equation for the velocity distribution f of the electrons. The rate of change $\frac{\partial f}{\partial t}\Big|_{coll}$ of f due to the interaction between the electrons and the lattice may in certain cases

be written

$$\left.\frac{\partial f}{\partial t}\right|_{coll} = - \frac{(f - f_0)}{\tau} \qquad (1,8)$$

where f_0 is the equilibrium value of f. The relaxation time τ exists and equation (1,8) is valid only if the energy absorbed or emitted by an electron in a collision is small compared with the initial energy of the electron. For acoustic phonons, this condition applies even at low temperatures.

Shockley and Bardeen (50S) derived an expression for the mean free path ℓ for the longitudinal mode. By substituting the effective mass in their expression by that for the cyclotron effective mass (equation (1,3)) and using the relations $\tau = \ell/v$ and $v = \frac{1}{\hbar} \frac{\partial E}{\partial k}$, we obtain

$$\tau = \frac{\rho c_\ell^2 \hbar \frac{\partial E}{\partial k}}{2E_1^2 k T k^2} \qquad (1,9)$$

where ρ is the density, c_ℓ is the velocity of long compressional waves in the crystal and $E_1 = \Delta E_c V_0 / \Delta V$. The quantity ΔE_c is the change in energy corresponding to the bottom of the conduction band due to a small change ΔV of the original volume V_0. Comparing this result with equation (1,6), one finds that for deformation potential scattering $s = -\frac{1}{2}$.

Scattering by transverse shear modes has been discussed by Herring (55H). The expression for the relaxation time is quite involved but the variation with temperature and energy is similar to that for longitudinal modes. Furthermore, the scattering is less than for longitudinal modes for spherical constant energy surfaces.

ii) Piezoelectric scattering

As in the previous case, this type of scattering is due to the acoustic mode of vibration. One can show, however, that a phase difference of 90^{o} exists between the matrix elements corresponding to the two cases. Hence they can be considered independently.

The electric polarization associated with the acoustic modes is found by using the form of the piezoelectric tensor determined by the crystal symmetry. The resulting value of the potential is then used to determine the matrix elements for scattering an electron of wave number $\underline{k}$ into a state of wave number $\underline{k}'$ by longitudinal as well as by transverse waves. Harrison (56H) performed this calculation for the crystallographic directions [001] , [011] and [111]. Again, replacing m^{*} by the relation in equation (1,3), Harrison's result becomes

$$\tau = \frac{\rho\, c_{\ell}^{2}\, h\, \kappa^{2}}{2\alpha\, \pi^{2}\, e^{2}\, c\, k\, T} \frac{\partial E}{\partial k} \qquad (1,10)$$

where c_ℓ is the acoustic velocity for long waves, c is the measured piezoelectric constant, κ is the dielectric constant and α is a constant which depends on the crystallographic direction.

For piezoelectric scattering then, $s = \frac{1}{2}$. If the material involved has a centre of symmetry as in the diamond lattice, the piezoelectric tensor will vanish. Hence piezoelectric scattering will not occur in Ge, but may occur in InSb since the zinc blende structure has no centre of symmetry.

b) Optical phonons

The optical branch of the lattice vibrations is especially important in polar semiconductors (37F, 57E). At low temperatures however, $k T < h \nu_0$ where ν_0 is one of the frequencies of the optical branch and the energy change in collisions is relatively large (unless the material is highly degenerate). This means that a relaxation time cannot always be defined in polar materials. However, at high temperatures, where $k T > h \nu_0$, a relaxation time exists, and using equation (1,6) of (53H) for $\frac{\partial f}{\partial t}\Big|_{coll}$, one can show that

$$\tau = \frac{a^3 M h \nu_0^2}{2e^4 k T} \frac{\partial E}{\partial k} \qquad (1,11)$$

for an arbitrary band shape, so that $s = \frac{1}{2}$. Here, M is the reduced mass of the ions and 'a' is the interionic distance.

Ehrenreich (61E) investigated by a variational procedure how far the theoretical formulas for the mobility, Hall coefficient and thermoelectric power could be formally reproduced by a solution of the Boltzmann equation with the assumption of a relaxation time varying in the manner given by equation (1,7), i.e. with parabolic bands. He found that $s = \frac{1}{2}$ for all three coefficients at high temperature, thus agreeing with Howarth and Sondheimer (53H). However, s falls with decreasing temperature to zero at $k T = h \nu_0$. For lower temperatures, the assumption fails completely, and at very low temperatures, s takes on different values for the three coefficients. Table (1,2), reproduced from (64M) gives the temperature at which $k T = h \nu_0$ for several III-V compounds, where ν_0 is the frequency of the longitudinal optical vibrations.

TABLE (1,2)

CRITICAL TEMPERATURES

InSb	264° K	GaSb	336° K
InAs	334° K	GaAs	408° K
InP	487° K	AlSb	482° K
		GaP	578° K

c) Ionized impurity scattering

Among lattice imperfections, only ionized impurities contribute significantly to scattering. A theory of ionized impurity scattering for a general band shape is given by Barrie (56B). The perturbing potential due to an ionized impurity is taken as

$$V(\underline{r}) = \frac{e^2}{\kappa\, \underline{r}} \exp(-q\,\underline{r})$$

where κ is the dielectric constant and q is the screening constant. From this, τ is found to be

$$\tau = \frac{\hbar\, \kappa^2\, k^2}{2\pi\, e^4\, N} \frac{\partial E}{\partial k} \left[\ln\left(1 + \frac{4k^2}{q^2}\right) - \frac{4k^2}{q^2 + 4k^2} \right]^{-1} \qquad (1,12)$$

giving a value of s equal to 3/2. Here N is the concentration of scattering centres.

d) Alloy scattering

A theory of this type of scattering using parabolic bands has been worked out by Nordheim (31N) and also by Brooks (55B). The potential energy of the electron is separated into a periodic part consisting of the average of the constituent potentials and a non-periodic part which contributes to the scattering. By replacing $m_L\, m_T^2$ by m^3 in Nordheim's result, (as quoted by Glicksman (58G)), we assume spherical constant energy surfaces and obtain for the relaxation time,

$$\tau = h^4 / \left[128^{1/2}\ \pi^3\ U\ V\ m^{3/2}\ E^{1/2}\ \alpha\ (1 - \alpha)\right] \qquad (1,13)$$

where U is an integral over scattering angles of the square of the matrix element for the difference of the potentials of the two components of the alloy, V is the atomic volume and α is the mole fraction of the minority component in the alloy. The scattering parameter, according to equation (1,7) is $-\frac{1}{2}$ for parabolic bands, but judging from the results of other mechanisms, it would be reasonable to assume that an arbitrary band shape would give the same result.

e) Scattering in III-V semiconducting compounds and alloys

The results of mobility measurements on InAs (56A), InP (58R) and InSb (55Ha) were compared with theoretical values obtained by Ehrenreich (57E, 59E). The latter concluded that at room temperature, scattering by optical phonons dominates for samples with carrier concentrations less than approximately 10^{19} cm^{-3}. At lower temperatures, however, phonon scattering is diminished and in heavily doped samples, ionized impurity scattering may predominate. However, magnetothermoelectric power measurements led Korenblit et al (64K) and Shalyt (62S) to the conclusion that piezoelectric scattering due to acoustic phonons dominates in InAs at 77°K and lower temperatures, except for the case of very heavily doped samples. There is ambiguity in distinguishing optical phonon scattering from piezoelectric scattering however, since both produce the same value of s.

The scattering mechanisms of III-V compounds were also investigated by Nernst-Ettinghausen measurements. Nasledov (61N) noted a sign reversal at $\sim 600^{\circ}K$ for GaAs and attributed this to acoustic phonons (deformation potential). He obtained similar results for InAs. The analysis did not account for the nonparabolicity of the conduction band, however. Rodot (59R) investigated longitudinal as well as transverse Nernst-Ettinghausen effects in InSb and found s to lie between 0 and $+\frac{1}{2}$. Sladek (60S) measured the magnetoresistance of high purity InSb at high fields and the best fit to the experimental curves were those for piezoelectric scattering.

Turning now to alloy semiconductors, it seems that alloy scattering is much more important in Ge-Si alloys (58G) than in III-V alloys. Ivanov-Omskii and Kolomets (60I) did not detect any alloy scattering with mobility measurements on $In_{1-x}Ga_xSb$ alloys. Ehrenreich (59E) concluded that it was also negligible in $InAs_{1-x}P_x$ alloys having analysed Weiss' mobility measurements (56W). Tietjen and Weisberg (65T) also reached the same conclusion regarding $GaAs_{1-x}P_x$ alloys after measuring the electron mobility in this system. They also compared the results from Brooks' expression for mobility due to alloy scattering with known mobilities for the compounds and concluded that alloy scattering should not dominate the electron mobility in any alloy of the III-V compounds. This effect would be largest in the GaAs rich end of the $In_{1-x}Ga_xAs$ system, where it would be approximately 40% of the total effect.

Leaf 24 omitted in page numbering.

CHAPTER II

THEORY

1. KANE MODEL

The compounds and alloys that were studied in this project all have the zinc blende structure and conduction and valence band extrema at the Γ point. Consequently, the Kane model will be applied to all experimental data. To prepare for this analysis the Kane model will now be developed into a suitable mathematical form.

As shown in the previous chapter, first order perturbation theory leads to a simplified Kane model which considers only one conduction band and three valence bands centered on $\underline{k} = 0$. The solution was:

$$E' \left[E' (E' - E_0) (E' + \Delta) - k^2 P^2 (E' + \frac{2}{3}\Delta)\right] = 0 \qquad (1,5)$$

with the four eigenvalues for $\underline{k} = 0$ being

$$E_1 = E_0$$

$$E_2 = E_3 = 0$$

$$E_4 = -\Delta$$

Since E' is measured from the top of the valence band, E_1 was identified as the bottom of the conduction band, separated from the valence band by the forbidden energy gap E_0. Similarly E_2 and E_3 are the top of the valence bands of the heavy and light holes while the third valence band

E_4 is split off by the spin orbit interaction Δ. The effects of higher and lower bands have been neglected. This model has been used extensively and has proved to be satisfactory for the III-V compounds.

Regarding the solution for the conduction band, the literature mentions two special cases derived from equation (1,5). The first solution assumes that kP and E_0 are much less than Δ whereas the second assumes that E_0 is much greater than Δ.

1) $kP,\ E_0 << \Delta$

$$E' = \frac{E_0}{2}\left[1 + \left(1 + \frac{8\,k^2\,P^2}{3\,E_0^2}\right)^{\frac{1}{2}}\right] \qquad (2,1)$$

2) $\Delta << E_0$

$$E' = \frac{E_0}{2}\left[1 + \left(1 + \frac{4\,k^2\,P^2}{E_0^2}\right)^{\frac{1}{2}}\right] \qquad (2,2)$$

With these approximations in mind, the author then sought a general solution for the conduction band, using as a trial solution:

$$E' = \frac{E_0}{2}\left[1 + \left(1 + \frac{\beta\,k^2\,P^2}{E_0^2}\right)^{\frac{1}{2}}\right] \qquad (2,3)$$

One could then solve for β such that equation (1,5) is satisfied. This parameter should take on different values from 8/3 to 4 for different values of $\eta = \Delta/E_0$. Ignoring the first E' in equation (1,5) and expanding, we obtain

$$(E')^3 + (E')^2 E_0(\eta-1) - E'(\eta E_0^2 + k^2P^2) - \frac{2}{3}\eta E_0 k^2 P^2 = 0$$

Substituting equation (2,3) into the above relation gives:

$$(E_0^3/8)\left[4 + 3\left(1 + \frac{\beta k^2 P^2}{E_0^2}\right)^{\frac{1}{2}} + \frac{3\beta k^2 P^2}{E_0^2} + \left(1 + \frac{\beta k^2 P^2}{E_0^2}\right)^{3/2}\right] +$$

$$(E_0^2/4)\left[2 + \frac{\beta k^2 P^2}{E_0^2} + 2\left(1 + \frac{\beta k^2 P^2}{E_0^2}\right)^{\frac{1}{2}}\right] E_0(\eta - 1) -$$

$$(E_0/2)\left[1 + \left(1 + \frac{\beta k^2 P^2}{E_0^2}\right)^{\frac{1}{2}}\right] (\eta E_0^2 + k^2 P^2) - \frac{2}{3}\eta E_0 k^2 P^2 = 0$$

Many terms will cancel. The terms with fractional powers are now expanded with the binomial theorem while neglecting terms involving k^4 etc., thus assuming that $kP << E_0$.

$$E_0 k^2 P^2 \left[\beta/4 + \eta(\beta/4 - 2/3) - 1\right] = 0$$

For $\underline{k} \neq 0$, this relation leads to

$$\beta = \frac{4 + 8\eta/3}{1 + \eta} \qquad \text{Cardona (61C)} \qquad (2,4)$$

The two extreme cases of $\eta = \infty$ (equation (2,1)) and $\eta = 0$ (equation (2,2)) may be obtained by calculating the appropriate value of β from equation (2,4) and substituting in equation (2,3). The intermediate cases may also be calculated in the same way.

The trial solution expressed by equation (2,3) has been shown to be valid. Since, by definition, $E = E' + \hbar^2k^2/2m$, one may then write

$$E = a k^2 + \frac{E_0}{2}\left[-1 + \left(1 + \frac{\beta k^2 P^2}{E_0^2}\right)^{\frac{1}{2}}\right] \qquad (2,5)$$

where $a = \hbar^2/2m$. The zero of energy has been shifted by E_0 to the bottom of the conduction band. This relation, along with equation (1,3) gives the energy dependence of the cyclotron effective mass in a Kane band.

$$\frac{1}{m^*} = \frac{1}{m} + (E_0^2 + \beta k^2 P^2)^{-\frac{1}{2}} \beta P^2/2\hbar^2 \qquad (2,6)$$

Thus, at the bottom of the conduction band where $\underline{k} = 0$,

$$\frac{1}{m_0^*} = \frac{1}{m} + \frac{\beta P^2}{2\hbar^2 E_0} \qquad (2,7)$$

By combining this relation with that for β, we obtain the well known expression for P^2.

$$P^2 = \frac{3a E_0 (E_0 + \Delta)\left(\frac{m}{m_0^*} - 1\right)}{(3 E_0 + 2\Delta)} \qquad (2,8)$$

Now P^2 and β may be eliminated from equation (2,5).

$$E = a k^2 + \frac{E_0}{2}\left[-1 + \left(1 + \frac{4a k^2}{E_0}\left(\frac{m}{m_0^*} - 1\right)\right)^{\frac{1}{2}}\right] \qquad (2,9)$$

The same result was obtained by Cardona (61C) who assumed that $E' << E_0 + \frac{2}{3}\Delta$. For E_0 sufficiently large and $m_0^* << m$, the above relation reduces to the standard parabolic band, in which case the effective mass is independent of energy:

$$E = \frac{\hbar^2 k^2}{2 m^*} \qquad (2,10)$$

From equation (2,9), one may calculate the inverse relation:

$$k = \left(\frac{E_0\, m}{2a\, m_0^*}\right)^{\frac{1}{2}} \left[1 + \frac{2E\, m_0^*}{E_0\, m} - \left(1 + \frac{4E\, m_0^*}{E_0\, m}\left(1 - \frac{m_0^*}{m}\right)\right)^{\frac{1}{2}}\right]^{\frac{1}{2}} \qquad (2,11)$$

These expressions are useful in that they are independent of the spin orbit splitting Δ, and may also be used to calculate m_0^*, the effective mass at the bottom of the (000) conduction band. Another equation may be obtained, however, by rewriting equation (1,5) but neglecting the first E' and measuring the energy from the bottom of the conduction band.

$$(E - a\,k^2)(E + E_0 - a\,k^2)(E + E_0 - a\,k^2 + \Delta) - k^2\,P^2\,(E + E_0 - a\,k^2 + \frac{2}{3}\,\Delta) = 0$$

If $E \gg a\,k^2$ however, this simplifies to the following expression:

$$E\,(E + E_0)(E + E_0 + \Delta) - k^2\,P^2\,(E + E_0 + \frac{2}{3}\,\Delta) = 0$$

from which one obtains

$$k = \left[\frac{E\,(E + E_0)\,(E + E_0 + \Delta)}{(E + E_0 + \frac{2}{3}\,\Delta)\,P^2}\right]^{\frac{1}{2}} \qquad (2,12)$$

Figure (2,1) shows the $E - \underline{k}$ variation one obtains from equations (1,5) (2,9) and (2,12) as well as from equation (32) of a publication by Kolodziejczak et al (66K) which takes into account the effect of higher and lower bands by second order perturbation theory. It will be noted that for InSb, equation (2,12) is a better approximation to equation (1,5) than is equation (2,9) at all energies. However, equation (2,9) is closer to Kolodziejczak's result. On the other hand, the latter assumed low

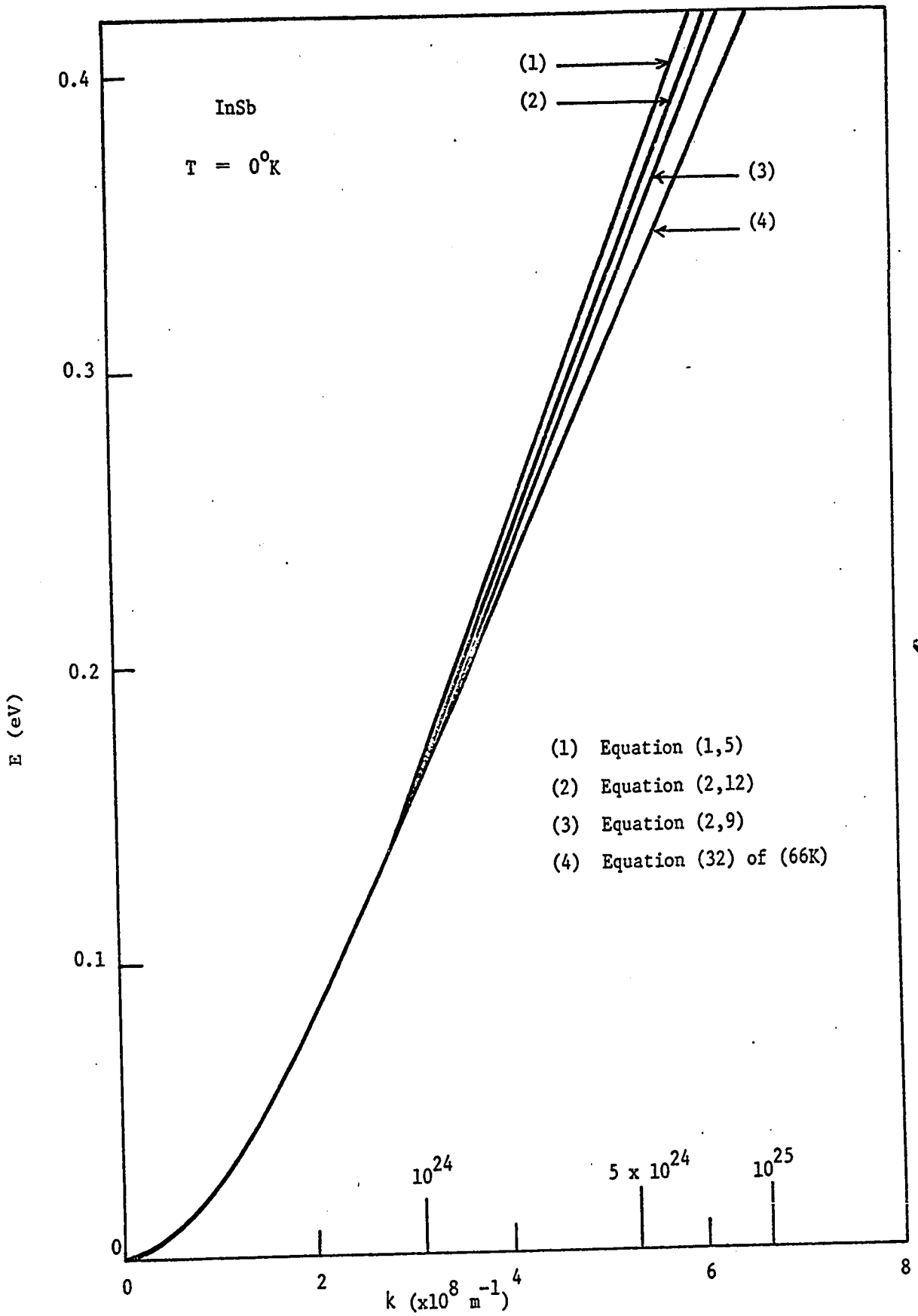

FIGURE (2,1) CONDUCTION BAND IN THE KANE MODEL

energies which was also done in the derivation of equation (2,9). Removing this assumption would raise curve 4 by an amount approximately equal to the difference between curves 2 and 3, since curve 3 assumes low energies and curve 2 does not. It then appears that curves 2 and 3 are good approximations to the complete Kane model. Both will be used in this thesis.

It must be realized however, that the value of E_0 in the Kane model should be replaced by E_0^*, the effective mass band gap (57E). E_0 is the actual intrinsic band gap of the material at a given temperature and will be smaller than the value at absolute zero because of the effects of both lattice dilatation and interaction with the phonon field. However, the band curvature, which determines the effective mass, depends only upon the lattice dilatation and hence E_0^* is the value the band gap would have if only dilatation and not the phonon field were effective, i.e., E_0^* would be expected to lie somewhere between the actual values of E_0 at absolute zero and at the temperature of investigation. This will be discussed further in Chapter IV.

2. MAGNETOTHERMOELECTRIC POWER

The transverse magnetothermoelectric effect or longitudinal Nernst-Ettinghausen effect is the e.m.f. which is observed in the direction of the applied temperature gradient when a magnetic field B is applied perpendicular to the temperature gradient. In the case of a single conduction band, with spherical constant energy surfaces, the thermoelectric power in zero magnetic field may be expressed (622,64K) as

$$\alpha_o = \frac{k}{e}\left[\frac{\int_0^\infty \xi\, k^{2s+1} \frac{\partial f_o}{\partial \xi} \left(\frac{\partial \xi}{\partial k}\right)^2 d\xi}{\int_0^\infty k^{2s+1} \frac{\partial f_o}{\partial \xi} \left(\frac{\partial \xi}{\partial k}\right)^2 d\xi} - \zeta\right] \qquad (2,13)$$

where ξ = E/kT

ζ = the Fermi energy divided by kT

f_o = the Fermi-Dirac distribution function

In a magnetic field, α_B becomes a function of both B and the scattering parameter s. As B tends to infinity, however, in the absence of quantization effects, α_B tends to a saturation value α_∞ which is independent of s, i.e.,

$$\alpha_\infty = \frac{k}{e}\left[\frac{\int_0^\infty \xi\, k^3 \frac{\partial f_o}{\partial \xi}\, d\xi}{\int_0^\infty k^3 \frac{\partial f_o}{\partial \xi}\, d\xi} - \zeta\right] \qquad (2,14)$$

Thus if the infinite field value α_∞ is determined and a particular band structure is assumed, the value of ζ may be obtained from equation (2,14) with no assumption concerning the scattering mechanism. Hence measurement of the zero field value α_o and substitution into equation (2,13) give a value for s. This in turn indicates which scattering mechanism is dominant.

The denominator in the last equation is proportional to the standard expression for the carrier concentration, assuming spherical constant energy surfaces, i.e.,

$$n = \frac{1}{3\pi^2} \int_0^\infty k^3 \frac{\partial f_o}{\partial \xi} \, d\xi \qquad (2,15)$$

Experimentally, n can be determined by extrapolating the values of the Hall coefficient R to an infinite field, giving R_∞, where

$$R_\infty = -\frac{1}{ne} \qquad (2,16)$$

The equations stated above will now be transformed to include the Kane model. Substitution of equation (2,12) into equations (2,13), (2,14) and (2,15) will give:

$$\alpha_o = \frac{k}{e} \left[\frac{I_1}{I_2} - \zeta \right] \qquad (2,17)$$

$$\alpha_\infty = \frac{k}{e} \left[\frac{I_3}{I_4} - \zeta \right] \qquad (2,18)$$

$$p^2 = E_0^2 \gamma \left(\frac{I_4}{3\pi^2 n} \right)^{2/3} \qquad (2,19)$$

where

$$I_1 = \int_0^\infty \frac{\xi \, G \exp(\xi - \zeta) \, d\xi}{\left[1 + \exp(\xi - \zeta)\right]^2}$$

$$I_2 = \int_0^\infty \frac{G \exp(\xi - \zeta) \, d\xi}{\left[1 + \exp(\xi - \zeta)\right]^2}$$

$$I_3 = \int_0^\infty \xi \left[\frac{\xi(\gamma\xi + 1)(\gamma\xi + 1 + \eta)}{(\gamma\xi + 1 + 2/3\,\eta)} \right]^{3/2} \frac{\exp(\xi - \zeta) \, d\xi}{\left[(1 + \exp(\xi - \zeta)\right]^2}$$

$$I_4 = \int_0^\infty \left[\frac{\xi(\gamma\xi + 1)(\gamma\xi + 1 + \eta)}{(\gamma\xi + 1 + 2/3\,\eta)} \right]^{3/2} \frac{\exp(\xi - \zeta) \, d\xi}{\left[1 + \exp(\xi - \zeta)\right]^2}$$

$$G = \left[\frac{\xi(\gamma\xi + 1)\ (\gamma\xi + 1 + \eta)}{(\gamma\xi + 1 + 2/3\ \eta)}\right]^{s+3/2} \left[\frac{(3\gamma\xi + 1)\ (\gamma\xi + 1) + (2\gamma\xi + 1)\eta}{(\gamma\xi + 1 + 2/3\ \eta)} - \frac{\gamma\xi\ (\gamma\xi + 1)\ (\gamma\xi + 1 + \eta)}{(\gamma\xi + 1 + 2/3\ \eta)^2}\right]^{-2}$$

$$\gamma = \frac{kT}{E_0}, \qquad \eta = \frac{\Delta}{E_0}$$

Equation (2,12) is particularly useful in this case because it is of the form

$$k = C\, m_0^*\, f(E)$$

where C is a constant. The m_0^* then cancels in equation (2,14) so that the effective mass need not be known to determine the Fermi energy. One can then solve for m_0^* by combining equations (2,19) and (2,8).

3. CONDUCTION IN A SINGLE SPHERICAL BAND

A) MAGNETORESISTANCE

Several factors may cause a transverse magnetoresistance to appear in a semiconductor, some of which are two band conduction, anisotropic relaxation time and inhomogeneities. Here, we will consider the simplest case, the magnetoresistance for a single spherical band centered on the Γ point due to an energy dependent relaxation time.

If an electric field E_x is applied in the x direction and a magnetic field in the z direction, the resultant current densities may be written as

$$J_x = A E_x - D E_y \tag{2,20}$$

$$J_y = D E_x + A E_y \tag{2,21}$$

where

$$A = ne^2 \left\langle \frac{\tau/m^*}{1 + e^2 B^2 (\tau/m^*)^2} \right\rangle \tag{2,22}$$

$$D = ne^3 B \left\langle \frac{(\tau/m^*)^2}{1 + e^2 B^2 (\tau/m^*)^2} \right\rangle \tag{2,23}$$

and the large bracket denotes the expected average with respect to the energy. The above definitions for A and D are more general than those given by Smith (59Sa) who assumes parabolic bands and therefore a constant effective mass. In III-V compounds, however, the effective mass varies with energy as illustrated for the Kane model by equation (2,6). Hence m^* was left inside the bracket in the last two equations. The averaging over the different states involves the relation (62Z)

$$\langle T \rangle = \frac{\int_0^\infty (-\frac{\partial f_o}{\partial E})\ T\, k^3\, dE}{\int_0^\infty (-\frac{\partial f_o}{\partial E})\ k^3\ dE} \tag{2,24}$$

Thus

$$A = (ne^2) \frac{\int_0^\infty \frac{(-\frac{\partial f_o}{\partial E})\ (\tau/m^*)\ k^3\, dE}{1 + e^2 B^2 (\tau/m^*)^2}}{\int_0^\infty (-\frac{\partial f_o}{\partial E})\ k^3\ dE}$$

$$= \frac{e^2}{3\pi^2} \int_0^\infty \frac{(-\frac{\partial f_o}{\partial E})\ (\tau/m^*)\ k^3\, dE}{1 + e^2 B^2 (\tau/m^*)^2}$$

$$D = ne^3 B \frac{\int_0^\infty \frac{(-\frac{\partial f_o}{\partial E})\ (\tau/m^*)^2\ k^3\ dE}{1 + e^2 B^2 (\tau/m^*)^2}}{\int_0^\infty (-\frac{\partial f_o}{\partial E})\ k^3\ dE}$$

$$= \frac{e^3 B}{3\pi^2} \int_0^\infty \frac{(-\frac{\partial f_o}{\partial E})\ (\tau/m^*)^2 k^3\ dE}{1 + e^2 B^2 (\tau/m^*)^2}$$

where n has been eliminated by using equation (2,15). Recalling the relations

$$\frac{1}{m^*} = \frac{1}{\hbar^2 k} \frac{\partial E}{\partial k}$$

$$\tau = t k^{2s-1} \frac{\partial E}{\partial k}$$

$$\xi = \frac{E}{kT}$$

we finally obtain

$$A = \frac{t}{3} (\frac{ekT}{\pi \hbar})^2 \int_0^\infty \frac{(-\frac{\partial f_o}{\partial \xi})\ k^{2s+1} (\frac{\partial \xi}{\partial k})^2 d\xi}{1 + \frac{e^2 B^2 t^2 (kT)^4}{\hbar^4} (\frac{\partial \xi}{\partial k})^4 k^{4s-4}} \qquad (2,25)$$

$$D = \frac{e^3 t^2 B (kT)^4}{3\pi^2 \hbar^4} \int_0^\infty \frac{(-\frac{\partial f_o}{\partial \xi})\ k^{4s-1} (\frac{\partial \xi}{\partial k})^4 d\xi}{1 + \frac{e^2 B^2 t^2 (kT)^4}{\hbar^4} (\frac{\partial \xi}{\partial k})^4 k^{4s-4}} \qquad (2,26)$$

The unknown t may be determined experimentally, since in the absence of a magnetic field, $A = A_0$ turns out to be the zero field conductivity σ_0. From equations (2,22) and (2,25),

$$A_0 = ne^2 \langle \tau/m^* \rangle = \sigma_0 = \frac{t}{3} \left(\frac{ekT}{\pi \hbar}\right)^2 \int_0^\infty \left(-\frac{\partial f_o}{\partial \xi}\right) k^{2s+1} \left(\frac{\partial \xi}{\partial k}\right)^2 d\xi$$

Thus

$$t = 3 \sigma_0 \left(\frac{\pi \hbar}{ekT}\right)^2 \Bigg/ \int_0^\infty \left(-\frac{\partial f_o}{\partial \xi}\right) k^{2s+1} \left(\frac{\partial \xi}{\partial k}\right)^2 d\xi \qquad (2,27)$$

These expressions for A and D will now allow one to predict the behavior of the magnetoresistance as a function of magnetic field. By applying the condition $J_y = 0$ for no transverse current,

$$J_x = (A + D^2/A)\, E_x = \sigma E_x$$

where σ is the field dependent conductivity which is now given by

$$\sigma = A + D^2/A \qquad (2,28)$$

The resistivity being just the reciprocal of this, we may write for the magnetoresistivity

$$\Delta\rho = \rho - \rho_0 = (A + D^2/A)^{-1} - A_0^{-1}$$

$$\frac{\Delta\rho}{\rho_0} = \frac{A_0}{A + D^2/A} - 1 \qquad (2,29)$$

where ρ_0 is the zero field resistivity.

B) HALL EFFECT

This phenomenon also involves the parameters A and D mentioned above. By definition the Hall coefficient R is given by

$$E_y = R B J_x$$

Thus we may write

$$J_x = -(A^2/D + D)\, E_y = -(A^2/D + D)\, R\, B\, J_x$$

$$R = \frac{-D/B}{A^2 + D^2} \qquad (2,30)$$

As above, we may calculate the change in R as a function of B.

$$\Delta R = R - R_0$$

$$= \frac{-D/B}{A^2 + D^2} + \frac{(D/B)_0}{A_0^2}$$

where $(D/B)_0$ is the limiting value of D/B as B tends to zero. The evaluation of this factor presents no problem as D is proportional to B. It may be shown that

$$\frac{\Delta R}{R_0} = \frac{A_0^2\, D}{B(D/B)_0\,(A^2 + D^2)} - 1 \qquad (2,31)$$

4. MAGNETORESISTIVITY AND HALL EFFECT FOR TWO BAND CONDUCTION

When two types of carriers are responsible for conduction in a semiconductor, the resistivity will depend on the magnetic field in the manner (59Sb) described by equation (2,32).

$$\rho = \rho_0 + \Delta\rho = \frac{(\sigma_1 + \sigma_2) + (\sigma_1\,\sigma_2\, B^2(\sigma_1 R_1^2 + \sigma_2 R_2^2)}{(\sigma_1 + \sigma_2)^2 + \sigma_1^2\,\sigma_2^2\, B^2\,(R_1 + R_2)^2} \qquad (2,32)$$

where σ_1, R_1 and σ_2, R_2 are the conductivities and Hall coefficients due to carriers in the two bands respectively. Both bands are assumed to have spherical constant energy surfaces and a constant effective mass. The corresponding Hall coefficient is described by

$$R = \frac{R_1\sigma_1^2 (1 + \sigma_2^2 R_2^2 B^2) + R_2\sigma_2^2 (1 + \sigma_1^2 R_1^2 B^2)}{(\sigma_1 + \sigma_2)^2 + \sigma_1^2 \sigma_2^2 B^2 (R_1 + R_2)^2} \qquad (2,33)$$

Smith derived these equations by imposing three conditions on the relaxation time, first that it exists, that it is isotropic and that it is independent of energy. As mentioned on page 17 of Chapter I, unless the material is highly degenerate, a relaxation time cannot be defined if the change in carrier energy upon scattering is large compared to the total energy of the carrier. Since the measured samples were degenerate in both bands, however, this would not present a problem. An isotropic relaxation time would require that both bands be centered upon $\underline{k} = 0$. The error introduced by an anisotropic τ will be considered in the following section. Finally, the relaxation time varies with energy as mentioned in Chapter I, but if the material is degenerate, only the electrons near the Fermi level will participate in the conduction so that the energy may be considered constant. This explanation also justifies the assumption that the effective mass is constant.

The next step is to transform the above equations to solve for σ_1, σ_2, R_1, R_2. The magnetoresistivity is

$$\Delta\rho = \frac{\sigma_0 + \sigma_1 \sigma_2 B^2 (\sigma_1 R_1^2 + \sigma_2 R_2^2)}{\sigma_0^2 + \sigma_1^2 \sigma_2^2 B^2 (R_1 + R_2)^2} - \frac{1}{\sigma_0}$$

and consequently the relative change in resistivity is

$$\frac{\Delta\rho}{\rho_0} = \frac{\frac{\sigma_1\sigma_2}{\sigma_0}(\sigma_1 R_1^2 + \sigma_2 R_2^2) - \frac{\sigma_1^2\sigma_2^2}{\sigma_0^2}(R_1 + R_2)^2}{B^{-2} + \frac{\sigma_1^2\sigma_2^2}{\sigma_0^2}(R_1 + R_2)^2} \qquad (2,34)$$

where the zero field conductivity is given by

$$\sigma_0 = \frac{1}{\rho_0} = \sigma_1 + \sigma_2 \qquad (2,35)$$

As far as the author is aware, he was the first to realize that a straight line could be obtained from equation (2,34). In fact, a plot of $\rho_0/\Delta\rho$ versus B^{-2} will yield a straight line of slope

$$p = \left[\frac{\sigma_1\sigma_2}{\sigma_0}(\sigma_1 R_1^2 + \sigma_2 R_2^2) - \frac{\sigma_1^2\sigma_2^2}{\sigma_0^2}(R_1 + R_2)^2\right]^{-1} \qquad (2,36)$$

and intercept on the $\rho_0/\Delta\rho$ axis of

$$q = \frac{p\,\sigma_1^2\sigma_2^2}{\sigma_0^2}(R_1 + R_2)^2 \qquad (2,37)$$

This result was used by Kwan (68K) who analysed the magnetoresistivity of highly doped n type InAs. The intercept corresponds to the saturation value of $\rho_0/\Delta\rho$ at infinite fields. Considering the Hall coefficient at infinite fields also,

$$R_\infty = \frac{R_1 R_2}{R_1 + R_2} \qquad (2,38)$$

Kwan's analysis involved R_0, the Hall coefficient extrapolated to zero

magnetic field, rather than R_∞. The last four equations express four measurable quantities in terms of four unknowns which may now be solved. From equations (2,35) and (2,38), one may write,

$$\sigma_2 = \sigma_0 - \sigma_1$$

$$R_2 = \frac{R_1 R_\infty}{R_1 - R_\infty}$$

Using these substitutions in equation (2,36), one may then show that

$$p = \frac{\sigma_0^2 (R_1 - R_\infty)^2}{\sigma_1 (\sigma_0 - \sigma_1) R_1^2 (R_\infty \sigma_0 - R_1 \sigma_1)^2} \qquad (2,39)$$

But from equation (2,37) it may also be shown that

$$p = \frac{q \sigma_0^2 (R_1 - R_\infty)^2}{R_1^4 \sigma_1^2 (\sigma_0 - \sigma_1)^2} \qquad (2,40)$$

By equating these two relations, one obtains

$$R_1^2 (\sigma_1 \sigma_0 - \sigma_1^2 - q \sigma_1^2) + R_1 (2q R_\infty \sigma_0 \sigma_1) - q R_\infty^2 \sigma_0^2 = 0$$

from which

$$R_1 = \left[\frac{q R_\infty \sigma_0}{\sigma_0 - \sigma_1 - q \sigma_1}\right] \left[-1 \pm \sqrt{1 + \frac{\sigma_0 - \sigma_1 - q \sigma_1}{q \sigma_1}}\right] \qquad (2,41)$$

Equations (2,39) and (2,41) may then be used for the solution by an iterative procedure that will be described in Chapter VI.

5. MAGNETORESISTANCE DUE TO ANISOTROPY

A) THEORY

This section will attempt to justify the analysis of the magnetoresistance due to two bands which assumed spherical constant energy surfaces and thus neglected effects due to anisotropy. When the constant energy surfaces are ellipsoids of revolution, a magnetoresistance will appear even though the material may be infinitely degenerate. To appreciate exactly what is caused by anisotropy, one should, however, return first to the case of a spherical band. If a constant effective mass and low magnetic fields are assumed, we may rewrite equations (2,22) and (2,23).

$$A \simeq \frac{ne^2}{m^*}\left[\langle\tau\rangle - \frac{e^2B^2}{m^{*2}}\langle\tau^3\rangle\right] \qquad (2,42)$$

$$D \simeq \frac{ne^3B}{m^{*2}}\langle\tau^2\rangle \qquad (2,43)$$

The Hall coefficient R_0, extrapolated to zero magnetic field may now be obtained from equation (2,30)

$$R_0 = \frac{-(D/B)_0}{A_0^2} = \frac{r}{ne} \qquad (2,44)$$

where $$r = \frac{\langle\tau^2\rangle}{\langle\tau\rangle^2}$$

Similarly, from equation (2,29), the magnetoresistivity

$$\frac{\Delta\rho}{\rho_0} \simeq \frac{e^2 B^2}{m^{*2}} \left[\frac{\langle \tau \rangle \langle \tau^3 \rangle - \langle \tau^2 \rangle^2}{\langle \tau \rangle^2} \right]$$

$$\simeq R_0^2 \sigma_0^2 B^2 \left[\frac{\langle \tau^3 \rangle \langle \tau \rangle}{\langle \tau^2 \rangle^2} - 1 \right]$$

$$\simeq R_0^2 \sigma_0^2 B^2 W \qquad (2,45)$$

where $$W = \frac{\langle \tau^3 \rangle \langle \tau \rangle}{\langle \tau^2 \rangle^2} - 1$$

When the bands are ellipsoids of revolution, the analysis is much more involved, since one must consider not only the direction of the axes of the ellipsoids but also the direction of the current and magnetic field with respect to these axes. The magnetoresistivity in small magnetic fields is (51P)

$$\frac{\Delta\rho}{\rho_0 B^2} = b + c(i\ell + jm + kn)^2 + d(i^2\ell^2 + j^2m^2 + k^2n^2) \qquad (2,46)$$

where i, j, k and ℓ, m, n are the direction cosines giving the directions of the current and magnetic field respectively. The constants b, c, and d depend on the directions of the axes of the ellipsoids and may be expressed in terms of $K = \frac{m_L}{m_T}$ where m_L and m_T are the longitudinal and transverse effective masses respectively.

Consider the case where the constant energy surfaces form ellipsoids along the <111> axes. Let the coordinate axes (x, y, z) lie along the <100> directions in the crystal. A derivation of the equations of motion (59Sd) will again lead to expressions for the current densities J_x and J_y. The results for the Hall coefficient and magnetoresistivity are

$$R_0 = \frac{r F}{ne} \qquad (2,47)$$

$$\frac{\Delta\rho}{\rho_0} = R_0^2 \sigma_0^2 B^2 S_{100}^{001} \qquad (2,48)$$

where $$F = \frac{3K(K+2)}{(2K+1)^2}$$

and $$S_{100}^{001} = \frac{1+W}{F} - 1 ,$$

the lower indices giving the current direction and the upper indices giving the magnetic field direction. Equation (2,47) holds for any crystal with cubic symmetry and for any direction, as long as the current is perpendicular to the magnetic field, and terms in B^2 may be neglected. The magnetoresistivity, however, is a function of orientation. When $K = 1$, the constant energy surfaces are spherical and the two equations above reduce to equations (2,44) and (2,45). Smith (59Sd) also quotes the results for two other specimen orientations:

$$S_{100}^{100} = \frac{2(W+1)(K-1)^2(2K+1)}{3K(K+2)^2}$$

$$S_{110}^{110} = \frac{1}{2} S_{100}^{100}$$

One can then show that

$$b = R_0^2 \sigma_0^2 S_{100}^{001}$$

$$c = -R_0^2 \sigma_0^2 S_{100}^{001} \qquad (2,49)$$

$$d = R_0^2 \sigma_0^2 S_{100}^{100}$$

B) APPLICATION

Equation (2,34) describes the magnetoresistivity due to the presence of two types of carriers, with other effects being neglected. However, each band may produce a magnetoresistivity because of an energy dependent τ and anisotropy. These contributions will now be calculated and compared with the two band magnetoresistivity. The form of the following analysis is identical to that of Harland (65H).

The total conductivity is

$$\sigma(B) = \sigma_1(B) + \sigma_2(B)$$

so that $$\frac{1}{\rho(B)} = \frac{1}{\rho_1(B)} + \frac{1}{\rho_2(B)}$$

whereas in zero magnetic field

$$\frac{1}{\rho_0} = \frac{1}{\rho_{10}} + \frac{1}{\rho_{20}}$$

where the last subscript refers to zero magnetic field.

$$\rho(B) = \frac{\rho_1(B)\,\rho_2(B)}{\rho_1(B) + \rho_2(B)}$$

If we write $$\rho_1(B) = \rho_{10} + \Delta\rho_1$$

$$\rho_2(B) = \rho_{20} + \Delta\rho_2$$

then

$$\rho(B) = \frac{\rho_{10}\,\rho_{20}\,(1 + \frac{\Delta\rho_1}{\rho_{10}})\,(1 + \frac{\Delta\rho_2}{\rho_{20}})}{\rho_{10} + \rho_{20} + \Delta\rho_1 + \Delta\rho_2}$$

The magnetoresistivity is then given by

$$\frac{\Delta\rho}{\rho_0} = \frac{(\rho_{10} + \rho_{20})\left(1 + \frac{\Delta\rho_1}{\rho_{10}}\right)\left(1 + \frac{\Delta\rho_2}{\rho_{20}}\right)}{\rho_{10} + \rho_{20} + \Delta\rho_1 + \Delta\rho_2} - 1$$

$$\simeq \frac{\rho_{10}\left(\frac{\Delta\rho_2}{\rho_{20}}\right) + \rho_{20}\left(\frac{\Delta\rho_1}{\rho_{10}}\right)}{\rho_{10} + \rho_{20}}$$

$$\simeq \frac{(R_1^2 \sigma_1^3 S_1 + R_2^2 \sigma_2^3 S_2) B^2}{\sigma_1 + \sigma_2} \qquad (2,50)$$

This is the net effect of the contributions from the individual bands. The magnetoresistivity due to two bands, to first order in B^2 may be found from equation (2,32):

$$\frac{\Delta\rho}{\rho_0 B^2} \simeq \frac{\sigma_1 \sigma_2 (\sigma_1 R_1 - \sigma_2 R_2)^2}{(\sigma_1 + \sigma_2)^2} \qquad (2,51)$$

The above analysis will now be applied to the two conduction bands in InSb, the (000) and the <111>.

Considering a typical set of results, we set $n(000) = 5n\langle 111\rangle$, $\mu(000) = 3\mu\langle 111\rangle$. Thus $\sigma_1 = 15\sigma_2$, $R_2 = 5R_1$ (2,52)

For the (000) band, which is known to be spherical, we may set $K = 1$ and neglect anisotropic effects. Two transverse cases will now be considered.

CASE 1 current direction [100]

magnetic field direction [010]

CASE 2 current direction [111]

magnetic field direction [11$\bar{2}$]

The coefficient c of equation (2,46) in such transverse cases will always be zero. The (000) magnetoresistivity is thus:

$$\frac{\Delta\rho_1}{\rho_{10}B^2} = b_1 = R_1^2 \sigma_1^2 W_1$$

since $S_1 = W_1$ for K = 1. For the <111> bands, the maximum magnetoresistivity will be obtained when $K = \infty$, i.e. when F = .75.

CASE 1

$$\frac{\Delta\rho_2}{\rho_{20}B^2} = b_2 = R_2^2 \sigma_2^2 S_{100}^{001}$$

$$= R_2^2 \sigma_2^2 (.333 + 1.333 W_2)$$

$$S_2 = .333 + 1.333 W_2$$

CASE 2

$$\frac{\Delta\rho_2}{\rho_{20}B^2} = b_2 + \frac{d_2}{3}$$

$$= R_2^2 \sigma_2^2 (.333 + 1.333 W_2 + .444 + 1.444 W_2)$$

$$S_2 = .777 + 1.777 W_2$$

We may now compute the combined effects of the bands by returning to

equation (2,50)

$$\text{CASE 1} \quad \frac{\Delta\rho}{\rho_0 B^2} = R_1^2 \sigma_1^2 (.94 W_1 + .00926 W_2 + .00231)$$

$$\text{CASE 2} \quad \frac{\Delta\rho}{\rho_0 B^2} = R_1^2 \sigma_1^2 (.94 W_1 + .0123 W_2 + .00540)$$

The two band magnetoresistivity may be obtained from equation (2,51).

$$\frac{\Delta\rho}{\rho_0 B^2} = .0260 \sigma_1^2 R_1^2$$

The contributions due to the individual bands are greatest for CASE 2. The first and second terms are due to the energy dependent relaxation times for the (000) and <111> bands respectively. For the (000) band, $E_F > 1000\ k\ T$ so that W_1 is insignificant. For the <111> bands, $E_F > 6\ k\ T$ so that $W_2 < .14$ and thus $.0123\ W_2$ is less than 7% of the two band term. The value of W_2 was obtained from equation (2,45) with the average values of τ, τ^2 and τ^3 being calculated by numerical integration in the manner suggested by equation (2,24). Scattering by ionized impurities ($s = 1.5$) was assumed along with a parabolic band of effective mass .2m. The anisotropy of the <111> bands accounts for the last term which is by for the largest and amounts to 25% of the two band term. For CASE 1, it is 9%. Since the InSb samples were polycrystalline, there would probably be some sort of average of the above and other cases coming into play. Also $K < \infty$ so that the contribution from the <111> bands is overestimated.

A similar analysis could be performed for large rather than small

values of B. Unfortunately, CASE 1 was the only one for which a theoretical expression was available. Smith (59Sd) states that for this case

$$\frac{\sigma_0}{\sigma_\infty} = \left\langle \frac{1}{\tau} \right\rangle \langle \tau \rangle \frac{(2K+1)^2}{3K(K+2)}$$

where σ_∞ is the infinite field conductivity. If it is assumed that the <111> bands are degenerate, then $\left\langle \frac{1}{\tau} \right\rangle \langle \tau \rangle = 1$. By repeating the analysis that was performed above, one can show that the anisotropy term is 8.4% of the two band term whereas for small fields, it was 8.9% of the corresponding two band term. It appears that approximately the same results are produced from high and low field calculations.

CHAPTER III

EQUIPMENT AND EXPERIMENTAL TECHNIQUE

1. PREPARATION OF INGOTS

A) $InAs_xSb_{1-x}$ AND $In_{1-x}Ga_xSb$ ALLOYS

Three compounds were needed to prepare ingots of $InAs_xSb_{1-x}$ and $In_{1-x}Ga_xSb$ alloys: InAs, InSb and GaSb. The first two were bought from Cominco in the form of n type polycrystalline ingots and had a carrier concentration of approximately 2×10^{16} cm^{-3}. The third compound, GaSb, was prepared by melting together stoichiometric quantities of 99.999% pure Ga and Sb bought from AIAG and Cominco respectively.

Both alloys were prepared by horizontal Bridgman techniques. This required a furnace with a "hot" zone separated from a "cold" zone by a steep temperature gradient. To prepare $InAs_xSb_{1-x}$ alloys for example the temperature of the hot zone was set higher than the melting point of InAs (1000^oC) while the "cold" zone temperature was lower than the melting point of InSb (525^oC), but not below 500^oC to avoid the loss of As by condensation. A steep gradient was provided by water cooled copper plates. For the $In_{1-x}Ga_xSb$ alloys, the hot zone temperature had to be greater than 712^oC, the melting point of GaSb while the cold zone as above was held below 525^oC.

An evacuated quartz capsule containing a known mixture of the two compounds to be alloyed was placed in the hot zone of the furnace and shaken to obtain a homogeneous solution. The capsule was then moved at a rate of 0.5 cm/day into the cold zone so that the ingot slowly froze from one end. The resulting ingot was about 15 cm long and 1 cm wide, the cross section being slightly elliptical. It was polycrystalline and generally had a single phase, the composition varying smoothly along the length of the ingot as shown by Figure (3,1). The composition of different points in the ingot was found by determining the lattice parameter a_o by X-ray powder photograph techniques. A powder camera 114.6 mm in diameter was used in conjunction with a Philips X-ray machine whose beam had an effective wavelength equal to 1.5418 A due to the copper doublet. The a_o value obtained in this way was compared with the a_o versus x curves published by Woolley et al (64 Wb) to obtain the composition. Since specimens were prepared from cross sectional slices cut from these ingots, the steep part of the curve in Figure (3,1) caused problems in obtaining relatively homogeneous specimens. However, by preparing several ingots of different mean composition (e.g. 70% InAs, 30% InSb) and lapping specimens down to 1 mm in thickness, it was possible to obtain a homogeneity of 1% or better for all specimens.

B) GaAs SINGLE CRYSTALS

The GaAs single crystal material was supplied by Merk, Monsanto and Northern Electric. The material was n type with the carrier concentration ranging from 9×10^{15} to 2×10^{18} cm^{-3}. The slices

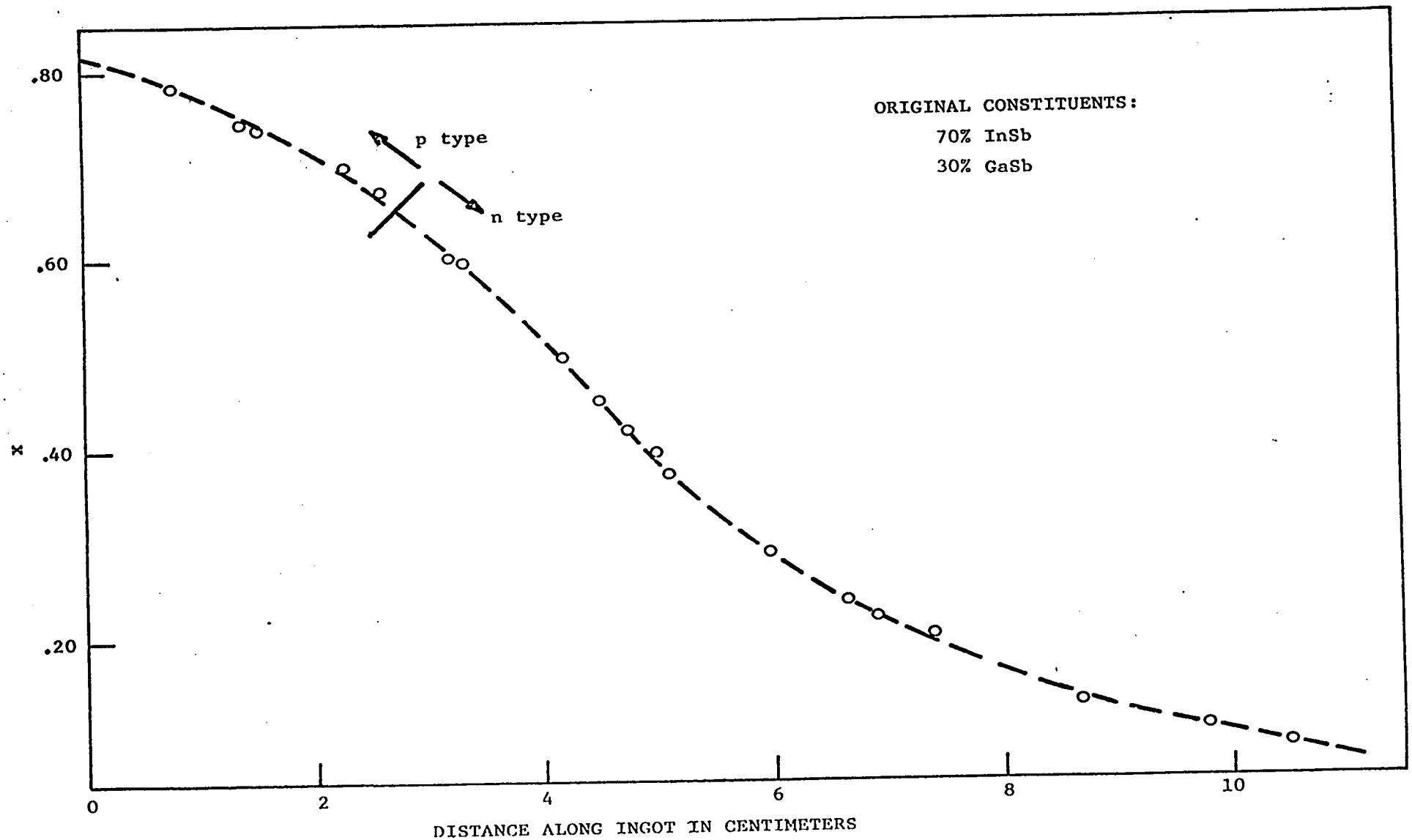

FIGURE (3,1) VARIATION OF x ALONG TYPICAL INGOT OF $In_{1-x}Ga_xSb$

obtained from Monsanto had been cut parallel to the (111) plane but the orientations of the others were unknown. In all cases, specimens were cut from these slices, with no regard for the crystallographic orientation. This will be shown to be unimportant.

C) InSb ALLOYED WITH In_2Te_3 AND In_2Se_3

The In_2Te_3 and In_2Se_3 materials were prepared from 99.999% pure elements bought from Cominco and Mining and Chemical Products Ltd. Stoichiometric quantities were molten together in evacuated quartz capsules. The InSb, as mentioned above, was obtained from Cominco and had an original electron concentration of 2×10^{16} cm^{-3}. Eighteen ingots of InSb alloyed with In_2Te_3 were prepared. Each weighed approximately six grams and contained a known quantity of In_2Te_3 varying from .02 to 1.5 percent. These ingots were annealed for 10 days at 500° C. This length of time is sufficient to allow equilibrium to be established in the alloy (60W). Another twelve ingots of InSb alloyed with In_2Se_3 were prepared but these required an annealing time of six weeks (61 Wb). The In_2Se_3 content varied from .02 to 1.5 percent.

The alloy compositions were calculated on the basis of the molecular weights of In_3Sb_3 and $In_2\square Te_3$, the square denoting a vacancy since In_2Te_3 (and In_2Se_3) has a defect zinc blende structure with one lattice site in three on the In sub-lattice vacant. There are still four valence electrons per lattice site as in the

zinc blende lattice. The percentages quoted above of In_2Te_3 (and In_2Se_3) are then those of Te (or Se) on the Sb sub-lattice. At low percentages, it has been shown that doping with In_2Te_3 or In_2Se_3 (60W, 61Wa) gives the same effect as doping with Te or Se. Thus specimens will be described by their atomic percentages of Te or Se which will vary from .01 to .75%.

In each of the two series of experiments, the ingots and specimens cut therefrom were assigned consecutive numbers. However, some ingots were found to contain blow holes and others were badly oxydized because of a crack in the capsule. This explains the missing numbers in the lists of the specimens. In some cases, two specimens were prepared and measured from the same ingot. The suffix A was then added to the name of one of the two specimens e.g. numbers 5 and 5A.

2. SAMPLE PREPARATION

A) CUTTING AND LAPPING

As mentioned above, cross sectional slices were cut from the $InAs_xSb_{1-x}$ and $In_{1-x}Ga_xSb$ ingots. The $InSb-In_2Te_3$ and $InSb-In_2Se_3$ ingots were smaller but had a uniform composition so that longitudinal slices could be cut from them. These operations were performed by gluing the ingots to arborite blocks with a mixture of glyptal and acetone and then cutting them with a .008" thick carborundum saw. The thickness of the slices was approximately 1.5 mm. The glue was then dissolved away with acetone and the slices thus obtained as

well as the GaAs slices were glued to arborite blocks and cut in the form of parallelepipeds of dimensions 10 x 2 x 1.5 mm.

Good results for the Hall coefficient and resistivity depended on the degree with which the opposite sides of the parallelepiped were parallel and the cross section rectangular. Accuracy in the Hall coefficient required a constant specimen thickness i.e., parallel opposite sides. Accurate resistivity measurements required a rectangular specimen cross section between the two resistivity probes on one side of the specimen since the dimensions were measured with a micrometer. Thus a careful lapping was performed at this stage using the adjustable lapping block shown in Figure (3,2). The specimen was glued to the block which was moved in figure-eight fashion on a glass plate covered with a mixture of water and 600 grit lapping powder. All four sides were lapped until the specimen cross section was approximately 0.9 x 1.4 mm. These dimensions were measured at different points along the specimen with a Moore and Wright micrometer accurate to one micron and found to be constant to better than 1%.

B) ELECTRICAL CONTACTS

Electrical contacts to the specimen was simplest for the case of the $InAs_xSb_{1-x}$ and $In_{1-x}Ga_xSb$ alloys. These were only measured at room temperature and resistivity measurements were not necessary. Two current contacts at the ends of the specimen and two Hall contacts

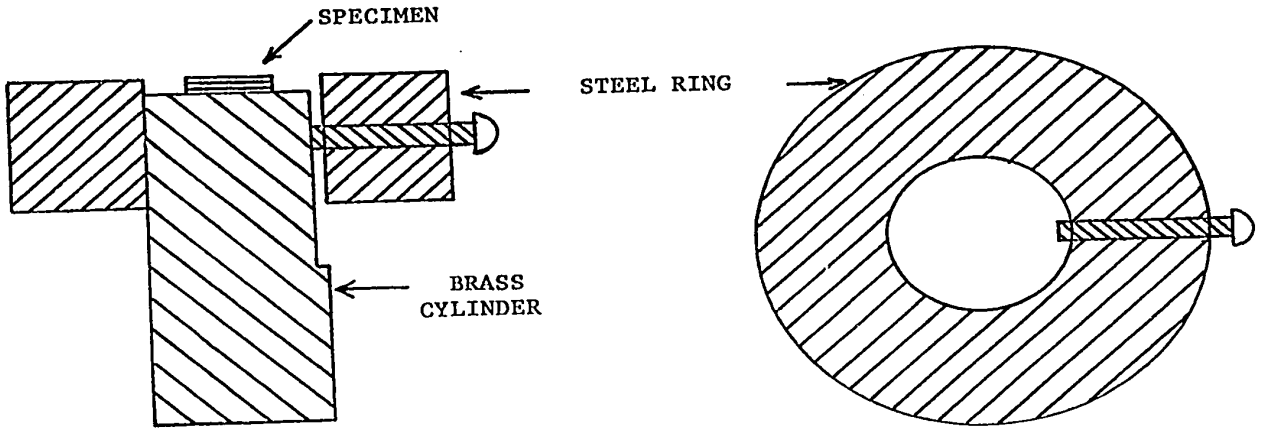

FIGURE (3,2) LAPPING BLOCK

on opposite sides were supplied by gold wires which were spark welded to the specimen by discharging through the contacts a 10μf capacitor charged to 10 volts. If one or more contacts were non-ohmic, the capacitor was discharged in both directions until ohmic contacts of approximately 1 ohm were obtained. Figure (3, 3a) illustrates the jig used for these measurements. Then came the magnetothermoelectric power measurements. Contacts for the latter were supplied by a special jig which will be described later.

In the InSb and GaAs projects, resistivity as well as Hall measurements were performed and greater care was taken in the contact preparation. The InSb contacts were obtained by the electroplating of tin. When the GaAs project was started, an evaporator was available so that these contacts were prepared by the evaporation of indium.

In the electroplating technique, the InSb specimen was masked with nail polish except for the end faces, one narrow strip on one side and two narrow strips on the other. The specimen, held by self-clasping tweezers, was etched in a solution of 1 part HNO_3 and 1 part HCl for ten seconds, rinsed in distilled water and finally dipped in a tin plating solution. The latter had been prepared with 1 part anhydrous stannic chloride, 1 part H_2SO_4 and 20 parts H_2O. With the specimen as the cathode and a platinum wire as the anode, a current of 1 ma was allowed to flow for approximately 30 minutes. The five exposed surfaces were then covered with a layer of tin about .1 mm thick. Acetone was then used to dissolve the nail polish. The contacts obtained in this way

were ohmic with a resistance of 1 or 2 ohms. The specimen was glued to a glass slide as shown in Figure (3, 3b) and silver paint was used to connect the tin contacts to # 32 enamelled copper wires which had been glued to the back side of the slide with baking vanish. The slide was then clamped in the specimen holder so that the specimen would lie horizontally in the cryostat. The # 32 copper wires were soldered to connecting pins which in turn were connected to copper leads coming out of the cryostat.

The end surfaces of the GaAs specimens were electroplated with tin as described above but indium was evaporated on the three side contacts. A copper foil was used through which two parallel slits had been cut with a razor blade. The slits were 1 mm long and separated by 6 mm. One side of the sample to be coated was centered over the slits and the whole assembly placed over the indium in the vacuum chamber of the evaporator. When the indium evaporated, it rose through the two slits of the copper foil and condensed on the specimen as two parallel narrow strips. The specimen was then turned over and centered over one of the slits. The evaporation procedure was repeated to obtain the last contact centered on one side of the specimen. At this stage the contacts were highly rectifying and had to be annealed. The specimen was heated to about 200^{o} C for 30 seconds in helium gas at a pressure of 30 mm of Hg. Contacts thus became ohmic with a resistance of approximately 5 ohms. The sample was then mounted on a glass slide as shown in Figure (3, 3b).

a)

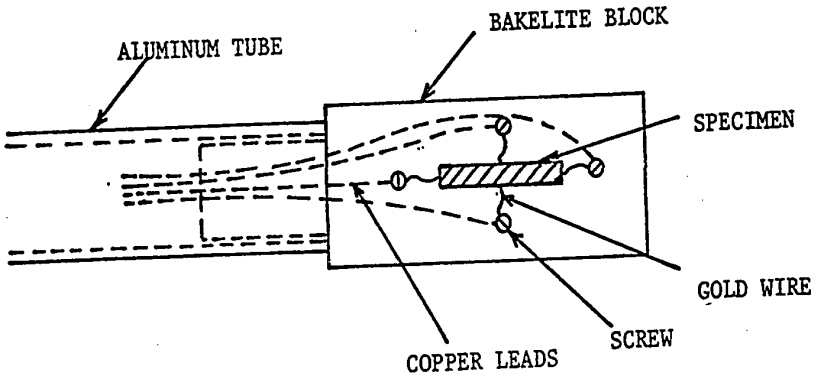

b)

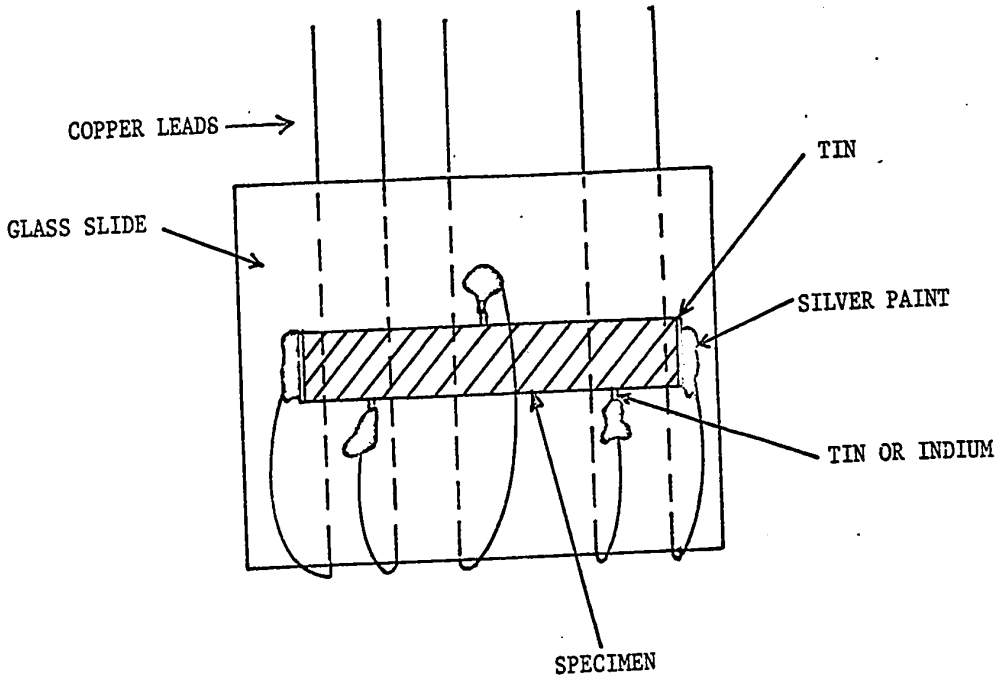

FIGURE (3,3) SPECIMEN CONNECTIONS

3. MEASUREMENTS

The first measurements by the author involved InSb alloyed with In_2Te_3 and were carried out in the old laboratory. The Hall and magnetoresistance apparatus had been mounted by Dr Harland and is described in the latter's Ph.D. thesis. When construction of the new Physics and Mathematics building was completed, the author mounted a new system in the present laboratory while retaining certain elements and ideas from the earlier apparatus. The electrical circuit and experimental method of the Hall effect and magnetoresistance measurements were basically the same in both laboratories so that there is no need to describe both in detail. The following sections will describe these measurements in the present laboratory but will also mention differences that occurred in the first experiments. All the magnetothermoelectric power measurements, on the other hand, were performed in the present laboratory.

A) ELECTROMAGNET

In the old laboratory a Pacific Electric electromagnet was used. With a pole gap of $1\frac{1}{2}$", it supplied a maximum field of 2.34 Wb/m^2 at a current of 200 amperes. The field calibration is shown in Table (3, 1a). The potential in the first column is that across one half of the magnetic field control resistor which was held at a constant temperature in a bath of boiling water. Dr Harland performed this calibration using a Rawson rotating coil gaussmeter. The absolute accuracy of the field is .01 Wb/m^2 whereas the relative accuracy is .001 Wb/m^2.

Most of the measurements however, were performed in the present building with a Magnion-Harvey-Wells 15 inch electromagnet Model L-158 along with the HS-10200 Power Supply and FFC-4 Field Regulator. With a gap of 1¼" and a maximum current of 205 amperes, a field of 3.20 Wb/m^2 is obtained. The desired field is simply dialed on the five decade switches and the power supply automatically drives up to that field. A rotating coil gaussmeter generates a 30 cps voltage proportional to the intensity of the magnetic field. A similar constant amplitude voltage is produced by the permanent magnet generator. This voltage is used as a precision reference voltage in measuring and controlling the field. It is attenuated through the five decade switches and compared with the signal from the gaussmeter probe. The difference, or error signal is amplified causing the power supply to act as a current amplifier in controlling the power of the magnet.

The field set accuracy is 5 parts in 10^5 and the stability 1 part in 10^6. The temperature stability is 5 parts in $10^7/^oF$ of ambient temperature with no effects due to changes in the temperature of the water flowing through the coils. The specimen was placed in the centre of the pole gap where over a cubic centimeter, the field is constant to 1 part in 10^5.

Unfortunately, the field sensed by the power supply is that at the gaussmeter probe which must be removed from the gap to make way for a cryostat or other sample holders. In other words, the specimen's electrical properties and the field at the specimen may not be measured

TABLE (3,1)

MAGNETIC FIELD CALIBRATIONS

a)		b)	
V (volts)	B (kilogauss)	B (outside) (kilogauss)	B (inside) (kilogauss)
.900	23.43	3.000	3.272
.850	23.21	4.000	4.363
.800	22.99	5.000	5.454
.750	22.75	6.000	6.545
.700	22.45	7.000	7.636
.650	22.13	8.000	8.727
.600	21.66	9.000	9.818
.550	21.13	10.000	10.909
.500	20.49	11.000	12.001
.475	20.12	12.000	13.093
.450	19.74	13.000	14.186
.425	19.34	14.000	15.281
.400	18.90	15.000	16.382
.375	18.45	16.000	17.487
.350	17.97	17.000	18.598
.325	17.49	18.000	19.723
.300	16.96	19.000	20.870
.275	16.38	20.000	22.031
.250	15.77	21.000	23.121
.225	14.99	22.000	24.146
.200	13.89	23.000	25.148
.175	12.53	24.000	26.140
.150	10.96	25.000	27.126
.125	9.22	26.000	28.105
.100	7.43	27.000	29.076
		28.000	30.043
		39.000	31.009
		30.000	31.976

N.B. 10 kilogauss = $1 Wb/m^2$

simultaneously. At the author's request, the shop technicians mounted the gaussmeter on a fixed platform. The gaussmeter itself, however, could be moved radially in and out of the pole gap by a micrometer adjustment with a range of 2". The author then proceeded with a field calibration which consisted of a comparison of the field at the centre of the pole gap with that at a position 1.10" away from the centre. With the gaussmeter at this "outside" position, it was possible to place the cryostat or other sample holder in the centre of the pole gap. At the "outside" position, the field dropped to about 90% of the field at the "inside" position as shown by Table (3, 1b) for 28 field settings from 3 to 30 kilogauss.

The calibration was performed by the following method. With the gaussmeter in the "outside" position, and the operating mode on "Field Set", the dials were set for 3.000 kilogauss. The current rose automatically until the field at the "outside" position was 3.000 kilogauss. The mode was then switched to "Sweep" but with a zero sweep velocity so that the current remained constant. The gaussmeter was moved to the "inside" position. The sensed field at this stage was different from the dialed field so that the error signal caused the galvanometer needle to deviate from the balance position. The dial setting was changed until the error signal was zero. As shown by Table (3, 1b) this dial setting was 3.272 kilogauss, the field at the "inside" position when the field was 3.000 kilogauss at the "outside" position. This procedure was repeated for 27 other field values.

B) CRYOSTAT

The cryostat used in this project was built at NRC and had been designed for use with the Pacific Electric Co. electromagnet described above. The original blueprint is shown in Figure (3, 4). The first InSb measurements performed in the old laboratory thus used the cryostat in its original form. However, the Magnion-Harvey-Wells electromagnet had pole caps whose angle was smaller and to use the cryostat with this magnet, it was necessary to lengthen the tail of the cryostat. These changes were done at NRC.

The cryostat consisted of an outer vacuum jacket, two refrigerant tanks, a radiation shield anchored to the upper (liquid nitrogen) tank and a silver specimen chamber separated from the lower (liquid helium) tank by a stainless steel thermal resistance. The specimen holder was made of bakelite in order to electrically insulate the specimen from the cryostat. A thin walled stainless steel tube connected the specimen holder to the cryostat head. A rotatable vacuum seal allowed alignment of the specimen in the magnetic field. The specimen was maintained at the temperature of the silver chamber by means of helium exchange gas.

The cryostat contained a copper wire resistance thermometer and a gold-cobalt versus copper thermocouple for use with the temperature control system. These are described in Dr Harland's thesis. Since the measurements reported here were performed at liquid helium and room temperatures, no further description of the temperature control system will be given.

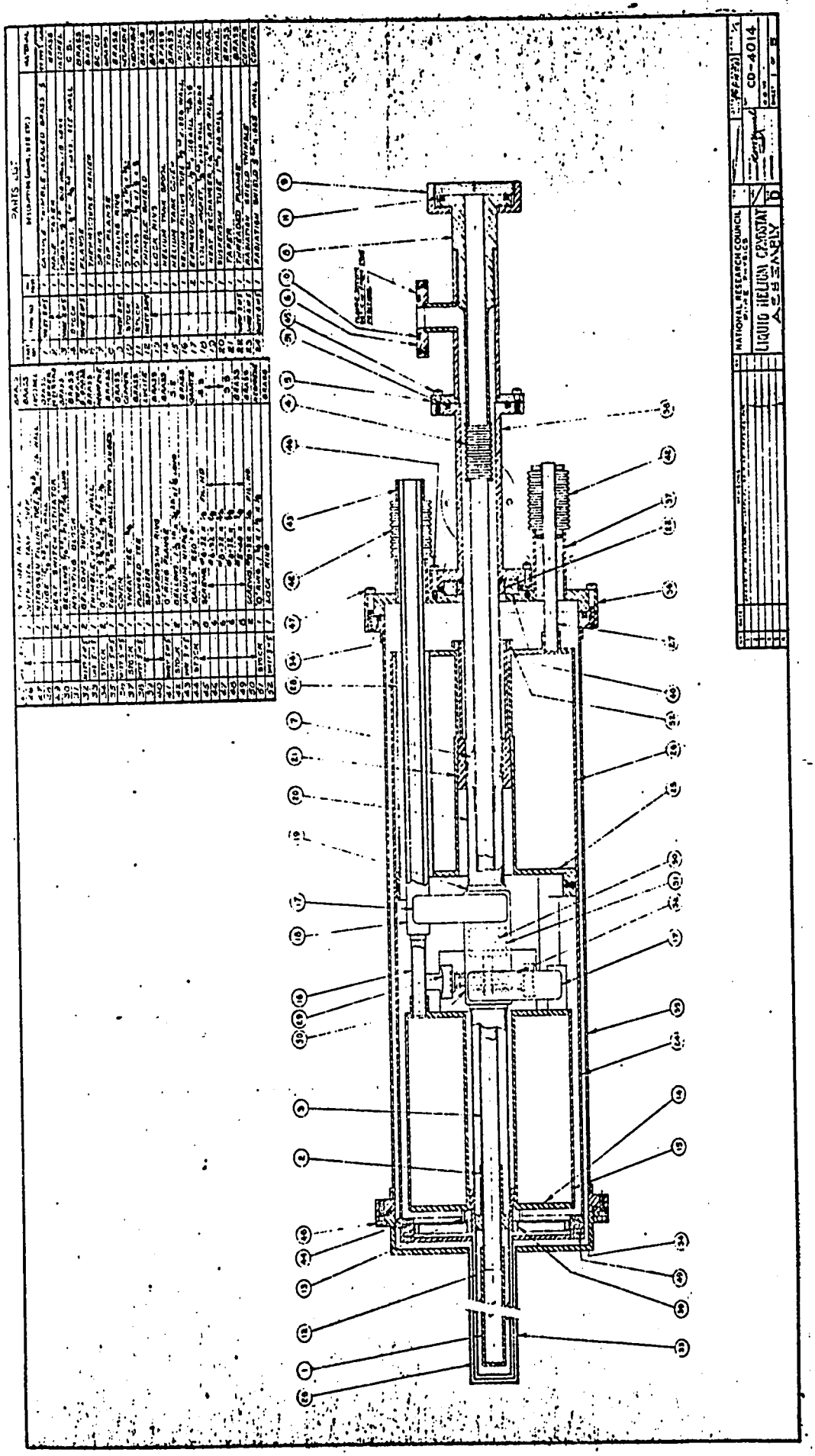

FIGURE (3,4) CRYOSTAT

C) HALL AND MAGNETORESISTANCE MEASUREMENTS

The current through the sample ($\sim$ 100 ma.) was supplied by two 12 volt automobile batteries in parallel. After 24 hours of operation, it varied less than 1 part in 10^5 in several hours. The current was controlled by a variable resistor in series with the specimen and determined from the potential drop across a 1 ohm standard resistance (Leeds and Northrup) measured with a Rubicon potentiometer. The resistivity of the specimen was obtained from the potential drop between the two contacts on the same side of the sample measured with a four figure digital voltmeter (Hewlett Packard Model 3440A with the 3443 High Gain plug-in). The signal was preamplified by an Astrodata Nanovolt Amplifier Model 120 whose noise level was less than .05 μv. Ten scales offered fixed gains varying from 200 to 2 million. In the old laboratory, a Philips recorder was used instead of the digital voltmeter. Its most sensitive scale gave a full scale reading for 1 mv. The preamplifier was a galvanometer amplifier built by Dr Harland and described in his thesis. Since the relative change in resistance due to the magnetic field was small, direct readings of the resistance as a function of field would be highly inaccurate. Thus a back-off system was used i.e. the reading of the zero field resistance voltage was nulled by opposing it to an equal voltage supplied by another automobile battery and a variable resistor. The effect of the magnetic field on the resistance voltage could be then amplified, say 20,000 times by the Nanovolt Amplifier and read on the digital voltmeter.

The $InAs_xSb_{1-x}$ and $In_{1-x}Ga_xSb$ alloys had two contacts on opposite sides which were used as Hall probes. Since in practice, these two contacts could never be perfectly aligned, a resistivity voltage appeared between them without a magnetic field and a back-off system similar to the above was used here also. Thus the voltage observed with the Nanovolt Amplifier-digital voltmeter combination would be due to the Hall effect only. The InSb and GaAs specimens had two contacts on one side. One of these was used as a Hall probe along with the contact on the opposite side. These two were badly misaligned and a back-off system was used to cancel the resistivity voltage.

The observed Hall voltage may have a contribution due to magnetoresistance. This problem was solved by measuring both Hall effect and magnetoresistance for forward and reverse magnetic field directions. Since the Hall voltage reverses with field but the magnetoresistance voltage does not, any contribution of the latter to the former will cancel in the average of the two field directions.

The circuit diagram is shown in Figure (3,5). A twelve position double deck switch with silver contacts was used to minimize electrical noise. All wires from the control panel to the specimen were shielded and passed through a soft iron pipe to reduce electromagnetic pickup. In the old laboratory, a series of copper switches in an oil bath to reduce thermal voltages was used instead of the twelve position switch.

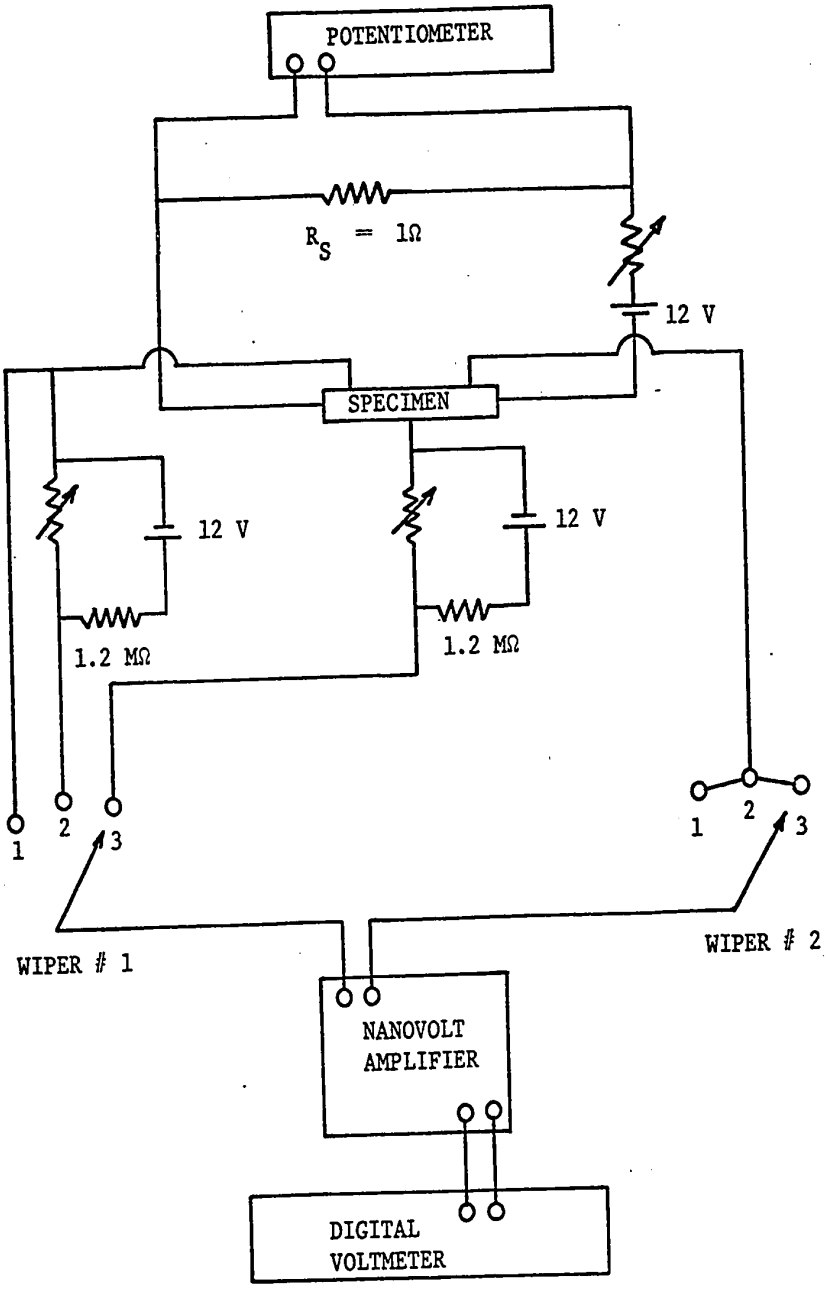

SWITCH FUNCTIONS:

1 RESISTANCE

2 MAGNETORESISTANCE

3 HALL EFFECT

FIGURE (3,5) HALL AND MAGNETORESISTANCE CIRCUIT

D) MAGNETOTHERMOELECTRIC POWER MEASUREMENTS.

These measurements were performed with an apparatus designed by the author and shown in Figure (3,6). The specimen was held in a horizontal position and contact with it was made through two insulated copper rods which were lowered onto it. A small wire heater was wound around one of the copper rods and the other acted as a heat sink. At the end of each rod, a length of copper-constantan thermocouple strip was glued so that these strips were in good contact with the specimen and each strip acted as the hot junction of a thermocouple. To improve the thermal contact with the specimen a small amount of indium was placed between the specimen and the thermocouple strip and a reasonable pressure applied by a screw adjustment of the copper rods. Separate cold junctions for each thermocouple were immersed in an oil bath at a known temperature so that the temperature of each end of the specimen could be determined independently and then the difference found. The thermoelectric e.m.f. between the ends of the specimen was measured across the two hot junctions leads of the thermocouples.

A temperature difference of approximately $2^{o}C$ was maintained between the ends of the sample by applying a regulated DC voltage to the heater with a Harrison Laboratories Constant Voltage Supply Model 6343A. The zero field thermoelectric power was observed and then nulled with the potentiometer on the Nanovolt Amplifier so that the change in thermoelectric power in a magnetic field could be measured accurately. Figure (3,7) illustrates the circuit diagram for these measurements.

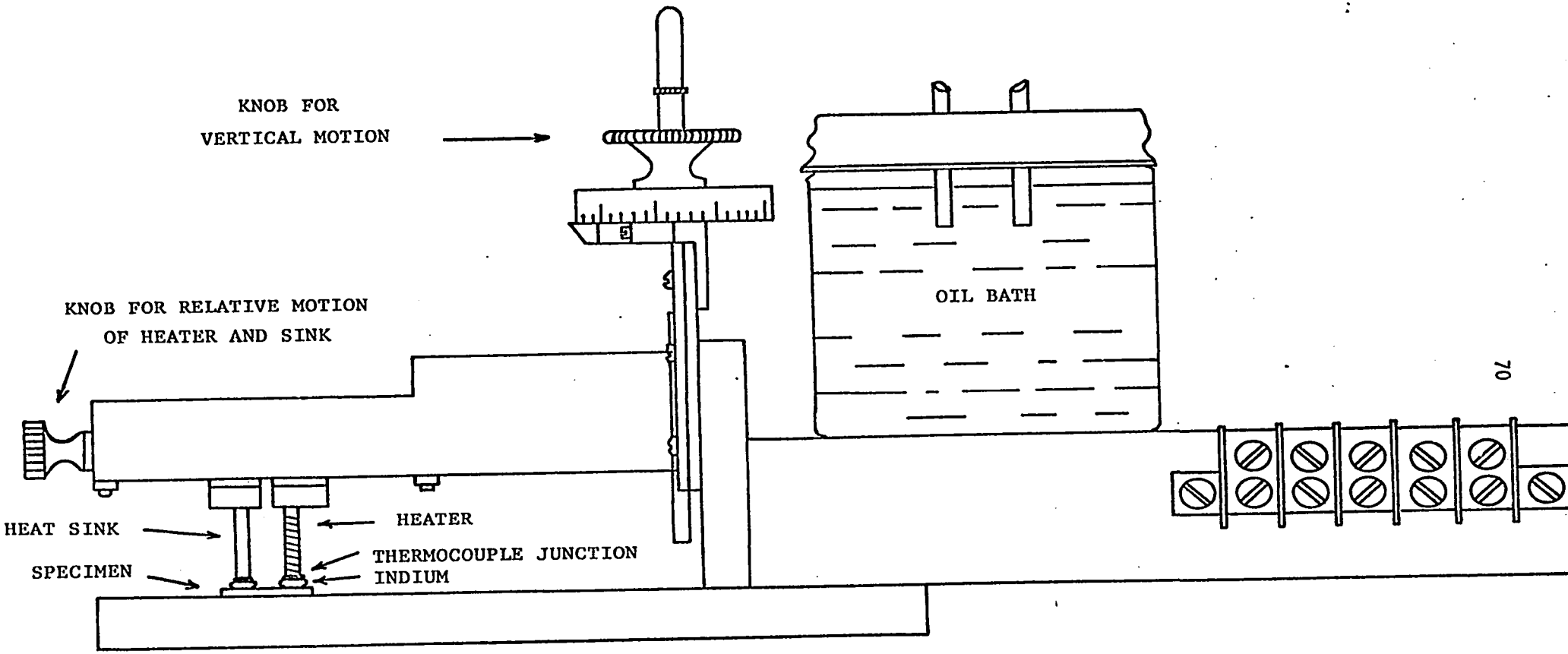

FIGURE (3,6) MAGNETOTHERMOELECTRIC POWER APPARATUS

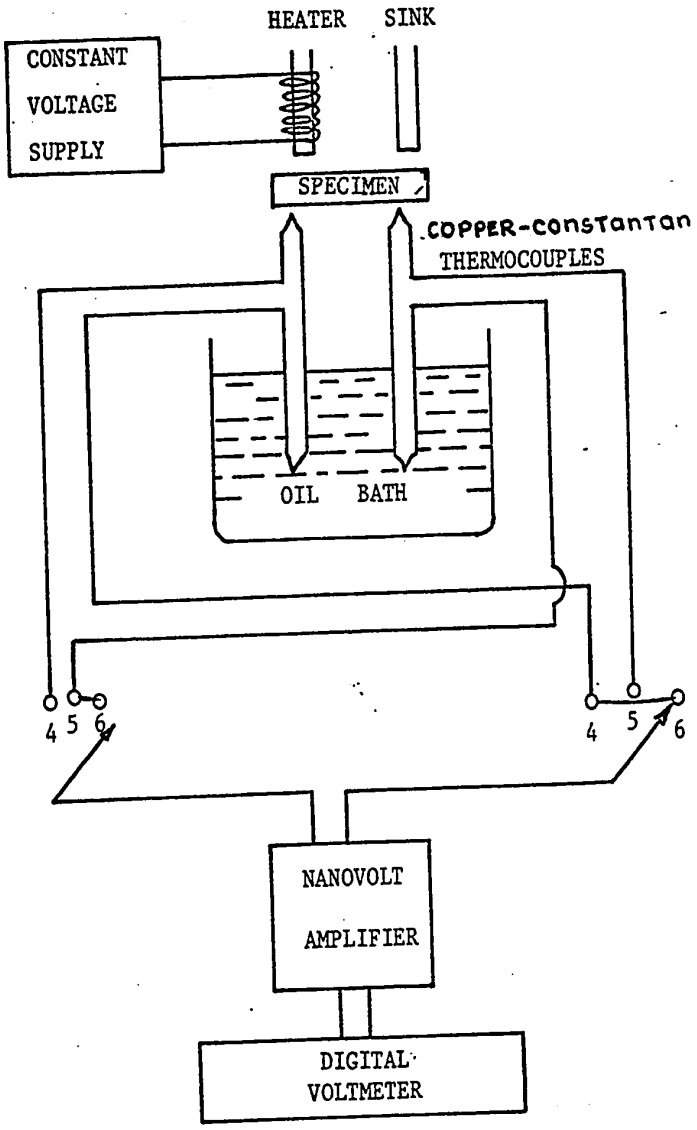

SWITCH FUNCTIONS

4 TEMPERATURE T_1

5 TEMPERATURE T_2

6 THERMOELECTRIC E.M.F.

FIGURE (3,7) MAGNETOTHERMOELECTRIC POWER CIRCUIT

CHAPTER IV

$InAs_xSb_{1-x}$ AND $In_{1-x}Ga_xSb$ ALLOYS

1. RESULTS

The results obtained with both the $InAs_xSb_{1-x}$ and $In_{1-x}Ga_xSb$ alloy systems will be presented in this chapter since the analyses are identical. Values of α_0, α_∞ and R_∞ (defined by equations (2,16), (2,17) and (2,18) were determined at room temperature for samples spaced over as wide a range in x as possible. For the $InAs_xSb_{1-x}$ system, results were obtained with x varying over the full range from 0 to 1, but for the $In_{1-x}Ga_xSb$ system, α_∞ could not be determined for $x > 0.87$. The reasons for this will be explained later.

The first step for both alloy systems involved the preparation of the material, followed by the cutting and lapping of a specimen to the desired size and shape as explained in the previous chapter. Then the Hall coefficient R was measured as a function of magnetic field. This variation is shown in Figure (4,1) for sample #8 of the $In_{1-x}Ga_xSb$ system. Over the observed range of magnetic fields (0 - 3.2 Wb/m^2), R never varied more than 5%, and as shown in the figure, R_∞ may easily be determined with a relative accuracy of less than 0.1%.

The thermoelectric power was also observed as a function of magnetic field. For most samples, practically complete saturation was

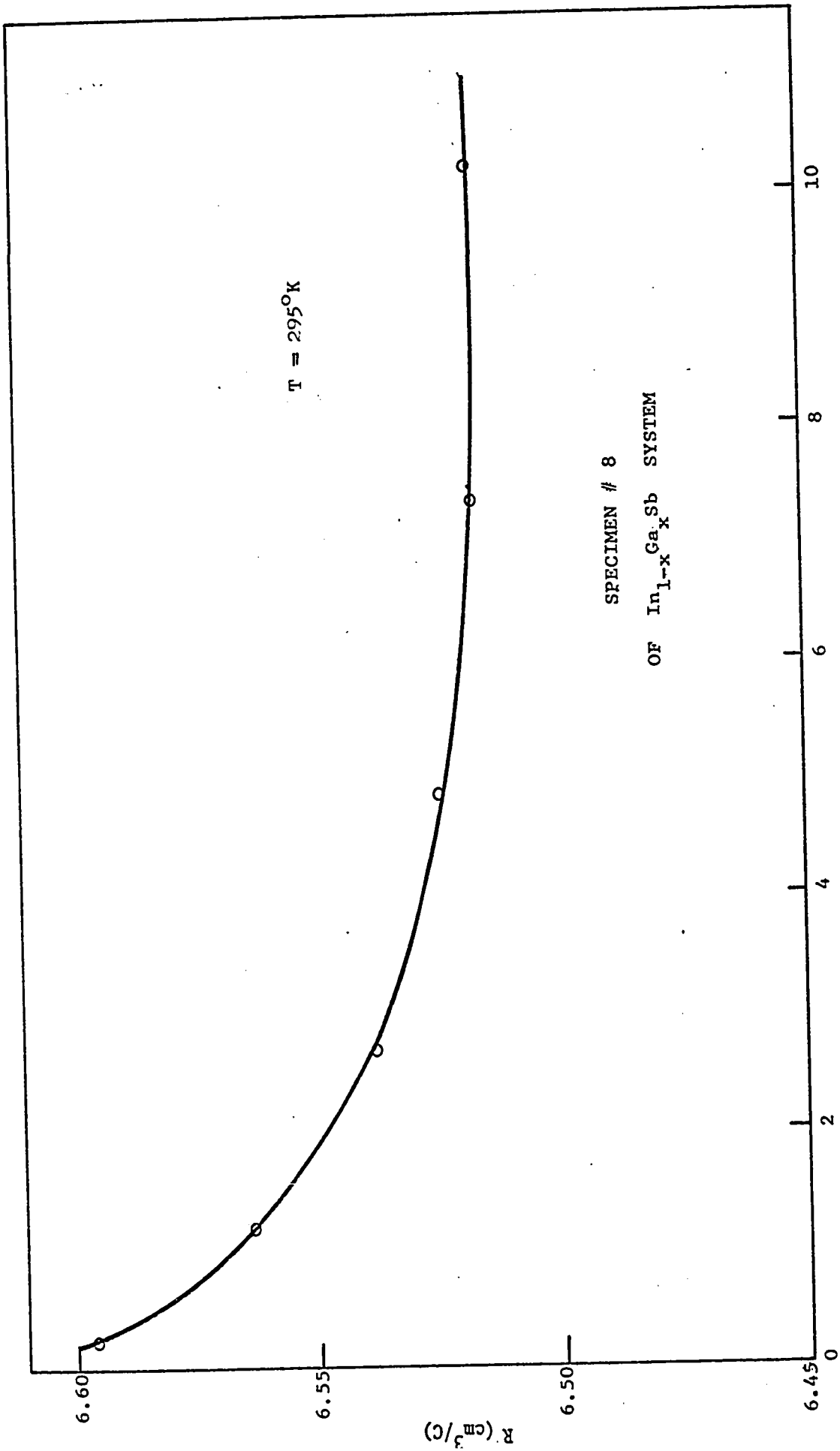

FIGURE (4,1) HALL COEFFICIENT VERSUS SQUARE OF MAGNETIC FIELD

obtained in the available magnetic fields, so that the value of α_∞ could easily be observed. Saturation requires $\mu B > 1$ and is illustrated by curve 1, Figure (4,2). For a few samples, however, α_B could only be seen to approach saturation (curve 2). Some of the least doped samples at or near the InSb end of the alloy systems did not exhibit saturation but diverged at higher fields (curve 3). It was concluded that quantum effects were responsible for the divergence. According to Anselm and Askerov (61A), the addition to α_0 arising from quantum effects is $\frac{k}{8e}\left(\frac{\hbar\omega}{kT}\right)^2$ where $\omega = \frac{eB}{m^*}$ is the cyclotron frequency. At 2 Wb/m^2, this contribution would be 2 $\mu V/^oK$ which is not too different from the observed effect.

To determine α_∞ from curves 2 and 3, it was necessary to use an empirical result of Shalyt (62S) who showed that for InAs

$$\Delta\alpha_B = \frac{A_1 B^2}{1 + A_2 B^2}$$

where A_1 and A_2 are constants and $\Delta\alpha_\infty$ is A_1/A_2. Hence if $B^2/\Delta\alpha_B$ is plotted as a function of B^2, a straight line of slope $1/\Delta\alpha_\infty$ should be obtained. Figure (4,3) shows that Shalyt's method produces straight lines for curves 1 and 2 of the previous figure and also for curve 3 before the onset of quantum effects. The same value for $\Delta\alpha_\infty$ is obtained with curve 1, whether it be taken from Figures (4,2) or (4,3). Thus it was always possible to determine $\Delta\alpha_\infty$ with the available magnetic fields.

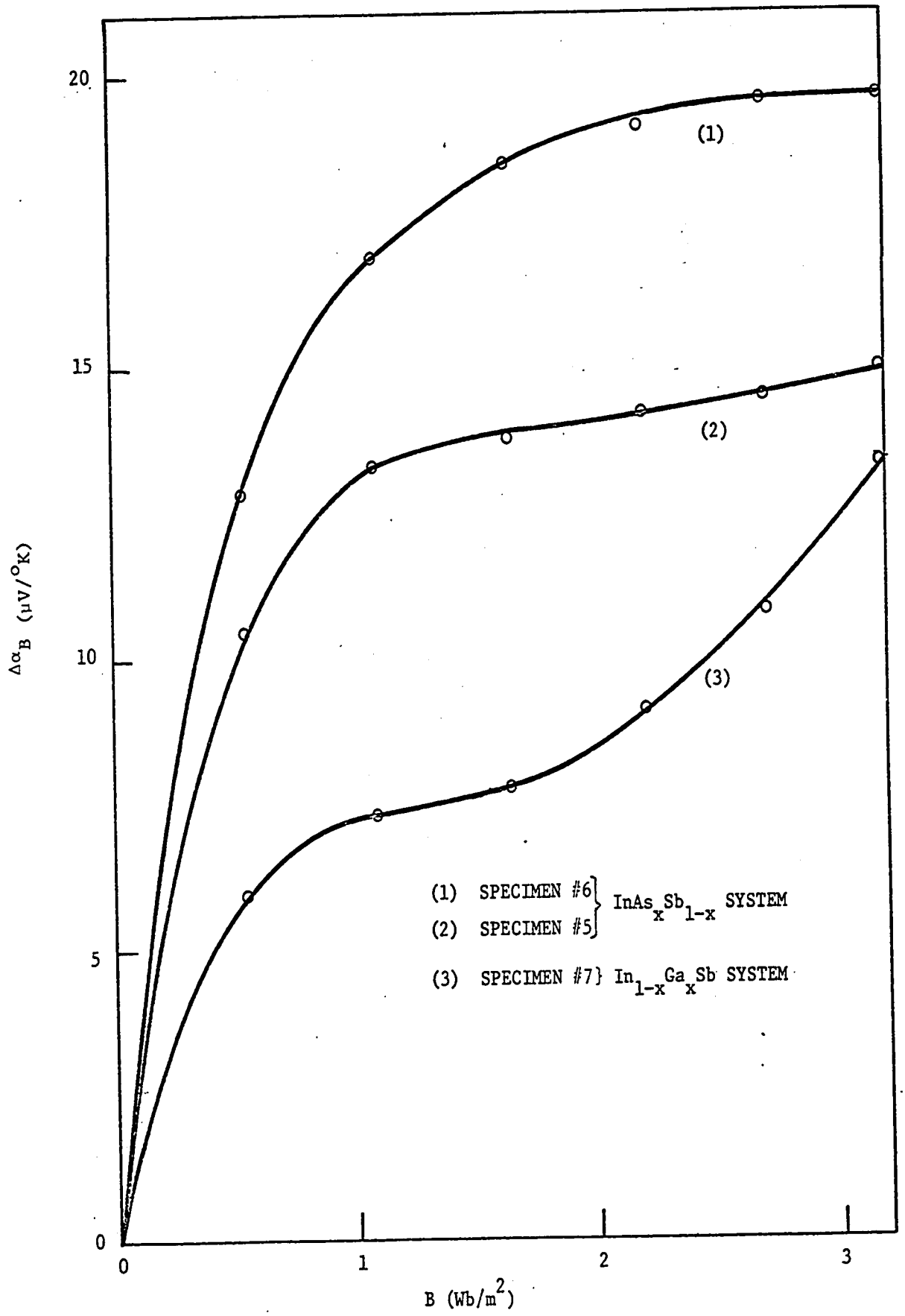

FIGURE (4,2) MAGNETIC FIELD DEPENDENCE OF THERMOELECTRIC POWER

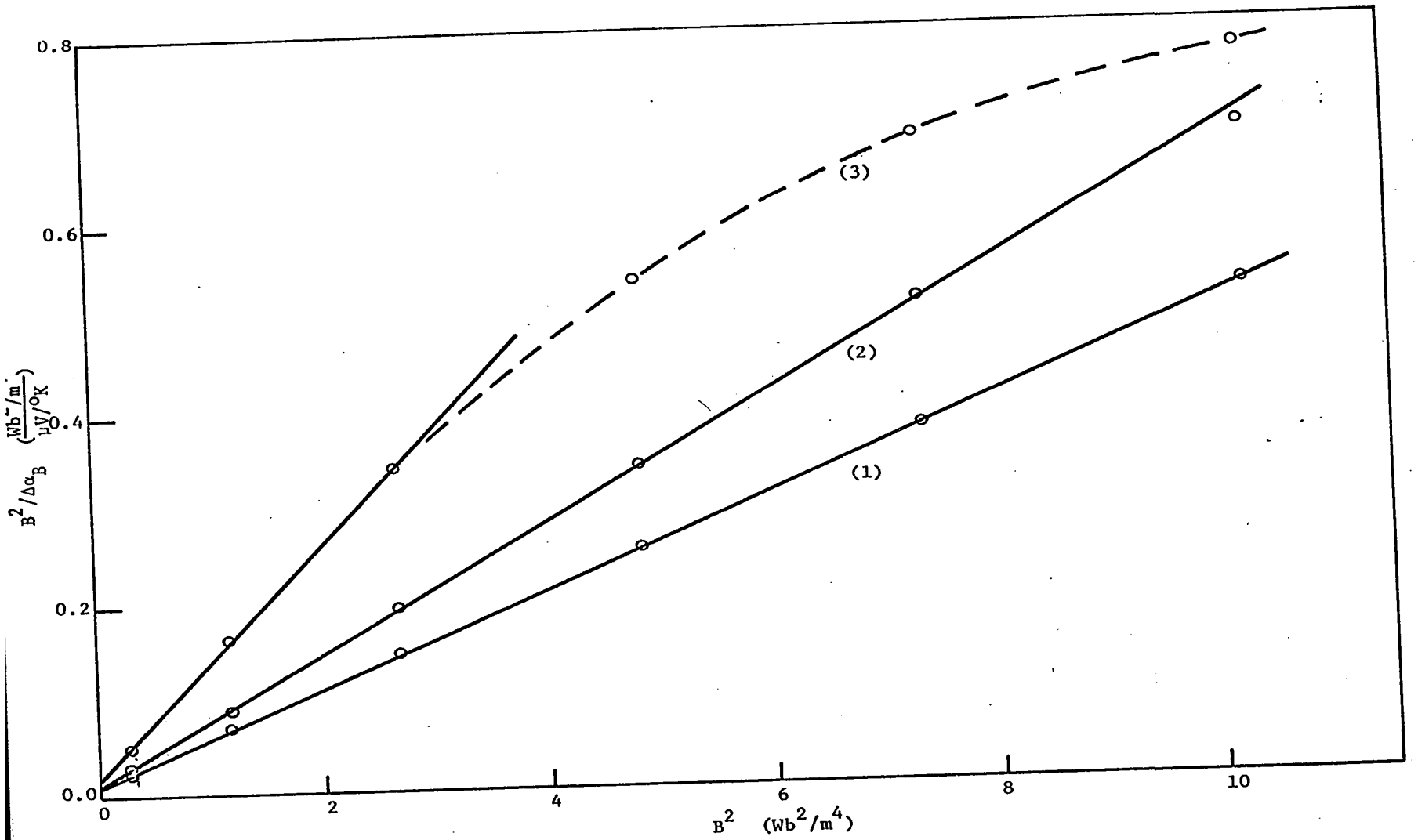

FIGURE (4,3) MAGNETIC FIELD DEPENDENCE OF THERMOELECTRIC POWER

TABLE (4,1)

DATA FROM THE $InAs_xSb_{1-x}$ ALLOYS

Specimen No.	x	α_o (μV/deg)	α_∞ (μV/deg)	R_∞ (cm^3/C)
1	0.000	281.7	290.0	189.7
2	0.000	189.7	181.3	40.62
3	0.000	260.1	265.8	129.3
4	0.055	287.6	304.1	224.2
5	0.140	248.4	263.3	139.2
6	0.275	218.5	238.2	95.92
7	0.400	181.3	200.4	54.53
8	0.400	183.2	204.9	55.22
9	0.480	201.4	220.5	70.69
10	0.580	199.0	207.7	62.12
11	0.710	192.9	201.4	53.30
12	0.840	214.9	216.0	55.18
13	0.870	183.0	180.2	29.58
14	0.880	177.0	173.6	28.82
15	0.915	192.2	186.2	31.57
16	0.960	264.3	256.3	80.80
17	0.985	227.4	222.1	51.88
18	1.000	356.0	357.0	268.0
19	1.000	237.0	232.0	54.00

TABLE (4,2)

DATA FROM THE $In_{1-x}Ga_xSb$ ALLOYS

Specimen No.	x	α_o (μV/deg)	α_∞ (μV/deg)	R_∞ (cm^3/C)
1	0.000	281.7	290.0	189.7
2	0.000	189.7	181.3	40.62
3	0.000	260.1	265.8	129.3
4	0.020	306.3	314.8	261.0
5	0.020	305.0	315.1	246.2
6	0.050	97.5	101.8	7.110
7	0.070	320.2	327.8	276.1
8	0.130	99.5	102.3	6.517
9	0.220	400.0	408.0	521.7
10	0.340	122.5	120.5	9.128
11	0.470	137.8	133.6	11.33
12	0.645	148.4	141.0	10.69
13	0.750	225.8	209.9	25.08
14	0.870	161.4	160.2	11.08

The results of the above measurements are summarized in Tables (4,1) and (4,2).

2. ESTIMATION OF EXPERIMENTAL ERRORS

Four main sources of error were present in the measurement of thermoelectric power with and without a magnetic field:

1. measurement of the e.m.f.
2. the thermoelectric power of copper
3. calibration of the thermocouple
4. imperfect thermal contact

The e.m.f. from the sample was fed into a preamplifier and then read on a four figure digital voltmeter. The error in this reading is estimated at less than .5%. When measuring the thermoelectric power of semiconductors, the second source of error is often ignored since metals have a very low thermoelectric power. Korenblit et al (64K) have taken this into account, stating that the thermoelectric power of copper is 1 $\mu V/^{o}K$. Here, most samples had a thermoelectric power greater than 200 $\mu V/^{o}K$ so that neglecting this effect introduces a .5% error. The calibration of the copper-constantan thermocouple was taken from standard references but impurities and strains can cause small deviations. The three sources of error just mentioned may be temporarily ignored, in view of the method used to deal with the error due to an imperfect thermal contact between specimen and thermocouple. This is by far the largest source of error and the most difficult to minimize. A calibration

of the apparatus was performed using the effective mass of InSb as a standard. The correct value was obtained when the thermoelectric power in an infinite magnetic field was increased by 5.0%. This correction factor was then applied to all measurements taken with this apparatus. It is estimated that deviations in the correction factor did not exceed 2% which would cause an error in the effective mass of less than 2%. Subsequent results for InAs, GaSb and also GaAs show this estimate to be valid. Inhomogeneities in the samples may also contribute to the scatter in the experimental points.

The carrier concentration was calculated from the Hall coefficient in a magnetic field. The latter as already mentioned could be determined with a relative accuracy of .1%. Themaximum error in the current was .01%. Most of the absolute error in the Hall coefficient however was due to that in the thickness of the sample which is estimated at .5%. Thus the error in the carrier concentration never exceeded .75%. Again errors due to inhomogeneity in the samples could be greater than this.

3. ANALYSIS

The Kane model could not be used in the analysis until it was decided which value to use for the E_0^* mentioned in Chapter II. It is known that E_0^* lies between E_0 and E_{00}, the intrinsic band gap values at the temperature of observation and at absolute zero respectively, i.e., E_0^* can be written as $E_0 + \Delta E_0$ where $0 < \Delta E_0 < (E_{00} - E_0)$. For InSb, it was shown (62Sa) that $E_0^* = 0.21$ eV, i.e., it is approximately

halfway between the values of E_0 and E_{00}. Furthermore, test calculations showed that the correction term ΔE_0 has little effect on the subsequent results. For example, a 50% change in the correction term caused less than 3% change in the resulting effective mass m_0^*. Hence, in the present work, ΔE_0 is arbitrarily chosen as $\frac{1}{2}(E_{00} - E_0)$, i.e., $E_0^* = \frac{1}{2}(E_{00} + E_0)$ for all cases. The values of E_0 have been taken from optical absorption data (64Wa) and the E_{00} values from Hall coefficient data (68C, 69C).

Another parameter involved in the Kane model was Δ, the valence band spin orbit splitting. This has not been determined for the alloys involved here, but electroreflectance data on similar alloys of this type indicate that Δ varies linearly with x (67T). Hence, a linear variation has been assumed between the known values for the compounds given below.

SPIN ORBIT SPLITTINGS		
InSb	0.82 eV	(66C)
InAs	0.38 eV	(67P)
GaSb	0.80 eV	(67C)

As above, small variations in Δ had little effect on subsequent results.

With values of E_0^* and Δ available, it was possible to proceed with the computations. When a Kane model (equation (2,12)) was substituted into the expressions for α_∞ and α_0 however, the integrals became too involved to solve analytically and hence were solved by numerical integration. These computations as well as those in the following chapters were performed on an IBM 360 computer. All programmes were written by the author and are listed at the end of the thesis.

First, the reduced Fermi level ζ was computed from equation (2,18) by combining an iterative procedure with numerical integration. Initially, ζ was set at -5, a value that was lower than the correct value for any specimen. Then followed a numerical integration by Simpson's rule with 2000 equal intervals between $\xi = 0$ and $\xi = 40$. (The quantity $\xi = E/kT$). At room temperature, $\xi = 40$ would give an electron an energy of about 1 eV. A negligible number of electrons would have an energy greater than this. The first and last terms were always several orders of magnitude smaller than the largest term which was situated near the centre of the 1 eV range. Test calculations with 1000 and 4000 terms over the same range showed that 2000 terms were more than sufficient for accurate results. The calculated value of the integral produced a value for α_∞ which was then compared with the experimental result. The initial calculated value was usually too high and Simpson's rule was applied again but with ζ increased by 1. This procedure was repeated until the calculated α_∞ was smaller than the experimental one. Then ζ was reduced by steps of .1 until the

calculated α_∞ was too large and so on until the smallest step was .001. Thus the reduced Fermi level corresponding to a measured α_∞ was known to .001 which is more accurate than is necessary considering the experimental error.

Then ζ was substituted into equation (2,19) to determine P^2. This calculation was done by numerical integration as described above. Then P^2 could be used in equation (2,8) to determine m_0^*/m.

Finally ζ was substituted into equation (2,17) to obtain the scattering parameter s. Again an iterative procedure was combined with a numerical integration as described above. The calculated values for ζ, m_0^*/m and s for the two alloy systems are summarized in Tables (4,3) and (4,4) and illustrated by Figures (4,4) to (4,7). The value of the Fermi level in itself is not interesting since it describes one particular sample only. It is required, however, for the determination of m_0^*/m and s. The results were good, being consistent with each other and with the existing literature. A discussion follows in the next section.

TABLE (4,3)

COMPUTED RESULTS FROM THE $InAs_xSb_{1-x}$ ALLOYS

Specimen No.	x	ζ	s	m_o^*/m
1	0.000	-0.28	0.50	0.0130
2	0.000	1.77	0.75	0.0133
3	0.000	0.17	0.60	0.0127
4	0.055	-0.45	0.44	0.0125
5	0.140	0.22	0.51	0.0113
6	0.275	0.72	0.51	0.0107
7	0.400	1.54	0.55	0.0104
8	0.400	1.43	0.51	0.0108
9	0.480	1.09	0.54	0.0108
10	0.580	1.29	0.61	0.0112
11	0.710	1.31	0.55	0.0133
12	0.840	0.87	0.53	0.0173
13	0.870	1.62	0.58	0.0192
14	0.880	1.78	0.59	0.0184
15	0.915	1.44	0.59	0.0202
16	0.960	0.08	0.53	0.0210
17	0.985	0.65	0.50	0.0213
18	1.000	-1.36	0.37	0.0221
19	1.000	0.46	0.48	0.0229

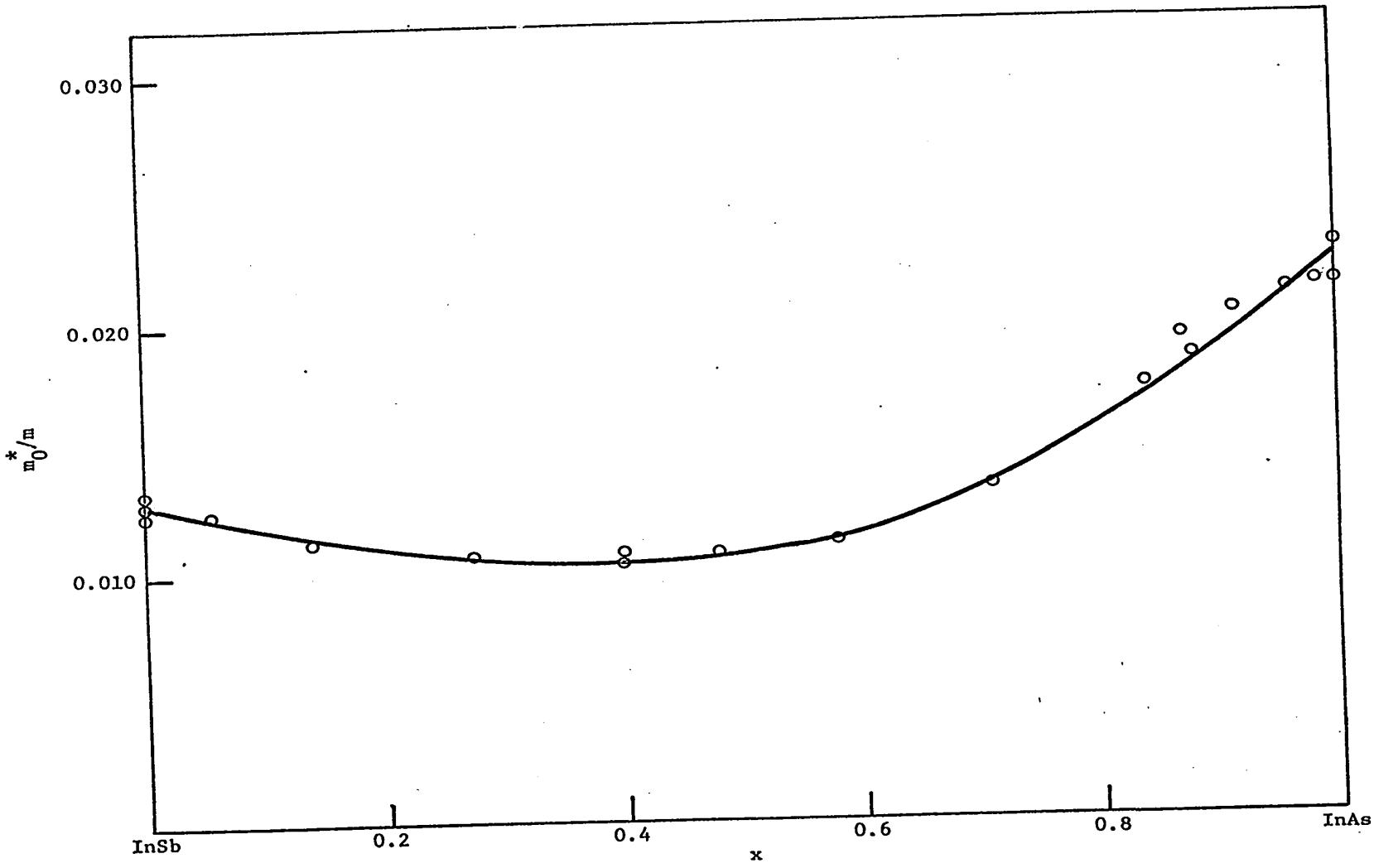

FIGURE (4,4) ELECTRON EFFECTIVE MASS IN $InAs_xSb_{1-x}$ ALLOYS

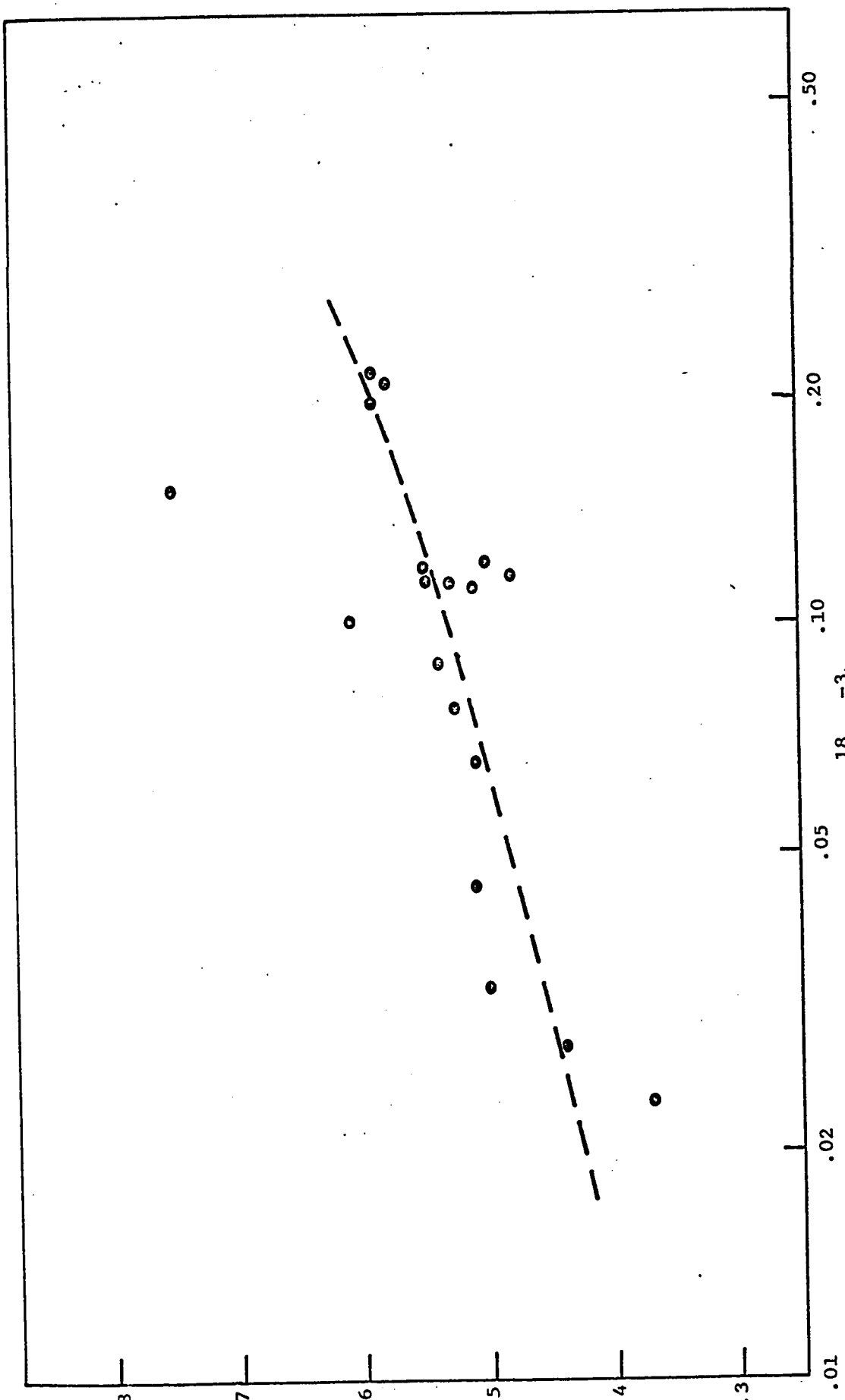

FIGURE (4,5) SCATTERING PARAMETER IN $InAs_xSb_{1-x}$ ALLOYS

TABLE (4,4)

COMPUTED RESULTS FROM THE $In_{1-x}Ga_xSb$ ALLOYS

Specimen No.	x	ζ	s	m_0^*/m
1	0.000	-0.28	0.50	0.0130
2	0.000	1.77	0.75	0.0133
3	0.000	0.17	0.60	0.0127
4	0.020	-0.60	0.53	0.0124
5	0.020	-0.60	0.51	0.0129
6	0.050	5.28	0.74	0.0141
7	0.070	-0.79	0.52	0.0135
8	0.130	5.14	0.75	0.0159
9	0.220	-1.87	0.46	0.0178
10	0.340	3.79	0.71	0.0196
11	0.470	3.07	0.66	0.0220
12	0.645	2.65	0.61	0.0275
13	0.750	0.83	0.58	0.0326
14	0.870	1.94	0.40	0.362

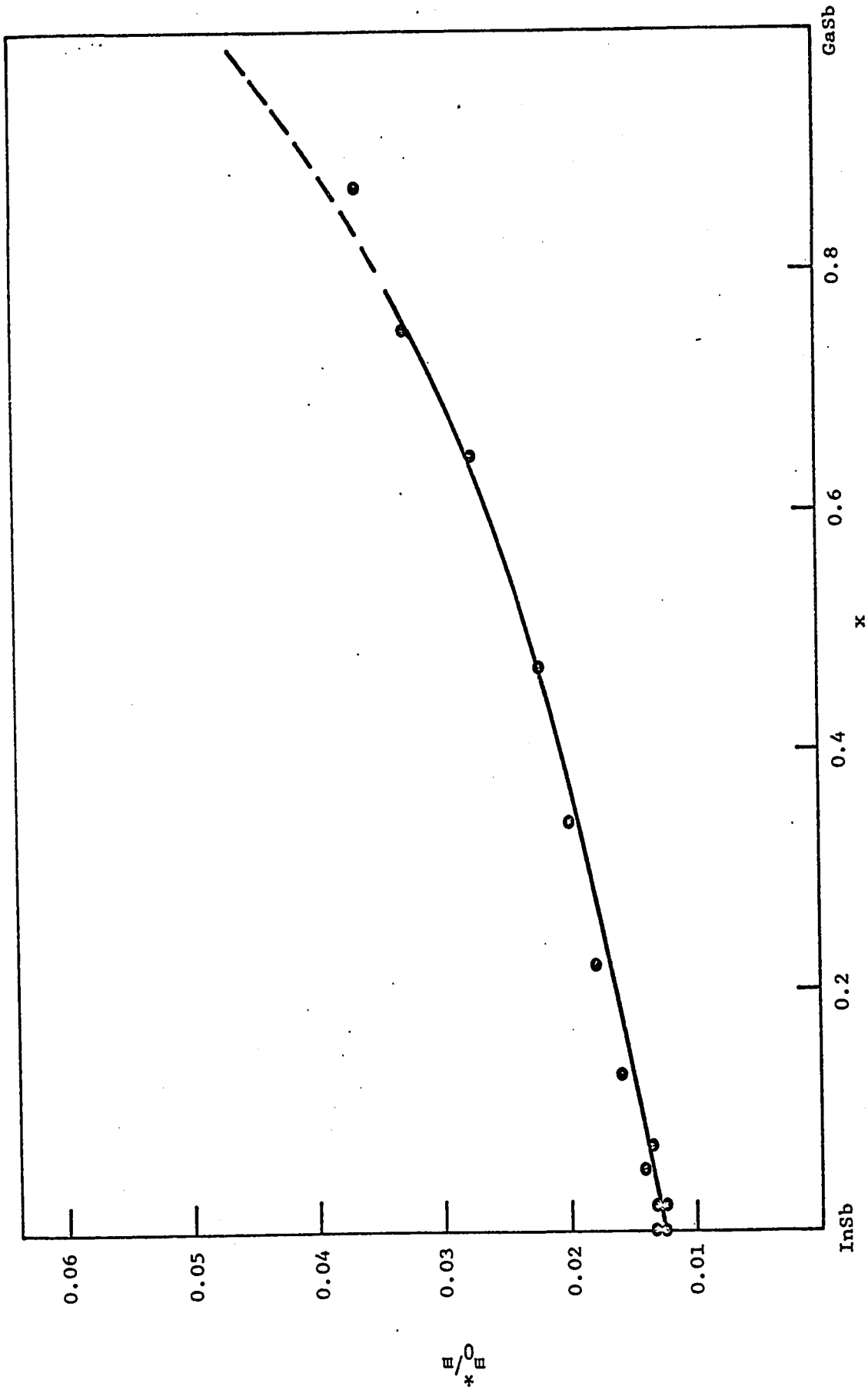

FIGURE (4,6) ELECTRON EFFECTIVE MASS IN $In_{1-x}Ga_xSb$ ALLOYS

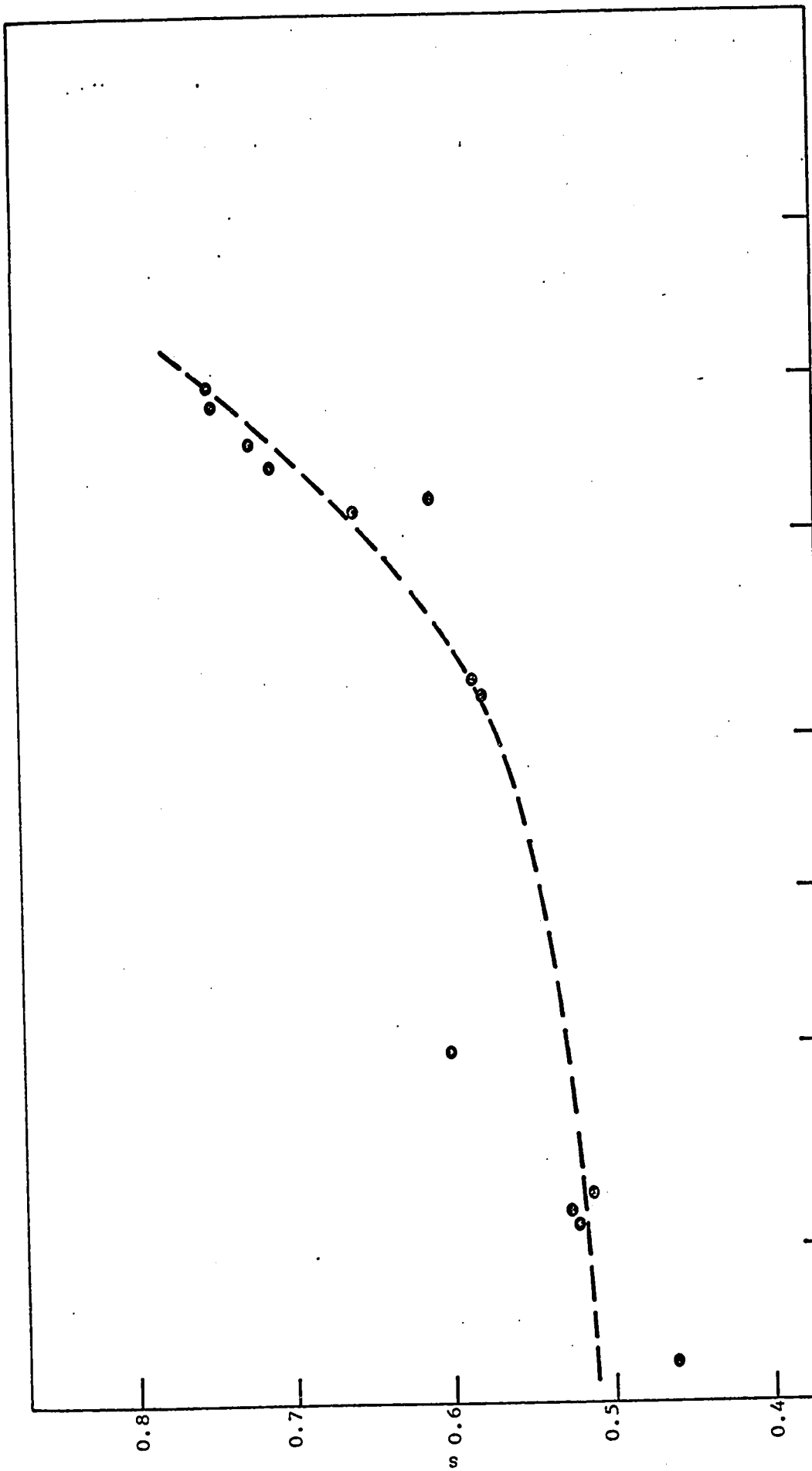

FIGURE (4,7) SCATTERING PARAMETER IN $In_{1-x}Ga_xSb$ ALLOYS

4. DISCUSSION

The combination of magnetothermoelectric power and Hall effect data led to the determination of m_0^*, the electron effective mass at the bottom of the (000) conduction band and the scattering parameter s as a function of composition for both alloy systems. It is noted that the effective mass values obtained for the compounds InSb (used as a standard), InAs and GaSb correspond very well with the already accepted values of Table (1,1). For the $InAs_xSb_{1-x}$ system, the curve of effective mass versus composition is parabolic with a shallow minimum of .010 m at approximately $x = .30$. The corresponding curve for the $In_{1-x}Ga_xSb$ system also has a parabolic behavior but the difference in the electron effective mass of the two compounds is large enough to prevent a minimum. Woolley and Thompson (64W) predicted a parabolic behavior for several III-V alloy systems including the two being discussed here by using a Kane model and the available data on band gaps at the Γ point. Since the matrix element P was not known, they assumed that $P^2 = 23$ eV for all compounds and alloys. This is not exactly true however. In work closely related to the author's, van Tongerloo and Woolley (68V) showed from Faraday rotation measurements that in the $InAs_xSb_{1-x}$ system, P^2 dips from the value of 21 eV for the two compounds to 18 eV at about $x = .40$. For this reason, the curve predicted by Woolley and Thompson has the correct shape but is slightly too low (68V). However, aside from an incorrect choice of P^2 and possibly of certain band gaps, their approach seems to be correct. The shape of the author's effective mass curves is consistent with their results.

The only previous experimental results were those of Potter and Kretschmar (64P) whose reflectivity and absorption measurements on thin films of $InAs_xSb_{1-x}$ indicated a monotonic increase of effective mass as x increased. However, the samples were highly doped and because of the Burstein shift, the optical absorption data gave higher values of optical energy gap than the correct instrinsic value E_0. Hence low effective mass values were obtained. This error being different for different samples, the deviation from linearity of the effective mass versus composition curve was not visible. Such an error did not occur in the author's results and the parabolic shape of the curve is clearly visible for both alloy systems.

The effective masses corresponding to the P^2 values obtained by van Tongerloo and Woolley are compared with the author's in Figure (4,8). The two curves coincide within experimental error. Figure (4,9) shows the author's effective mass results for the $In_{1-x}Ga_xSb$ system as well as those obtained from Faraday rotation and infrared reflectivity measurements in this laboratory (69A). Once again, the curves agree within experimental error.

The samples used in the thermoelectric power measurements were doped highly enough so that hole conduction could be ignored but not enough to cause any deformation in the conduction band or to have two conduction band phenomena. The latter effect did occur, however, near the GaSb end of the $In_{1-x}Ga_xSb$ system since the <111> band of GaSb is only .08 eV above the (000) band. Electrons in the upper band have

a mobility of less than .1 m^2/volt sec (66H) so that the saturation condition ($\mu B > 1$) would only be attained if B were greater than 100,000 gauss (10 Wb/m^2). This is why saturation could not be observed in the available magnetic fields for $x > .87$. The <111> band minimum of InSb, however, is at least .40 eV above the (000) band minimum as will be shown later. The samples were not doped highly enough to populate this band to any extent. Similarly in InAs, the <111> band minimum is .62 eV above the (000) band minimum (68K) thus avoiding the possibility of two band conduction.

The observed values of s only vary from .4 to .75 because of the relatively small range of carrier concentrations. Nevertheless, one can see that at the lower carrier concentrations s is approximately $\frac{1}{2}$ but tends towards $\frac{3}{2}$ for the more highly doped samples (Figures (4,5) and (4,7)). The value $s = \frac{3}{2}$ would indicate ionized impurity scattering which is reasonable for highly doped samples. However $s = \frac{1}{2}$ corresponds to either piezoelectric scattering or optical phonon scattering. Korenblit et al (64K) found that $s \simeq \frac{1}{2}$ for low n in InAs at $95^{\circ}K$ and attributed this to piezoelectric scattering. Ehrenreich (57E, 59E) has shown that polar scattering by optical phonons dominates in InSb, InP and InAs from $200^{\circ}K$ to $500^{\circ}K$. He dismisses the importance of piezoelectric scattering in these compounds above $100^{\circ}K$. We then conclude that in the samples measured here at room temperature ($295^{\circ}K$), namely InSb, InAs and the alloy systems $InAs_xSb_{1-x}$ and $In_{1-x}Ga_xSb$, the dominant scattering mechanism is that by optical phonons. In discussing this type of scattering however, Chapter I noted that a

relaxation time could only be defined at "high" temperatures for these compounds, i.e., at temperatures such that $kT > \hbar\omega$ where $\hbar\omega$ is the phonon energy. Table (1, 2) shows that for longitudinal optical vibrations, this condition is just satisfied at room temperature for InSb but for InAs and GaSb, one would have to go to approximately $50^{o}K$ above room temperature. Since values near $\frac{1}{2}$ were observed in these compounds and in the two alloy system it is suggested that the temperatures in Table (1,2) are slightly too high. This point will be discussed more fully in the chapter dealing with the GaAs results.

Since alloy scattering corresponds to an s value of $-\frac{1}{2}$, and no sample gave an s value less than $+ .3$, it is clear that this mechanism is unimportant in the two alloys systems that were measured. These results are consistent with the mobility measurements on $In_{1-x}Ga_xSb$ alloys (60I). As mentioned in Chapter I, Tietjen and Weisberg (65T) calculated the effect of alloy scattering in several alloys of III-V compounds and found that the largest effect of alloy scattering would be found in $In_{1-x}Ga_xAs$ alloys. For high values of x, alloy scattering could account for 40% of the total effect. Magnetothermoelectric measurements on this system would thus be of interest.

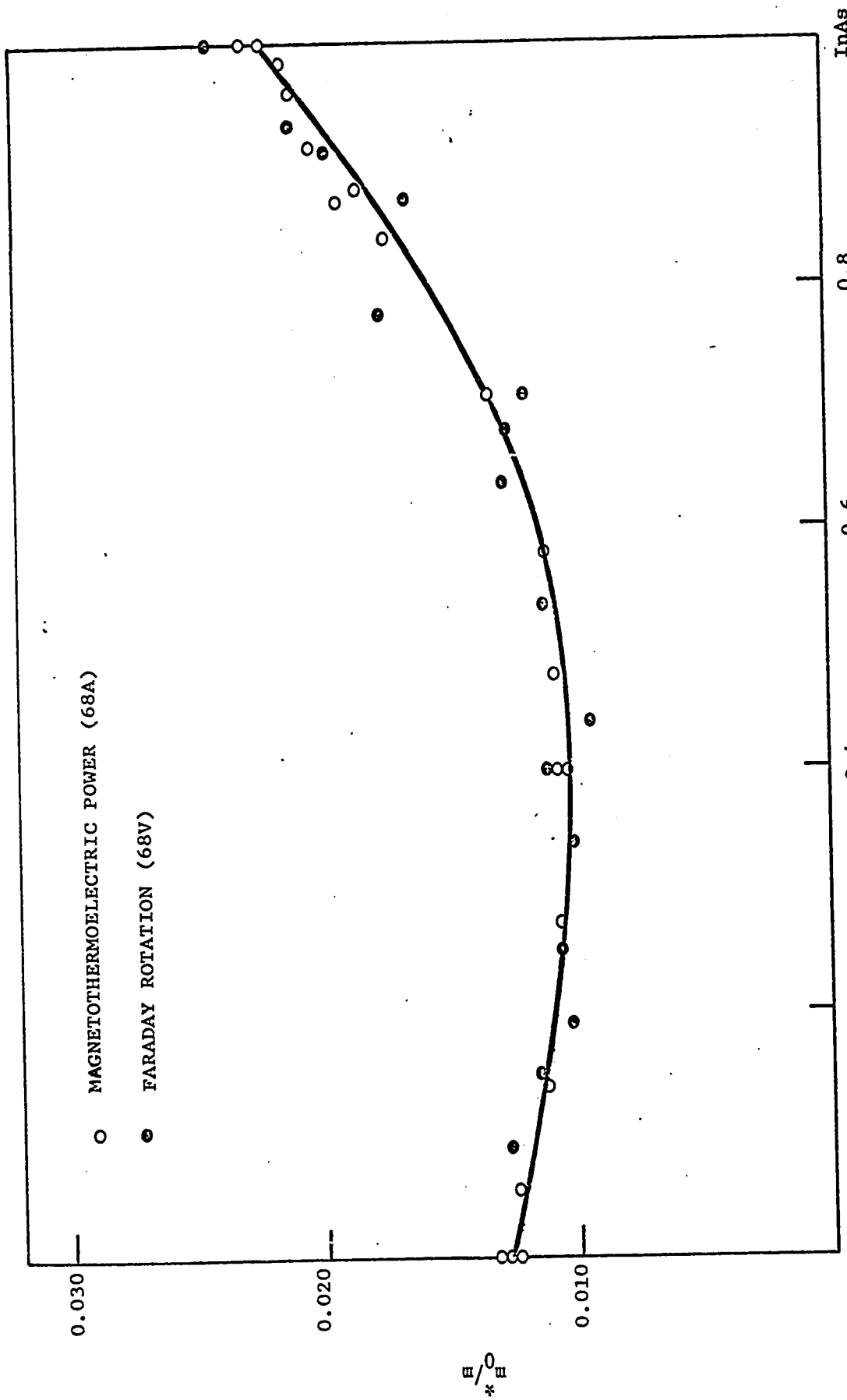

FIGURE (4,8) ELECTRON EFFECTIVE MASS IN $InAs_xSb_{1-x}$ ALLOYS

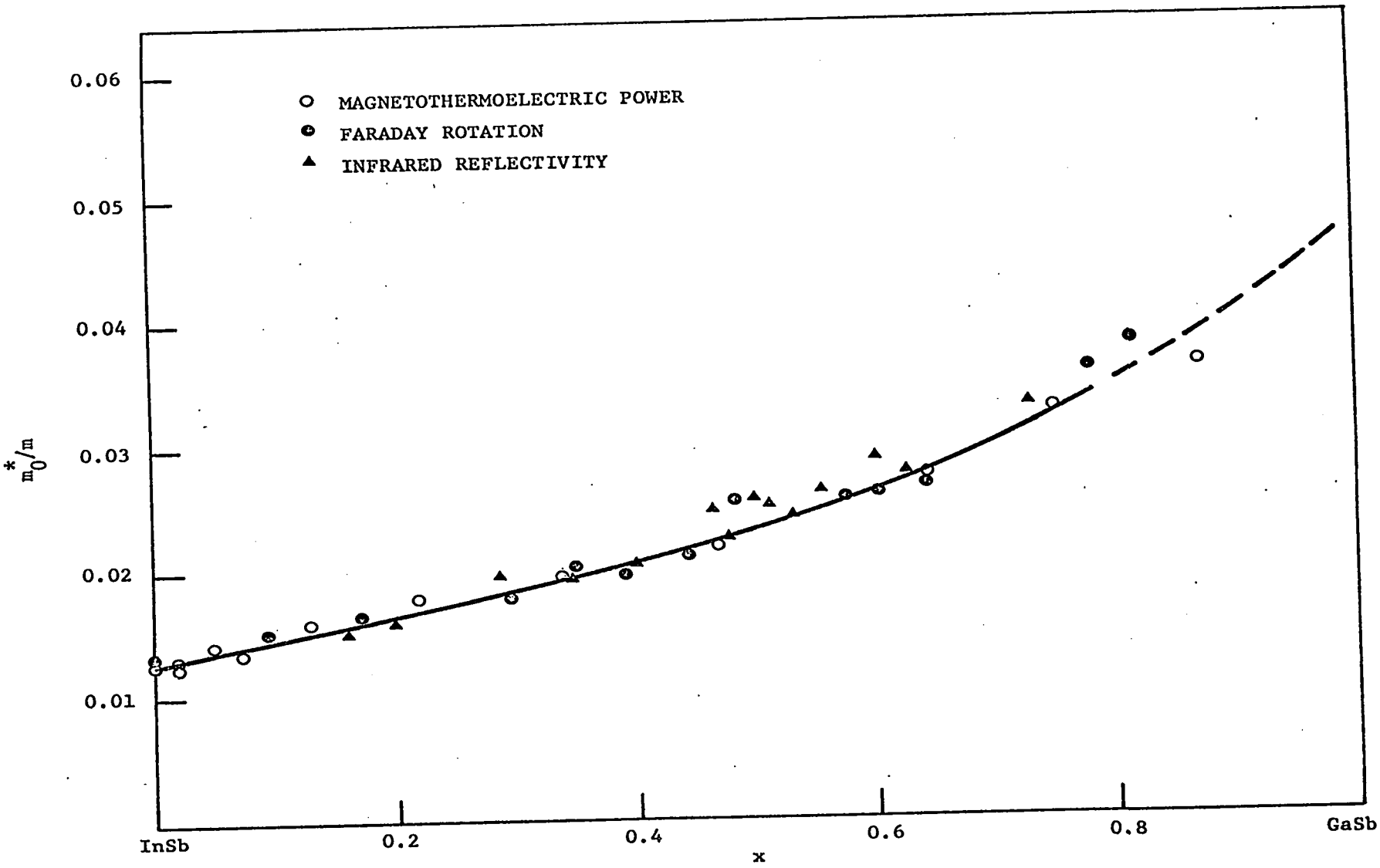

FIGURE (4,9) ELECTRON EFFECTIVE MASS IN $In_{1-x}Ga_xSb$ ALLOYS

CHAPTER V

GaAs SINGLE CRYSTALS

1. RESULTS

The magnetoresistance and Hall coefficient of single crystals of GaAs were measured as a function of magnetic field at room temperature. The samples were n type, being doped with Te or Sn, the electron concentration varying from 10^{16} to 10^{18} cm^{-3}. For these experiments, the crystallographic orientation of the samples was ignored, so that spherical constant energy surfaces will be assumed in the analysis of the data.

First the resistivity ρ_0 in the absence of a magnetic field was determined using the arrangement of Figure (3,3b). Then the magnetoresistivity $\Delta\rho$ was measured as a function of magnetic field B. This yielded a plot of $\Delta\rho/\rho_0$ versus B as shown in Figures (5,1) and (5,2) for samples 1 and 5 respectively. The back-off voltage method described in Chapter III allowed accurate determinations of $\Delta\rho/\rho_0$. Then the Hall coefficient R was measured as a function of magnetic field e.g. Figure (5,3). By extrapolating to zero field, a value for R_0 was obtained. This led to a plot of $\Delta R/R_0$ as shown in Figures (5,4) and (5,5). Due to the uncertainty in R_0, the quantity $\Delta R/R_0$ was much less accurate than $\Delta\rho/\rho_0$ since one cannot back-off the zero field Hall coefficient, whereas it is easy to back-off the zero field resistivity voltage. Since $\Delta R/R_0$ is small, the choice of R_0 is extremely critical and large

errors in ΔR may occur. This is why these experiments were performed only for the least doped samples where ΔR is reasonably large. For the highly doped samples, ΔR is barely detectable. The purpose of these experiments was to plot $R_0/\Delta R$ versus B^{-2}. Reasonable straight lines were obtained e.g.Figure (5,6) The magnetoresistivity ratio $\Delta\rho/\rho_0$ is independent of the dimensions of the sample and depends only on the measured voltages. The absolute error in this ratio may go as high as 2% when the magnetoresistance signal is very low but is generally less than 1%.

Along with experimental data, Figures (5,1), (5,2), (5,4) and (5,5) show theoretical curves for different values of s. These will be discussed later. It was found that a straight line was obtained when $\rho_0/\Delta\rho$ or $R_0/\Delta R$ was plotted versus B^{-2} as shown by Figure (5,6). The vertical intercept represents $\rho_0/\Delta\rho_\infty$ or $R_0/\Delta R_\infty$ where the subscript denotes the value in an infinite magnetic field. Table (5,1) summarizes the above results for 12 samples of GaAs arranged in ascending order of carrier concentration. For the 5 most highly doped samples, the variation of the Hall coefficient with magnetic field was too small to measure with reasonable accuracy. Thus R_0 and R_∞ are listed as identical numbers for these samples.

2. ANALYSIS

Since $R_\infty = -\frac{1}{ne}$, it is a simple matter to compute the carrier concentration n. The latter may then be used to determine the

TABLE (5,1)

MEASURED PARAMETERS OF GaAs AT 295°K

Specimen No.	Dopant	ρ_0 ($\times 10^{-6}$ ohm m)	R_0 (cm^3/C)	R_∞ (cm^3/C)	$\rho_0/\Delta\rho_\infty$	$R_0/\Delta R_\infty$
1	Sn	1806.0	818.6	802.9	.506	52
2	Sn	400.3	145.4	141.0	3.806	33
3	Sn	145.5	50.60	48.58	8.039	25
4	Te	46.29	17.63	17.22	12.40	43
5	Te	33.28	11.20	10.94	12.42	43
6	Te	23.55	7.465	7.313	14.68	49
7	Sn	23.05	6.155	6.086	15.55	90
8	Sn	9.792	1.979	1.979	33.66	
9	Te	7.868	1.935	1.935	45.64	
10	Te	6.525	1.540	1.540	69.37	
11	Te	5.383	1.125	1.125	75.60	
12	Te	4.330	.789	.789	82.00	

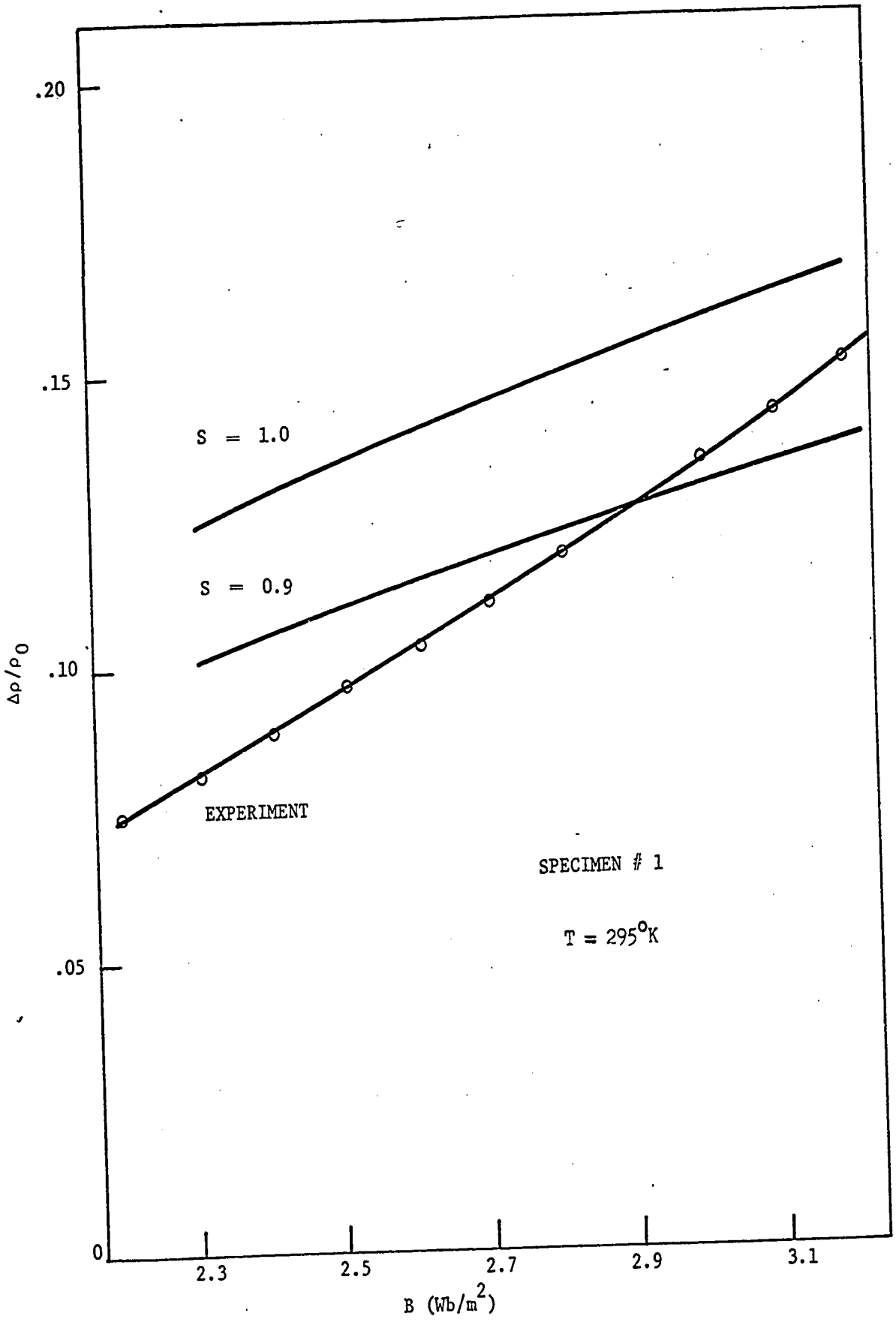

FIGURE (5,1) MAGNETORESISTIVITY OF GaAs

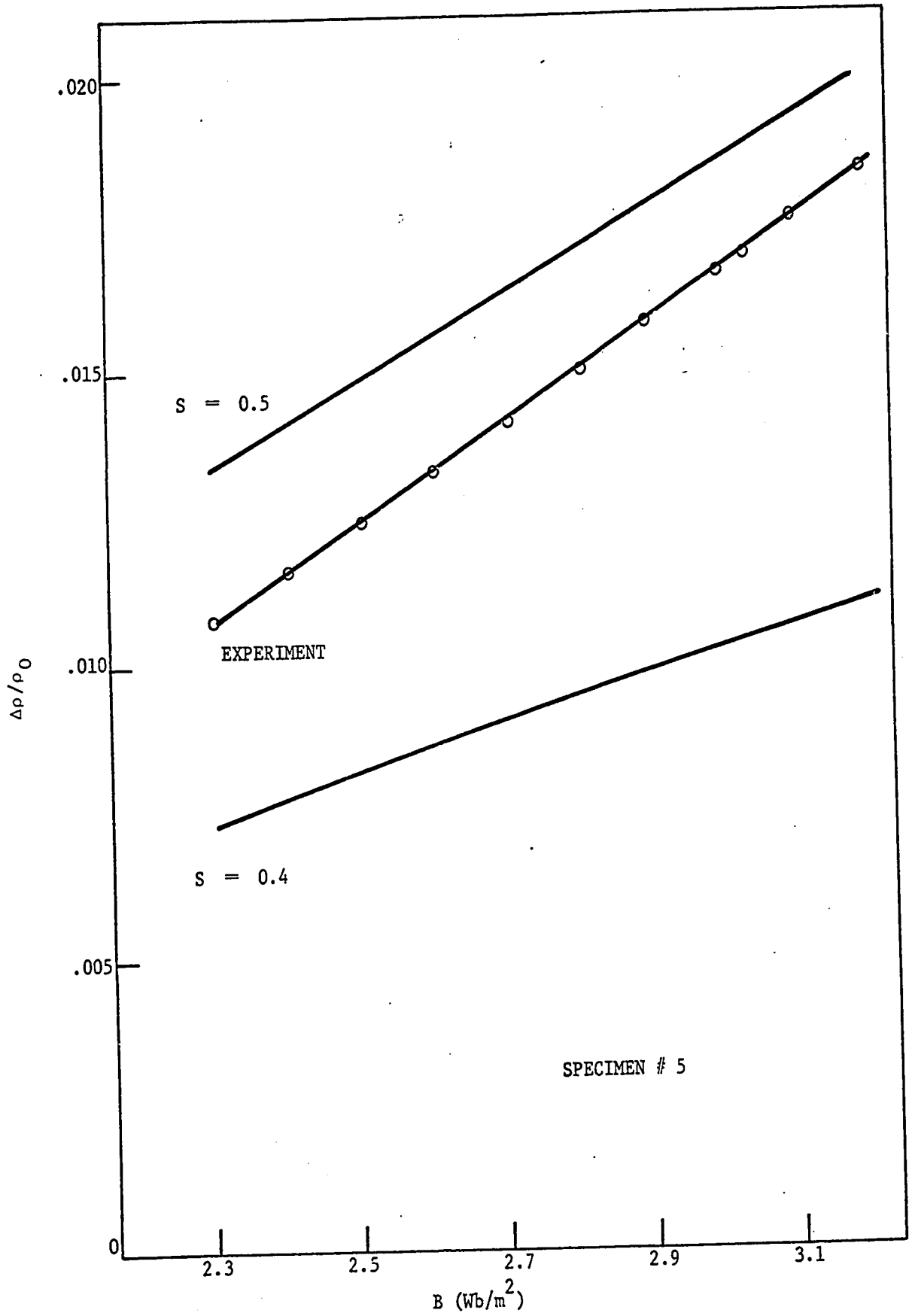

FIGURE (5,2) MAGNETORESISTIVITY OF GaAs

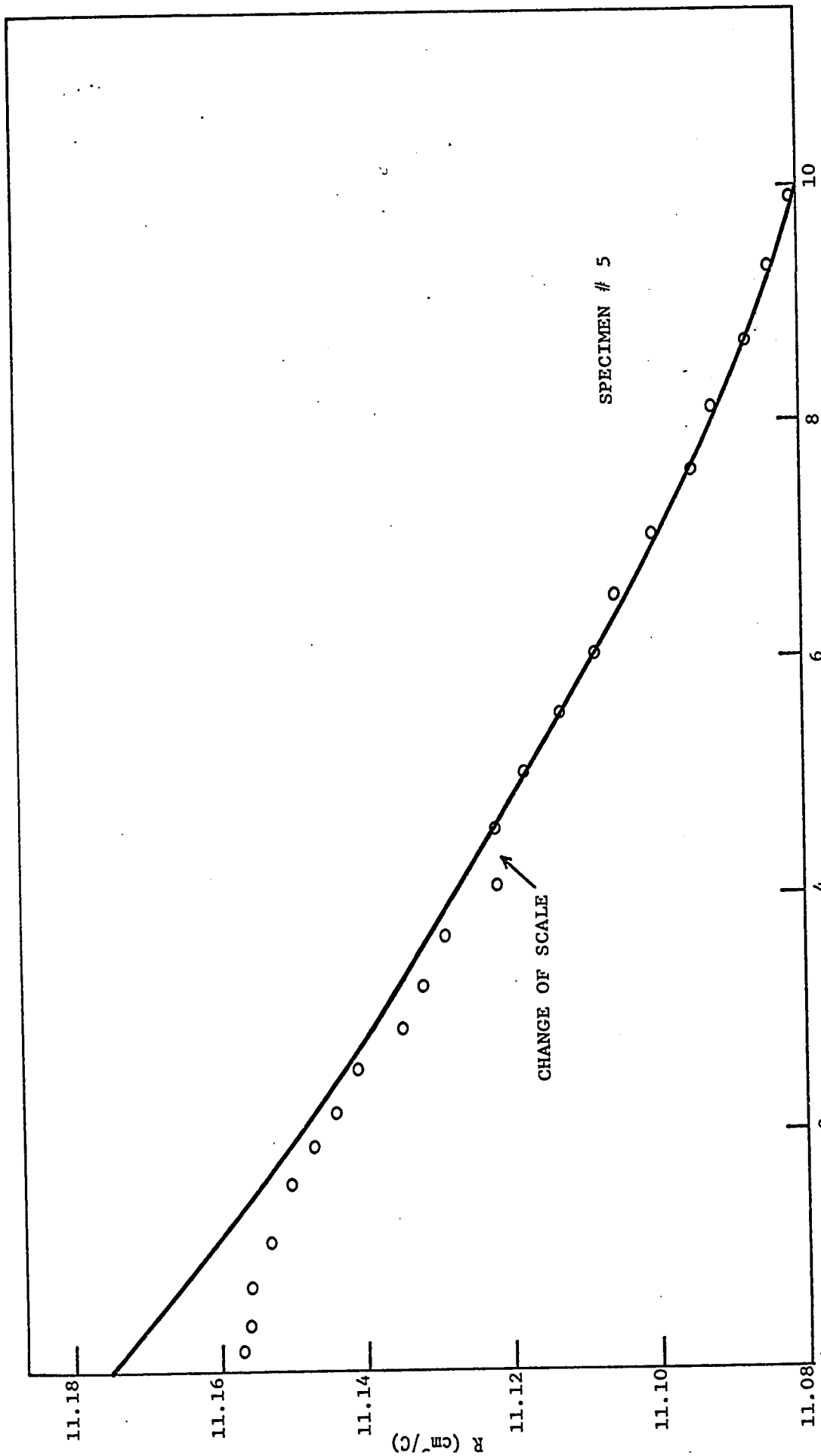

FIGURE (5,3) HALL COEFFICIENT VERSUS B^2 IN GaAs

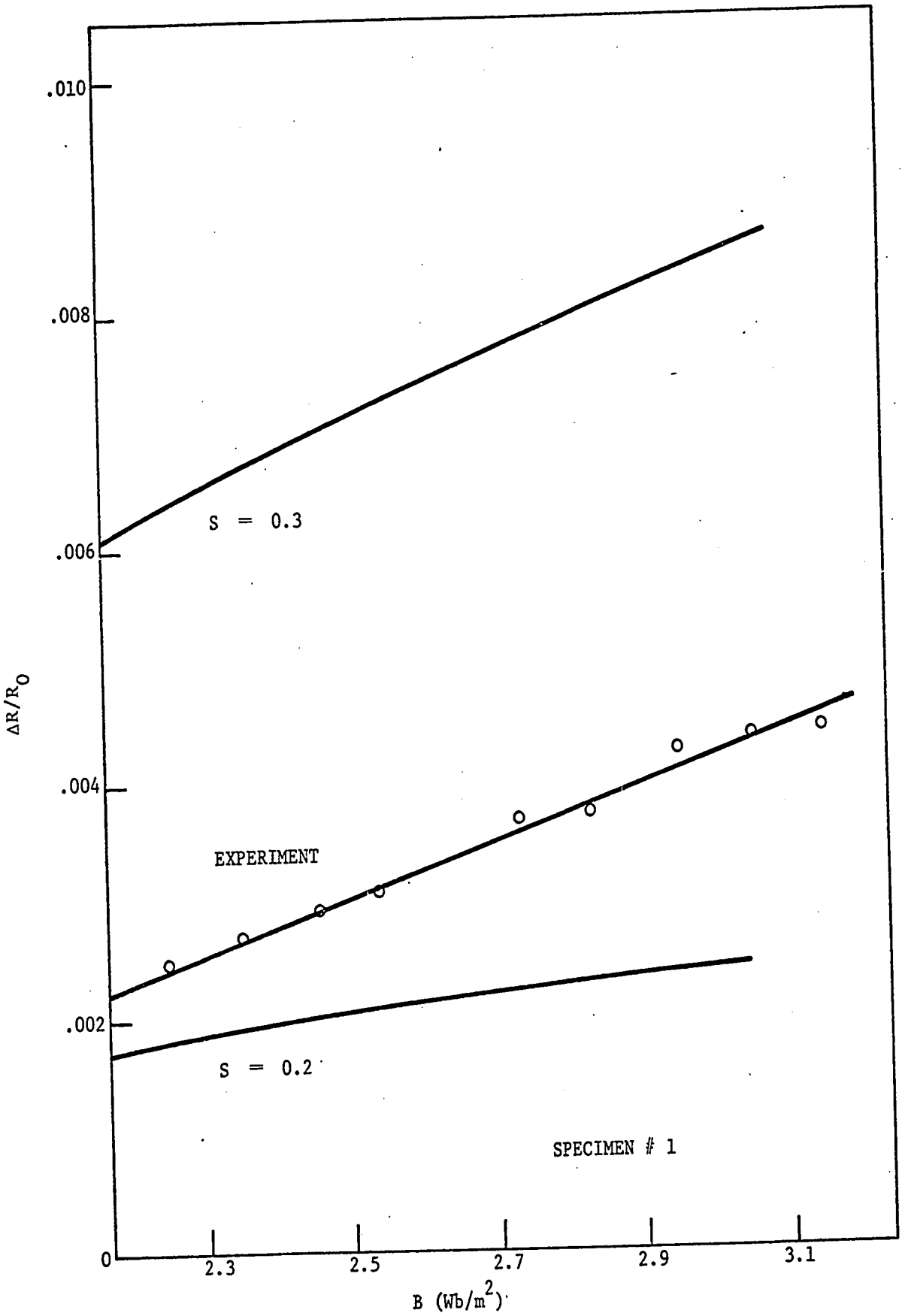

FIGURE (5,4) CHANGE OF HALL COEFFICIENT VERSUS B IN GaAs

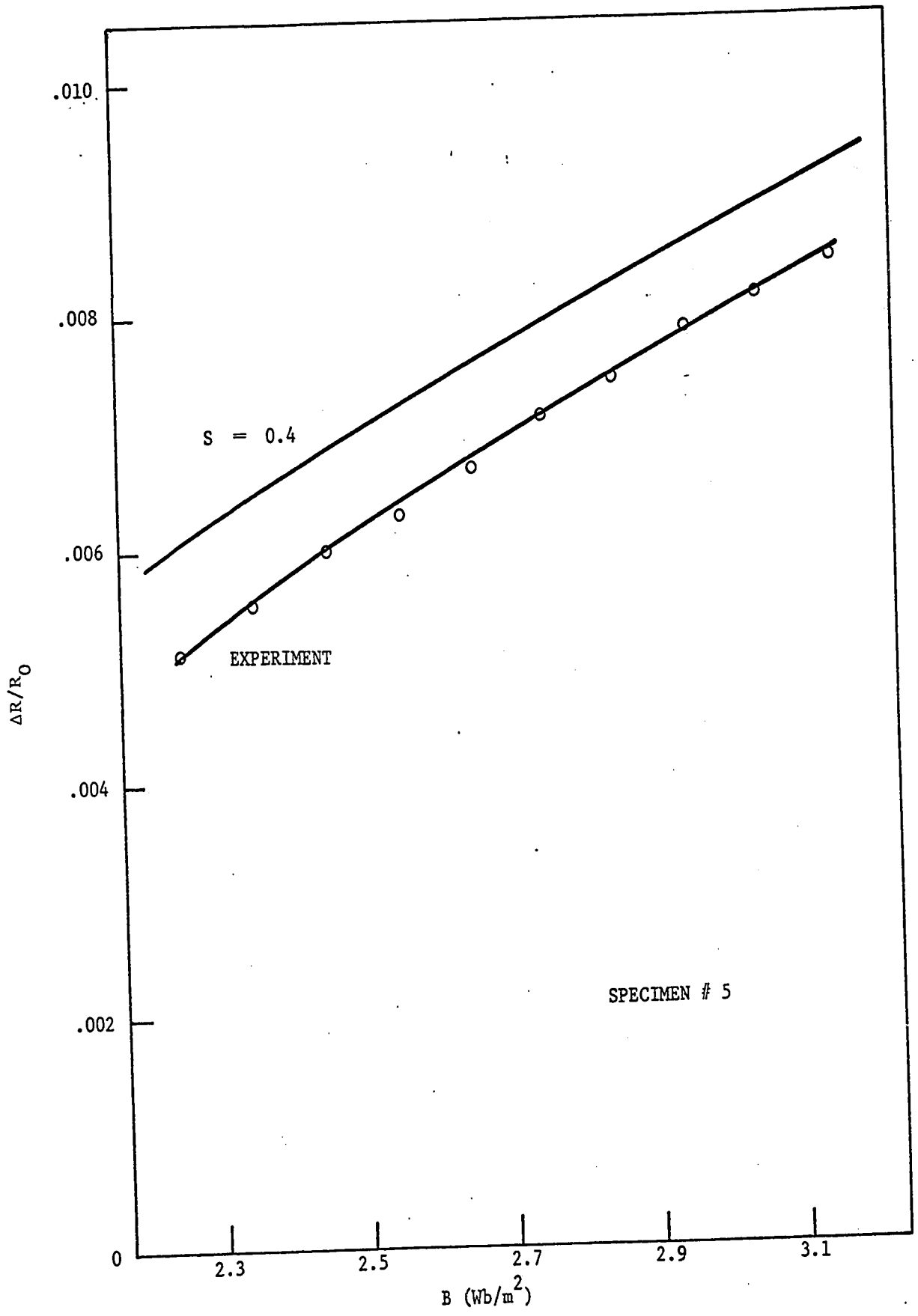

FIGURE (5,5) CHANGE OF HALL COEFFICIENT VERSUS B IN GaAs

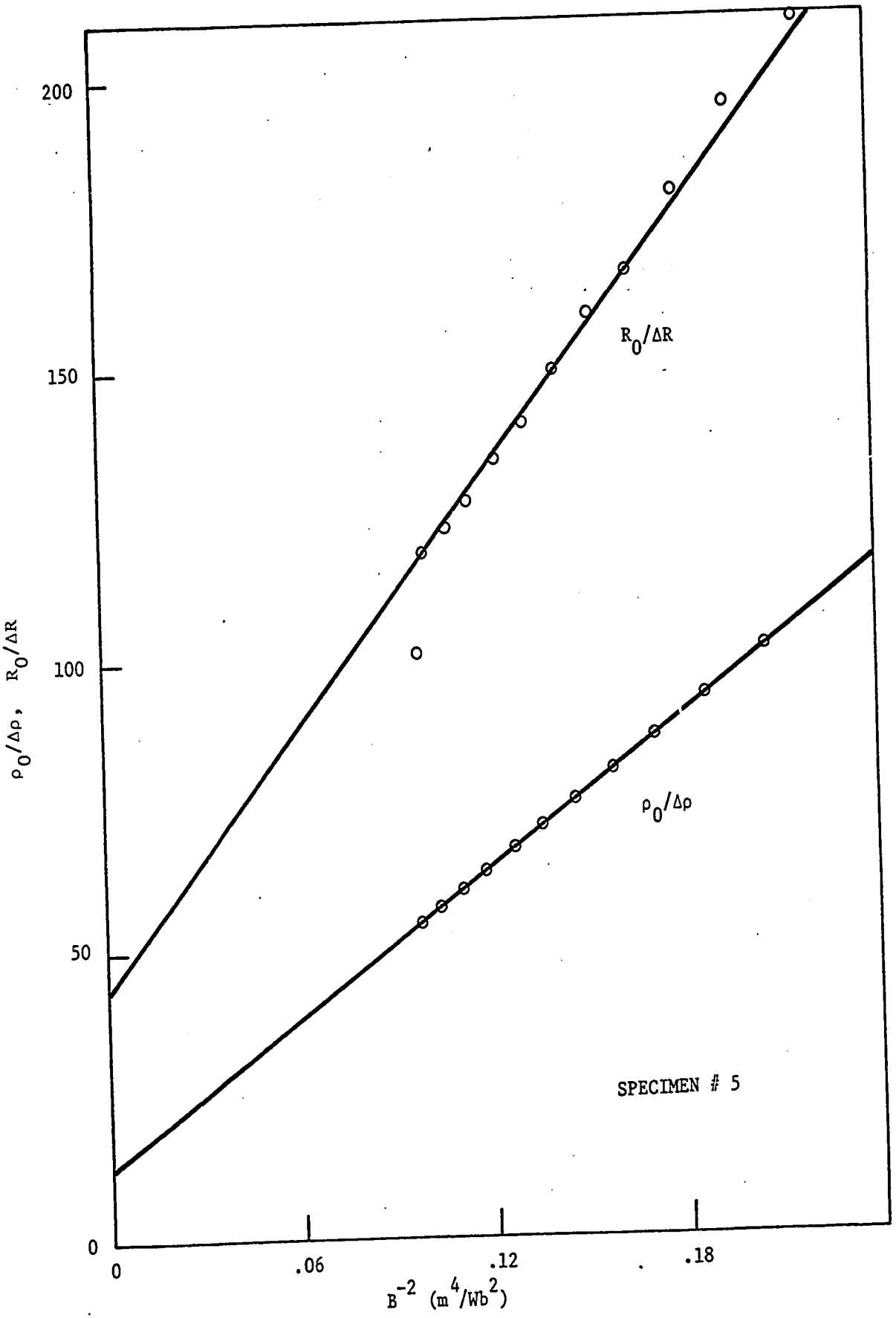

FIGURE (5,6) $\rho_0/\Delta\rho$ AND $R_0/\Delta R$ VERSUS B^{-2} IN GaAs

Fermi level, according to equation (2,15). To perform this calculation, a Kane model was assumed, with the energy-wave vector relation being given by equation (2,11). The effective mass m_0^* at the bottom of the conduction band was assumed to be .072 m and the energy gap 1.41 eV. A computer programme was used which combined an iterative procedure with numerical integration. This programme is similar to that described in the previous chapter. The Fermi level is varied until the value of the integral in equation (2,15) gives the correct carrier concentration. The mobility $\mu = R_\infty / \rho_0$ was also calculated. The Fermi level being known, it was then possible to predict the Hall coefficient and magnetoresistivity as a function of field by varying B in equations (2,29) and (2,31). This was done for different values of the scattering parameter s as illustrated by Figures (5,1), (5,2), (5,4) and (5,5). It is apparent from these curves that increasing s raises the curve as well as its slope. For specimens 1 and 5 as well as for the others, the slope of the experimental magnetoresistivity curve is too high to coincide with the theoretical curve for any value of s. The discrepancy is greatest for the purest specimens. On the other hand, the Hall coefficient curve could be made to coincide with some value of s. These considerations may be illustrated more readily by using the values of $\rho_0/\Delta\rho_\infty$ and $R_0/\Delta R_\infty$ that were listed in Table (5,1). By setting $B = \infty$ in equations (2,29) and (2,31) one may, by an iterative procedure, determine which values of s are consistent with the experimental results. The s values denoted by $s(\rho)$ in Table (5,2) satisfy the magnetoresistivity data only at $B = \infty$ but those denoted by s(R)

fit the Hall data over the whole range of B. As expected from the above discussion different results were obtained for $s(\rho)$ and $s(R)$. All computations related to equations (2,15), (2,29) and (2,31) involved iterative procedures combined with numerical integration as shown by Programmes 3, 4 and 5 at the end of the thesis.

The magnetothermoelectric power was measured for specimens 3 and 4 with the same technique and analysis as for the two alloy systems. Thus equation (2,12) was used to express the k versus E relationship. This equation is only accurate if $m_0^* \ll m$, which is a fair approximation for GaAs. As mentioned above, however, it allows one to express α_∞, the thermoelectric power in an infinite field, in a manner which is independent of the effective mass. Once the Fermi level is obtained from α_∞, the effective mass may be calculated from equations (2,8) and (2,19). Then α_0 may be used to obtain s. These results are shown in Table (5,3).

3. DISCUSSION

In the GaAs project, the measured variation of the Hall coefficient and resistivity with magnetic field was compared with the theoretical variation. It was assumed that these variations were due only to the energy dependent relaxation time of electrons in the (000) conduction band. Thus conduction due to holes or to electrons in higher bands was neglected. Since even the purest sample had an electron concen-

TABLE (5,2)

COMPUTED PARAMETERS OF GaAs AT 295°K

Specimen No.	ζ	μ (m^2/Vs)	s(ρ)	s(R)
1	- 4.169	.444	1.45	.33
2	- 2.402	.352	.78	.39
3	- 1.283	.334	.61	.44
4	- 0.079	.372	.55	.39
5	0.508	.329	.59	.42
6	1.091	.311	.59	.42
7	1.394	.264	.60	.36
8	3.748	.202	.65	
9	3.831	.246	.60	
10	4.512	.236	.58	
11	5.551	.209	.64	
12	6.976	.182	.73	

TABLE (5,3)

MAGNETOTHERMOELECTRIC POWER RESULTS

Specimen No.	α_0 (μV/deg)	α_∞ (μV/deg)	ζ	m_0^*/m	s
3	356.0	337.0	- 1.240	.070	.38
4	275.0	253.0	- 0.060	.071	.44

tration of almost 10^{22} m^{-3}, the hole concentration would be approximately 10^{3} m^{-3} since $np \simeq 10^{25}$ m^{-6} for GaAs at room temperature. Hole conduction is thus negligible. Conduction due to electrons in higher bands would occur only if the latter are relatively close to the (000) minimum. Optical measurements of band gap as a function of pressure led Edwards et al (59E) to the conclusion that the <100> minimum in GaAs is situated 0.5 eV above the (000) minimum at atmospheric pressure. Measurements of Hall coefficient versus temperature gave Aukerman and Willardson (60A) a value of $\Delta E = 0.38$ eV. In a review article, Welker and Weiss (56W) show the band gap versus composition for the alloy GaP_xAs_{1-x}. These data were obtained by Folberth (55F) from fundamental optical absorption measurements. The band gap curve consists of two straight line segments with a break at $x \sim .5$. It is known that the absolute minimum in GaAs is at (000) whereas it is at <100> for GaP. Thus by extrapolating back both line segments, one can determine the height of the subsidiary minima in both compounds. In the case of GaAs it would be in the <100> direction at a height of 0.40 eV above the absolute minimum. Supposing that ΔE is as low as 0.30 eV and that electrons in the upper band have an effective mass of 1.2 m (60E), there would be about 25 times as many electrons in the (000) band as in the <100> band in the most highly doped sample. Also, the mobility of the <100> electrons is at least 30 times smaller than that of the (000) electrons (67H). Thus the contribution of the higher band to the conductivity would be negligible.

Thus in these experiments, theassumption that only the (000) electrons contribute to the conductivity is valid. It is known that this band has spherical constant energy surfaces (59G) so that the neglect of specimen orientation is justified. A glance at Table (5,1) will show that even with the samples cut at random orientations, there is a continuous increase of $\rho_0/\Delta\rho_\infty$ for increasing n. Further proof that the measured electrons were in a spherical band can be deduced by noting that $\Delta\rho_\infty/\rho_0$ decreases rapidly towards zero as the carrier concentration is increased. It is known that in a spherical degenerate band only electrons near the Fermi level contribute to the conduction. Thus the relaxation time τ is effectively constant and no magnetoresistance is observed.

Having disposed of the various possible causes of magnetic field dependence of the Hall coefficient and resistivity other than that of energy dependent relaxation time in a single spherical band, one would expect that the theoretical and experimental curves would agree. As mentioned above, however, the magnetoresistivity curves did not coincide with theoretical ones for any value of s, the discrepancy being greatest for the purer samples. On the other hand, the Hall coefficient curves gave good agreement with $s \sim .40$. The same s value was obtained from magnetothermoelectric power measurements which produced electron effective mass values of .070 m and .071 m,close to the accepted value. The value $s = .40$ therefore seems to be valid.

As mentioned in Chapter I, at high temperatures, $s = \frac{1}{2}$ for optical phonons but drops to zero at "critical temperatures" listed

in Table (1,2) for different materials and finally to negative values for lower temperatures. During the discussion of the alloy results, it was suggested that the "critical temperatures" listed for InSb, InAs and GaSb were too high since good results were obtained at room temperature. The same might be said for GaAs since the results are also consistent. Nevertheless, one might accept from Table (1,2) that the "critical temperature" for GaAs is higher than those of the other compounds. One might then expect that provided optical phonon scattering is still involved, the s obtained with GaAs will be lower i.e., farther from $\frac{1}{2}$ than that obtained with the other compounds and alloys. This in fact was observed. For the experiments involving the magnetothermoelectric power of the two alloy systems, s was generally $\frac{1}{2}$ or greater while for GaAs, it was found to be .40 from Hall and magnetothermoelectric power measurements. It is then concluded that optical phonons dominate the scattering in GaAs at room temperature, in agreement with Ehrenreich (60E).

It remains to be seen why the magnetoresistivity curves did not coincide with theoretical ones for any value of s and consequently produced from the data at $B = \infty$ an s value higher than that from the other types of measurement. The reason, whatever it is, has a much larger effect on the magnetoresistivity than on the Hall effect or magnetothermoelectric power. This fact reminds one of Glicksman's work (59G) which showed the influence of contact size on the magnetoresistance of GaAs. It was found that large contact areas introduce a contribution to the magnetoresistance by a shorting out of the Hall voltage in the vicinity of the contacts whereas consistent results are obtained, within

experimental error, with .002" wide gold wire contacts. The author's contacts were wider than this (∿ .01") but the above argument does not seem to apply to the arrangement used by the author (Figure (3,3b)).

Another possible explanation involves impurity levels associated with the (000) and <100> conduction bands. In this case, one would expect different results from Sn and Te doped specimens. Unfortunately, the same range of electron density n was not available with the two types of specimens. For example, the three most highly doped specimens were Te doped. These displayed a small magnetoresistance discrepancy which may be due to a Te impurity level associated with the subsidiary <100> band. However, Craford et al (68Ca) have shown this Te level to be ∿.04 eV below the <100> minimum which is approximately .40 eV or 16 kT above the (000) minimum. The Fermi level of the most highly doped specimen is only 7 kT above the (000) minimum. Thus no magnetoresistance could be caused by the impurity level.

The author is led to the conclusion that the small magnetoresistance discrepancy common to specimens 3 to 12 which are either Sn or Te doped is due to small inhomogeneities. These are large enough to create a small magnetoresistance but too small to cause any appreciable scatter in the variation of mobility with n (Figure (5,7)). According to Proshko and Shveikin (67Pa), this explanation could also apply to specimens 1 and 2 which produced much larger discrepancies. These workers used laser radiations to measure the transmission of heavily doped GaAs and found that the lower the impurity concentration, the greater were the deviations from the average value.

There is however, another possible explanation for the large magnetoresistance discrepancy obtained with specimens 1 and 2 which were both Sn doped. This effect may be due to an intermediate Sn donor level which only merges with the (000) band in the more highly doped specimens. To confirm this statement, Te doped specimens with the same n as specimens 1 and 2 would have to be studied and found to have a much smaller (or larger) magnetoresistance discrepancy if the Te level is shallower (or deeper) than the Sn level. The author is not aware of any literature concerning the activation energy of Sn doped levels in GaAs. Some support for the above argument can be found however, by studying the mobility of specimens containing different dopants and by following the analysis of Csavinski (61Ca) which will now be outlined briefly.

Csavinski analysed Furukawa's (60F) measurements on heavily doped Ge which showed the mobility of Sb doped specimens to be 20 to 40% larger than that of As doped specimens at the same n and that the difference increased for increasing n. If ionized impurity scattering dominates, it follows that the scattering cross section depends on the ionized impurity and this dependence is more important in highly doped samples where the electrons screen the impurity ions more effectively so that the short range potential which is characteristic of a certain impurity becomes more important. It is then shown that the ratio of the mobilities of the Sb and As doped specimens is given by

$$\frac{\mu(Sb)}{\mu(As)} = 1 + \frac{q_1 + q_2}{Q\ (Sb^+)}$$

where $Q(Sb^+)$ is the scattering cross section of an Sb ion. From the fact that the ionization energy of an As donor is 30% greater than that of an Sb donor (59F), it is shown that $q_1 + q_2$ is a positive quantity so that $\mu(Sb) > \mu(As)$.

In Figure (5,7) the author has shown that $\mu(Te) > \mu(Sn)$ for any n. Williams (65W) also observed this effect. By analogy with the above, we may say that the ionization energy is greater for the Sn level than for the Te level in GaAs. This could explain the large magnetoresistance of the "pure" Sn doped specimens whose impurity level had not yet merged with the (000) band. There are of course differences between the Ge case studied by Csavinski and that of GaAs. For instance, polar scattering is much more important in GaAs. These are just speculations however, until it is shown that Te doped specimens with $n \sim 10^{22}\ m^{-3}$ produce results different from those of specimens 1 and 2. A study of the Hall coefficient versus temperature with Basinski's type of analysis (66Ba) would complete the picture by yielding the activation energy of the various donors.

Willardson and Duga (60Wa) measured the magnetoresistance of GaAs as a function of magnetic field and reported a satisfactory agreement between theoretical and experimental curves. Their calculations were based on a spherical parabolic conduction band, the charge carriers being scattered by acoustical lattice vibrations and ionized impurities. However, the author has shown, in agreement with Ehrenreich, that polar scattering dominates in GaAs at room temperature. A small correction would also be introduced by the use of a Kane band rather than a parabolic one.

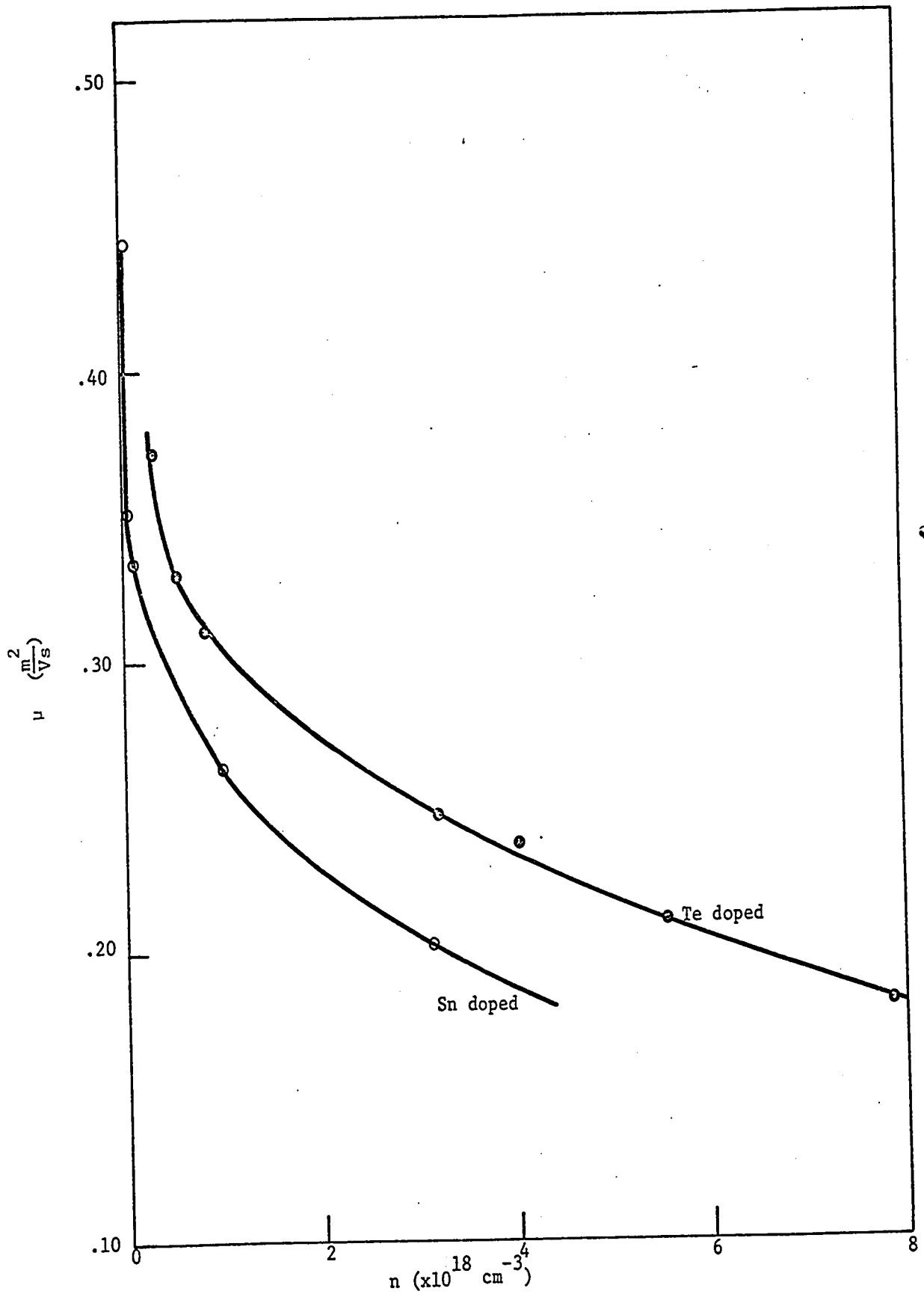

FIGURE (5,7) MOBILITY VERSUS ELECTRON DENSITY IN GaAs

CHAPTER VI

n type InSb

1. RESULTS

Two series of experiments were performed on polycrystalline n type InSb at 4.2°K. The first series involved specimens alloyed with In_2Te_3 while the second involved specimens alloyed with In_2Se_3. Again the magnetoresistance and Hall coefficient were measured as a function of magnetic field. The Hall coefficient tended to a saturation value R_∞ for infinite fields but the total observed change was always less than 2%. Figure (6,1) shows how R_∞ varied with y, the atomic percent of Te and Se. The corresponding resistivity curves are shown in Figures (6,2) and (6,3). These results are similar to those obtained by Woolley et al (60W, 61Wa). Typical magnetoresistivity curves are shown in Figure (6,4). Both series of experiments confirmed the prediction of Chapter II that a straight line would be observed with two band conduction if $\rho_0/\Delta\rho$ were plotted versus B^{-2} (Figure 6,5)). Only a slight curvature is observed with some specimens at small fields. The summary of slopes p and intercepts q as well as the other results mentioned above are given in Tables (6,1) and (6,2).

TABLE (6,1)

DATA FROM InSb-In_2Te_3

Specimen No.	y (% Te)	ρ_0 ($\times 10^{-6}$ ohm m)	R_∞ ($\times 10^{-6}$ m^3/C)	p (Wb^2/m^4)	q
2	.050	1.231	.8569	254.0	25.2
3	.250	1.929	.7420	447.0	21.3
4	.125	1.914	.8020	233.0	10.1
4A	.125	2.198	.8670	88.7	3.17
5	.375	2.326	.7800	334.0	11.6
5A	.375	2.166	.7305	720.0	20.6
6	.025	1.248	1.123	116.5	14.4
6A	.025	1.273	1.185	111.3	15.1
7	.390	2.586	.8240	902.0	33.7
8	.755	3.798	.8620	362.0	6.30
9	.485	2.742	.7800	467.0	9.20
12	.120	1.707	.9265	179.6	14.3
13	.011	1.439	1.970	44.5	7.66
14	.180	1.972	.8480	217.9	10.9
15	.060	1.364	.8850	367.0	44.9
17	.220	2.020	.8350	349.0	20.4
18	.615	2.852	.8070	592.0	3.60

TABLE (6,2)

DATA FROM $InSb-In_2Se_3$

Specimen No.	y (% Se)	ρ_0 ($\times 10^{-6}$ ohm m)	R_∞ ($\times 10^{-6}$ m^3/C)	p (Wb^2/m^4)	q
1	.280	2.111	.9680	406.0	22.8
2	.150	2.007	.9893	335.0	19.3
3	.050	1.680	1.128	182.3	20.1
4	.430	3.039	1.197	197.5	7.22
6	.635	2.887	1.099	80.3	2.50
7	.760	3.355	1.183	163.8	5.27
10	.027	1.584	1.190	113.0	13.9
12	.009	1.687	2.106	60.9	6.00

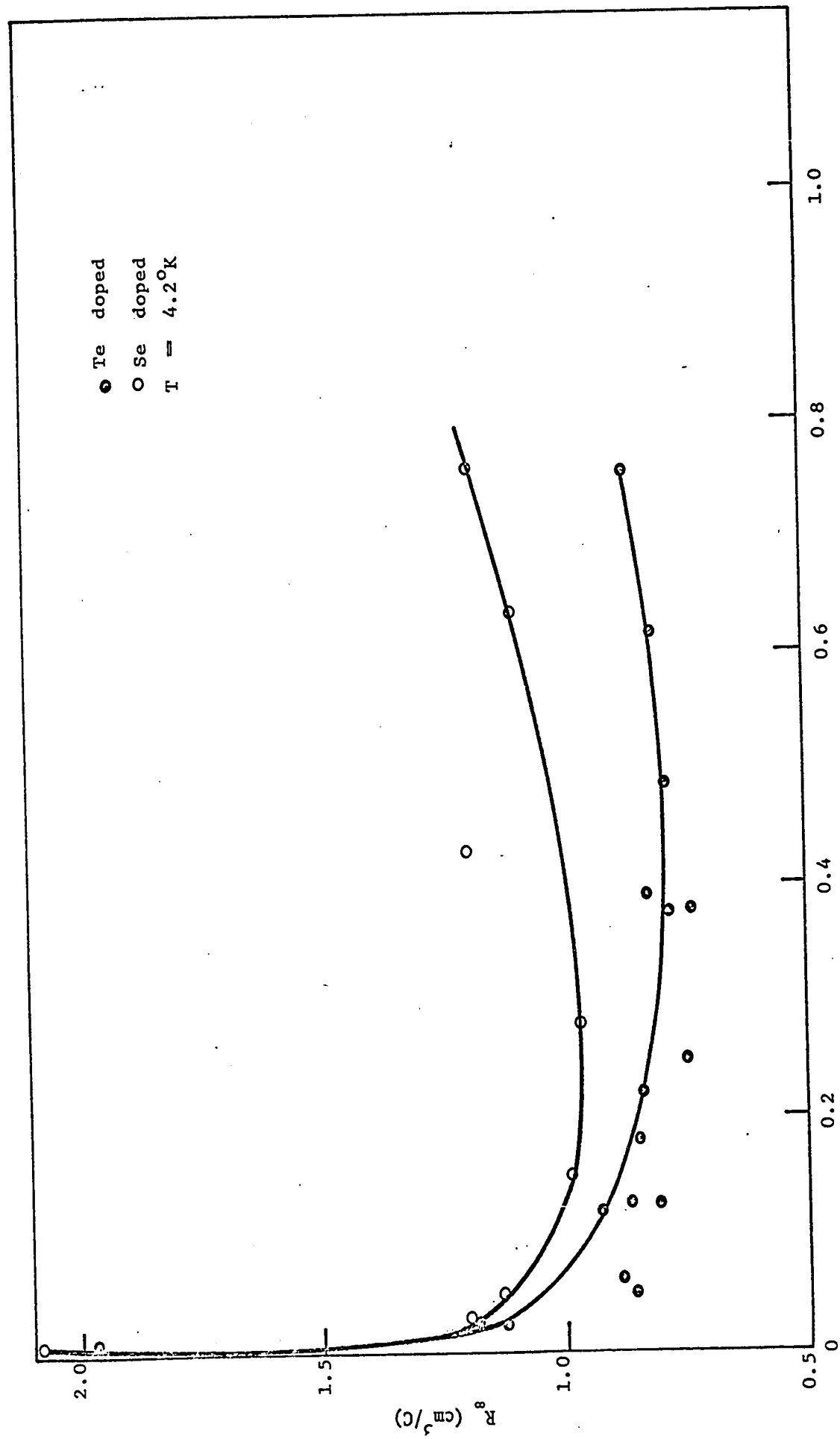

FIGURE (6,1) HALL COEFFICIENT OF InSb AS A FUNCTION OF DOPING

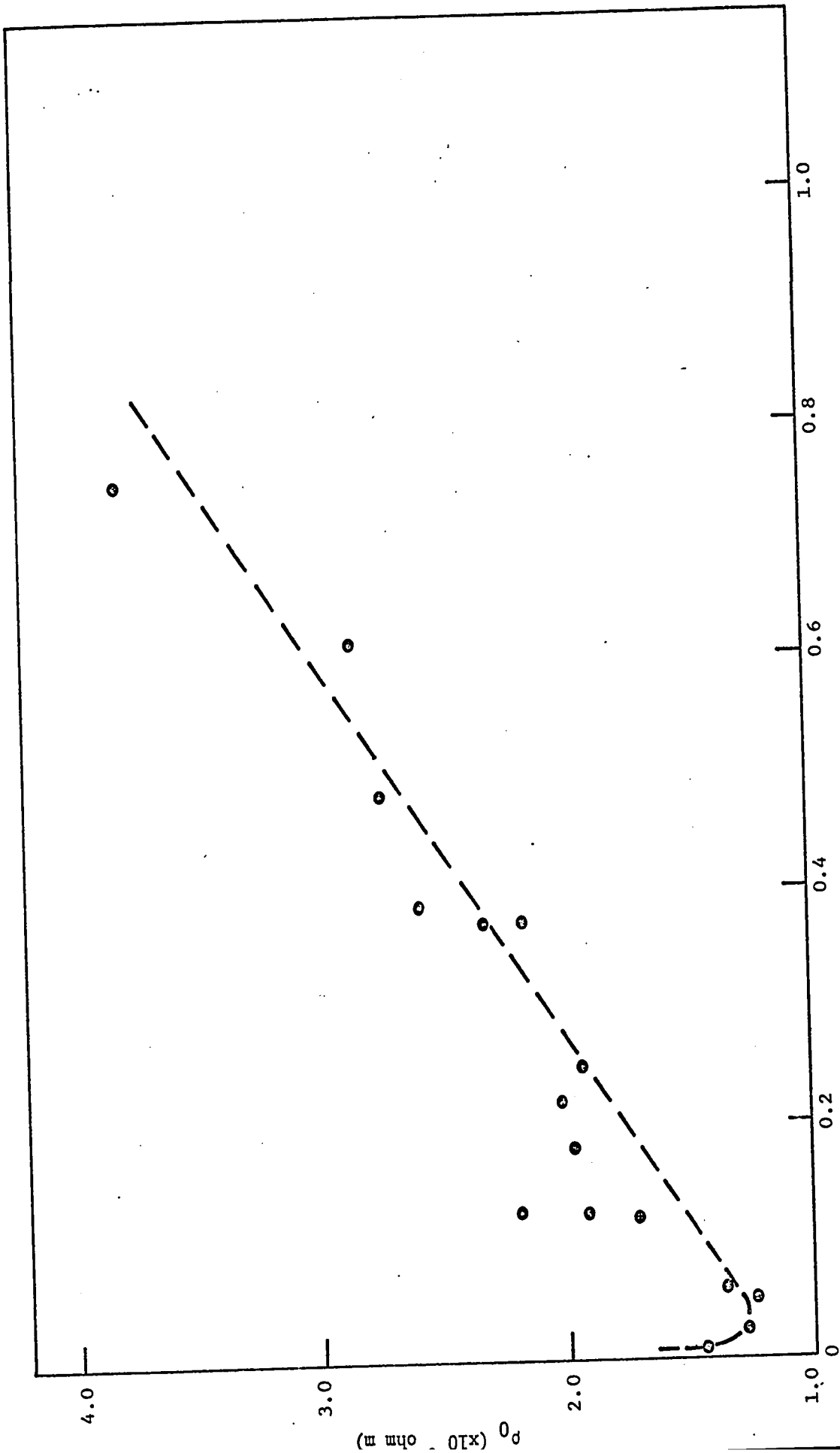

FIGURE (6,2) RESISTIVITY OF InSb VERSUS TELLURIUM CONTENT

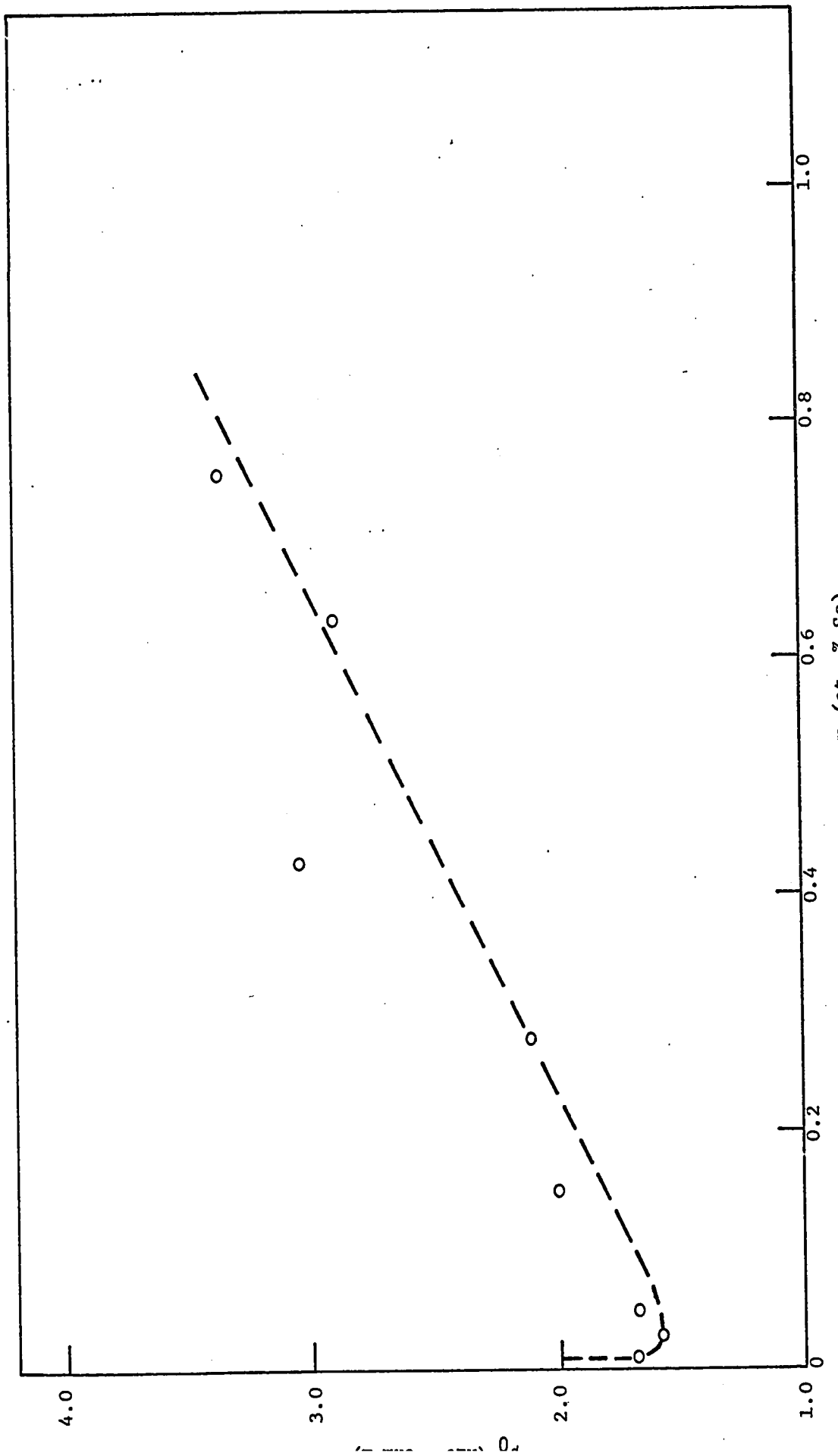

FIGURE (6,3) RESISTIVITY OF InSb VERSUS SELENIUM CONTENT

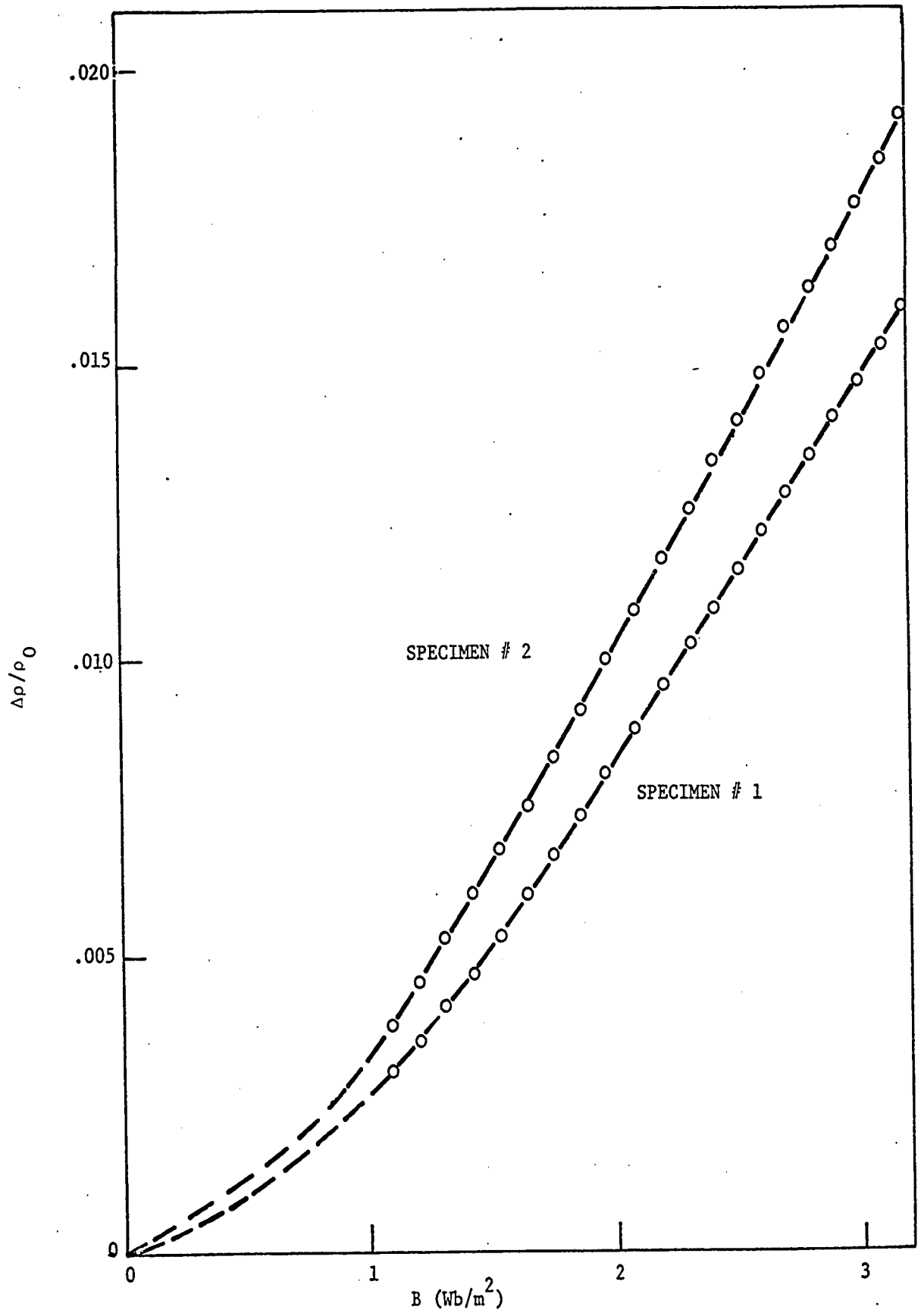

FIGURE (6,4) MAGNETORESISTIVITY OF $InSb\text{-}In_2Se_3$

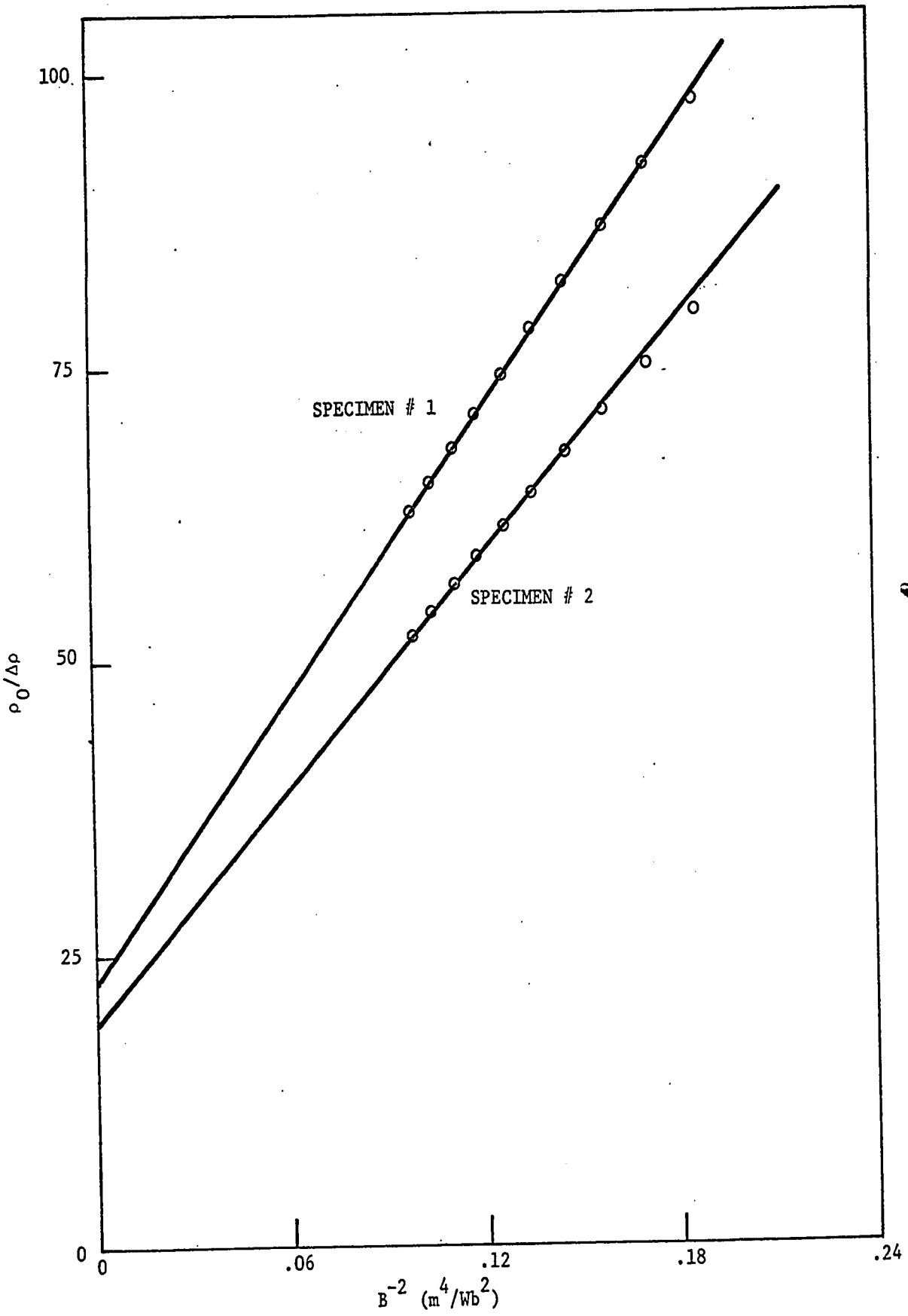

FIGURE (6,5) $\rho_0/\Delta\rho$ VERSUS B^{-2} FOR $InSb\text{-}In_2Se_3$

2. ANALYSIS

The slight curvature mentioned above for lower fields (Figure (6,5)) may be due to the assumption in equation (2,34) that

$$R_1 = \frac{1}{n_1 e} \qquad R_2 = \frac{1}{n_2 e}$$

i.e., the high field condition for arbitrary band shapes. As shown in Chapter II, at small fields, the Hall coefficient is also affected by the band shape and the Fermi level of the specimen. In Figure (6,5), the intercept represents the inverse of the magnetoresistivity at infinite magnetic fields so that if the high field slope and corresponding intercept are chosen, the above equations are valid.

The four measured parameters R_∞, ρ_0, p and q were fed into a computer to solve for the four unknowns R_1, R_2, σ_1, and σ_2 by an iterative procedure. First a value for σ_1 equal to $.55\ \sigma_0$ was chosen, i.e., the band whose conductivity is σ_1 is assumed to contribute just over one half of the total conductivity σ_0. The remaining conductivity σ_2 is provided by the other band. Presumably, the conductivity of the (000) band will be higher than that of the <111> band and will be denoted by σ_1. The smaller conductivity σ_2 will then be assigned to the <111> band. With $\sigma_1 = .55\ \sigma_0$, R_1 was calculated with the aid of equation (2,41). The result was then tested with equation (2,39) and generally found to be incorrect. The fraction .55 was gradually raised until equation (2,39) was satisfied. At this point, σ_1 and R_1 were the correct values from which σ_2 and R_2 were easily determined from equations (2,35) and (2,38) respectively. The carrier concentrations

now being known from the Hall coefficients, the mobilities could then be determined from the relations

$$\sigma_1 = n_1 e \mu_1 \qquad \sigma_2 = n_2 e \mu_2$$

The results discussed so far are shown in Tables (6,3) and (6,4) and Figures (6,6) to (6,9).

The known carrier concentrations were then used to solve for the Fermi levels of each of the two bands separately. A Kane model (equation (2,12)) was assumed for the (000) band while the <111> band was taken as parabolic (equation (2,10)). Each of these equations was used with equation (2,15) to calculate the corresponding Fermi level by numerical integration in an iterative procedure. The following parameters were used for the Kane band analysis: $E_0 = .25$ eV, $\Delta = .82$ eV, $m_0^* = .013$ m. Since the effective mass m_1^* of the <111> band electrons was not known, the calculation was performed for different values. The multiplicity of the <111> band was set equal to 4. This in effect assumes that the <111> minima are located at the band edge as in Ge (59Se). If the Fermi level of each band is measured from the bottom of that band, the difference in energy ΔE between the minima may be written

$$\Delta E = E_{F_1} - E_{F_2}$$

where E_{F_1} and E_{F_2} are the Fermi levels of the (000) and <111> bands respectively. The values of Fermi level and ΔE are listed in Tables

(6,5) and (6,6) assuming $m_1^* = .2\ m$, the corresponding value for GaSb (69V) and Ge (56D). The choice of m_1^* is not critical, however, since ΔE is relatively independent of m_1^*. A glance at Table (6,7) shows that for specimen 18 of the In_2Te_3 series, the value calculated for ΔE changes about 1% when the effective mass is doubled.

The variation of ΔE with y is illustrated by Figure (6,10) for both series of experiments. For clarity, specimens for which y is less than .25% have been omitted from this graph since their calculated n_2 values are mostly the result of noise and scatter, the real values being negligible, as one can conclude from Figures (6,6) and (6,7). Although a considerable amount of scatter is present, it is evident that ΔE decreases with increasing y. The two curves have different slopes but produce a common value of $\Delta E = .43$ eV for pure InSb.

3. ERROR DUE TO ANISOTROPY

In Chapter I, it was mentioned that at high and low magnetic fields, a contribution of up to 25% of the two band magnetoresistance signal may appear due to anisotropy of the <111> conduction band of InSb. A few test calculations were performed to see what effect on ΔE is obtained when the slope p and intercept q of the magnetoresistivity curve are changed. Table (6,8) shows these for sample #1 alloyed with In_2Se_3. The first line shows the observed slope and intercept. Only a slight change is observed in n_1. However n_2 changes by approximately

a factor of two when the slope or the intercept or both are doubled. This brings about a corresponding change in E_{F_2} but ΔE changes by no more than 3% in the table.

TABLE (6,3)

CARRIER DENSITIES AND MOBILITIES OF $InSb-In_2Te_3$

Specimen No.	y (% Te)	n_1 ($x10^{24}$ m^{-3})	n_2 ($x10^{24}$ m^{-3})	μ_1 (m^2/Vs)	μ_2 (m^2/Vs)
2	.050	6.892	.3923	.7184	.3051
3	.250	7.484	.9286	.4068	.2064
4	.125	6.673	1.110	.4569	.1914
4A	.125	5.145	2.055	.4914	.1518
5	.375	6.687	1.316	.3679	.1699
5A	.375	7.841	.7037	.3530	.1616
6	0.25	5.198	.3604	.9389	.3367
6A	.025	4.932	.3359	.9702	.3538
7	.390	6.869	.7063	.3323	.1853
8	.755	5.335	1.907	.2682	.1116
9	.485	6.799	1.204	.3122	.1279
12	.120	5.924	.8133	.5811	.2634
13	.011	2.940	.2289	1.445	.3931
14	.180	6.269	1.092	.4692	.2050
15	.060	6.696	.3573	.6653	.3410
17	.220	6.549	.9266	.4397	.2273
18	.615	6.808	.9267	.3118	.0707

TABLE (6,4)

CARRIER DENSITIES AND MOBILITIES OF $InSb-In_2Se_3$

Specimen No.	y (% Se)	n_1 ($\times 10^{24}$ m^{-3})	n_2 ($\times 10^{24}$ m^{-3})	μ_1 (m^2/Vs)	μ_2 (m^2/Vs)
1	.280	5.923	.5256	.4791	.2268
2	.150	5.799	.5107	.5162	.2289
3	0.50	5.084	.4499	.7027	.3175
4	.430	4.311	.9043	.4407	.1709
6	.635	3.912	1.768	.4909	.1368
7	.760	4.053	1.223	.4128	.1532
10	.027	4.738	.5079	.7964	.3306
12	.009	2.764	.1997	1.317	.2975

TABLE (6,5)

FERMI LEVELS AND BAND SEPARATION OF $InSb-In_2Te_3$

Specimen No.	y (% Te)	$\frac{E_{F_1}}{kT}$	$\frac{E_{F_2}}{kT}$	ΔE (eV)
2	.050	1121.0	10.6	.403
3	.250	1161.0	18.9	.414
4	.125	1105.7	21.3	.393
4A	.125	988.7	32.2	.347
5	.375	1106.7	23.9	.393
5A	.375	1184.1	15.7	.424
6	.025	993.1	10.0	.357
6A	.025	970.8	9.6	.349
7	.390	1119.4	15.8	.400
8	.755	1004.4	30.6	.353
9	.485	1114.5	22.5	.396
12	.120	1050.7	17.3	.375
13	.011	772.5	7.3	.278
14	.180	1076.6	21.1	.383
15	.060	1107.3	10.0	.398
17	.220	1096.9	18.9	.391
18	.615	1115.2	18.9	.398

TABLE (6,6)

FERMI LEVELS AND BAND SEPARATION OF $InSb-In_2Se_3$

Specimen No.	y (% Se)	$\frac{E_{F_1}}{kT}$	$\frac{E_{F_2}}{kT}$	ΔE (eV)
1	.280	1050.7	12.9	.377
2	.150	1041.2	12.7	.373
3	.050	983.6	11.6	.353
4	.430	915.4	18.6	.325
6	.635	878.1	29.1	.308
7	.760	891.0	22.8	.315
10	.027	954.0	12.6	.342
12	.009	751.4	6.7	.270

TABLE (6,7)

EFFECT OF m_1^*/m on ΔE FOR $InSb-In_2Te_3$, SPECIMEN # 18

m_1^*/m	$\frac{E_{F_1}}{kT}$	$\frac{E_{F_2}}{kT}$	ΔE (eV)
.15	1115.2	25.2	.3954
.20	1115.2	18.9	.3977
.25	1115.2	15.1	.3991
.30	1115.2	12.6	.4000

TABLE (6,8)

EFFECT OF p AND q ON ΔE FOR $InSb-In_2Se_3$, SPECIMEN # 1

p (Wb^2/m^4)	q	n_1 ($\times 10^{24}\ m^{-3}$)	n_2 ($\times 10^{24}\ m^{-3}$)	ΔE (eV)
406.0	22.8	5.923	.5256	.3765
812.0	45.6	6.164	.2850	.3847
406.0	45.6	5.504	.9443	.3624
812.0	22.8	6.208	.2402	.3862

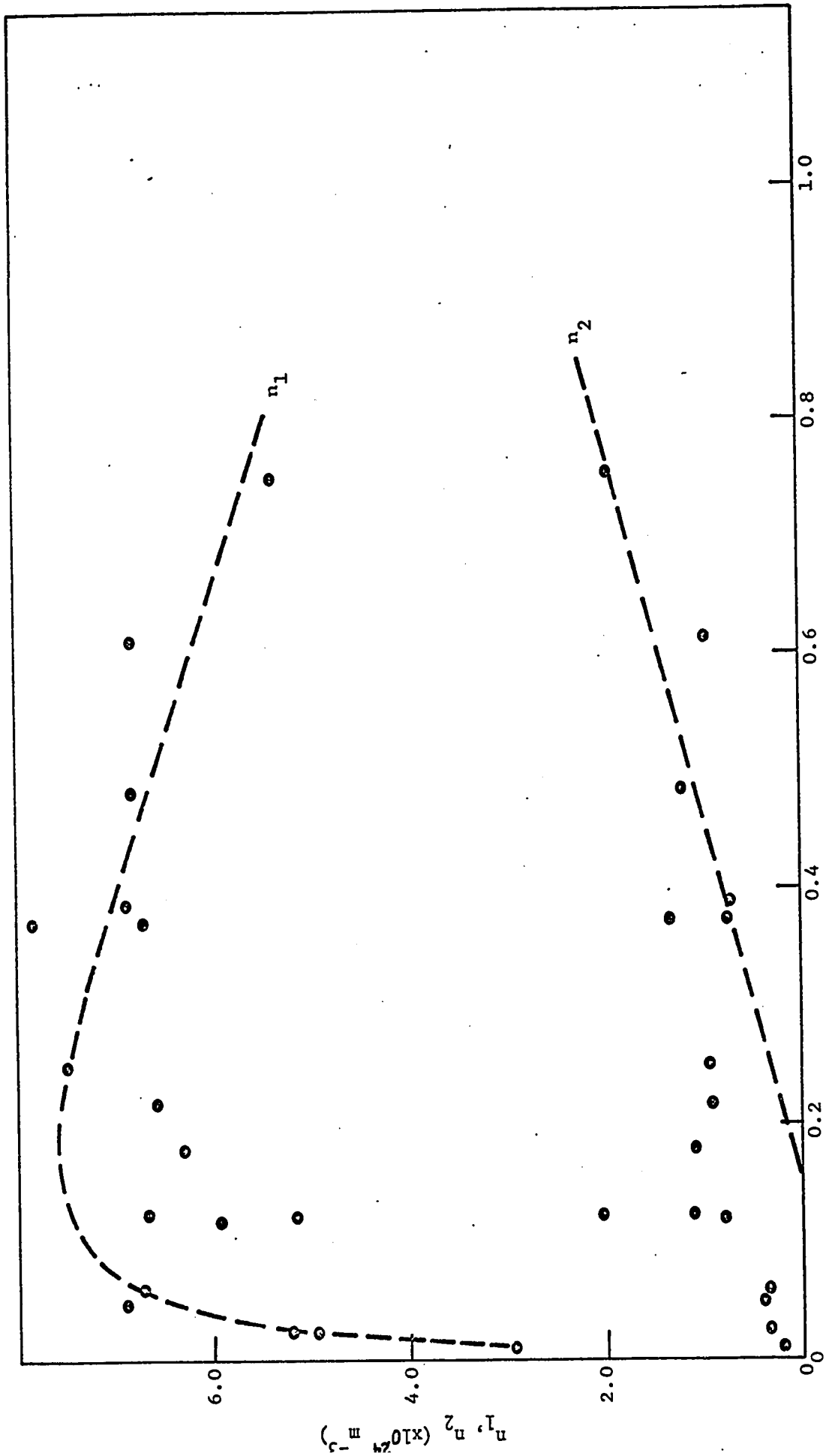

FIGURE (6,6) n_1 AND n_2 IN InSb VERSUS TELLURIUM CONTENT

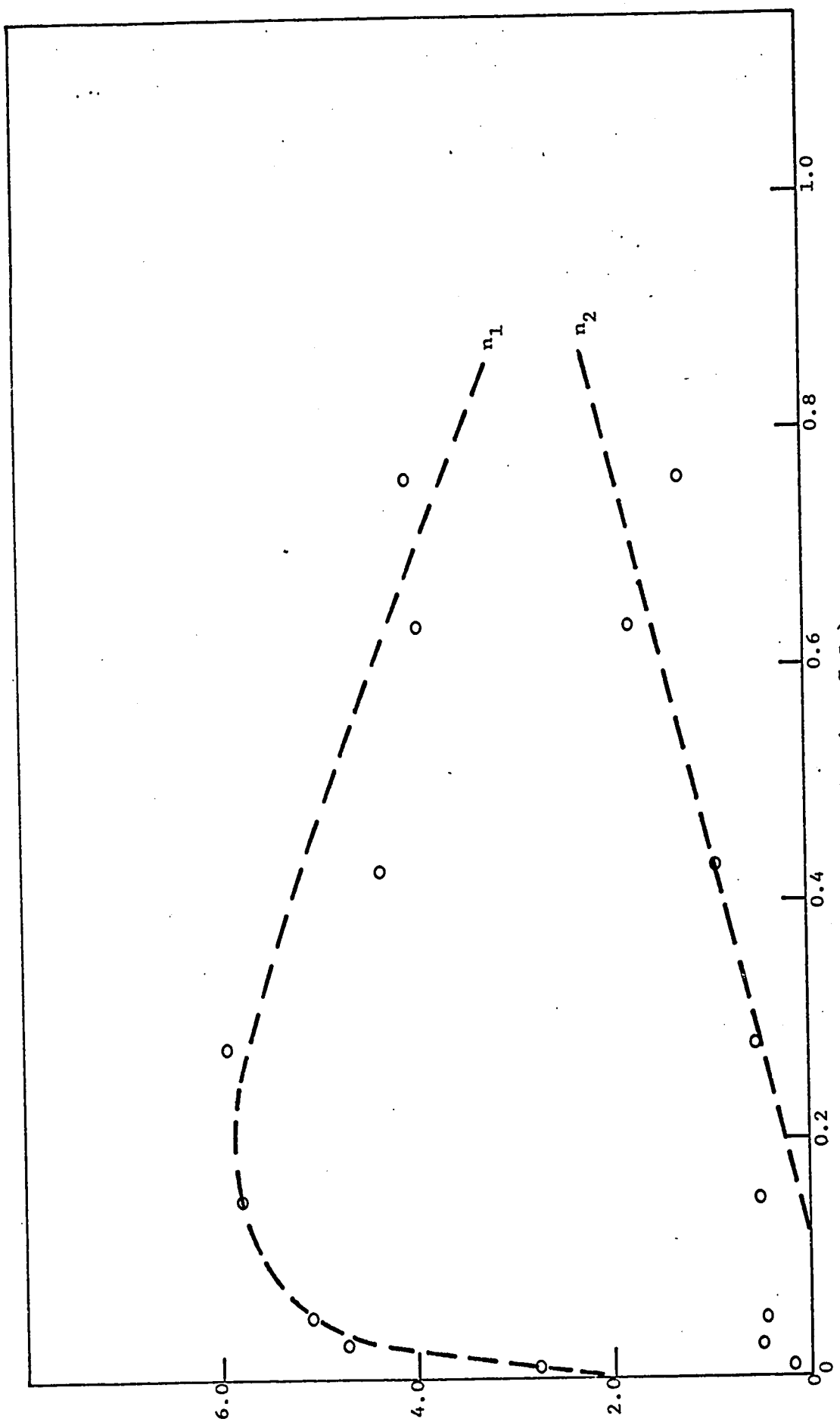

FIGURE (6,7) n_1 AND n_2 IN InSb VERSUS SELENIUM CONTENT

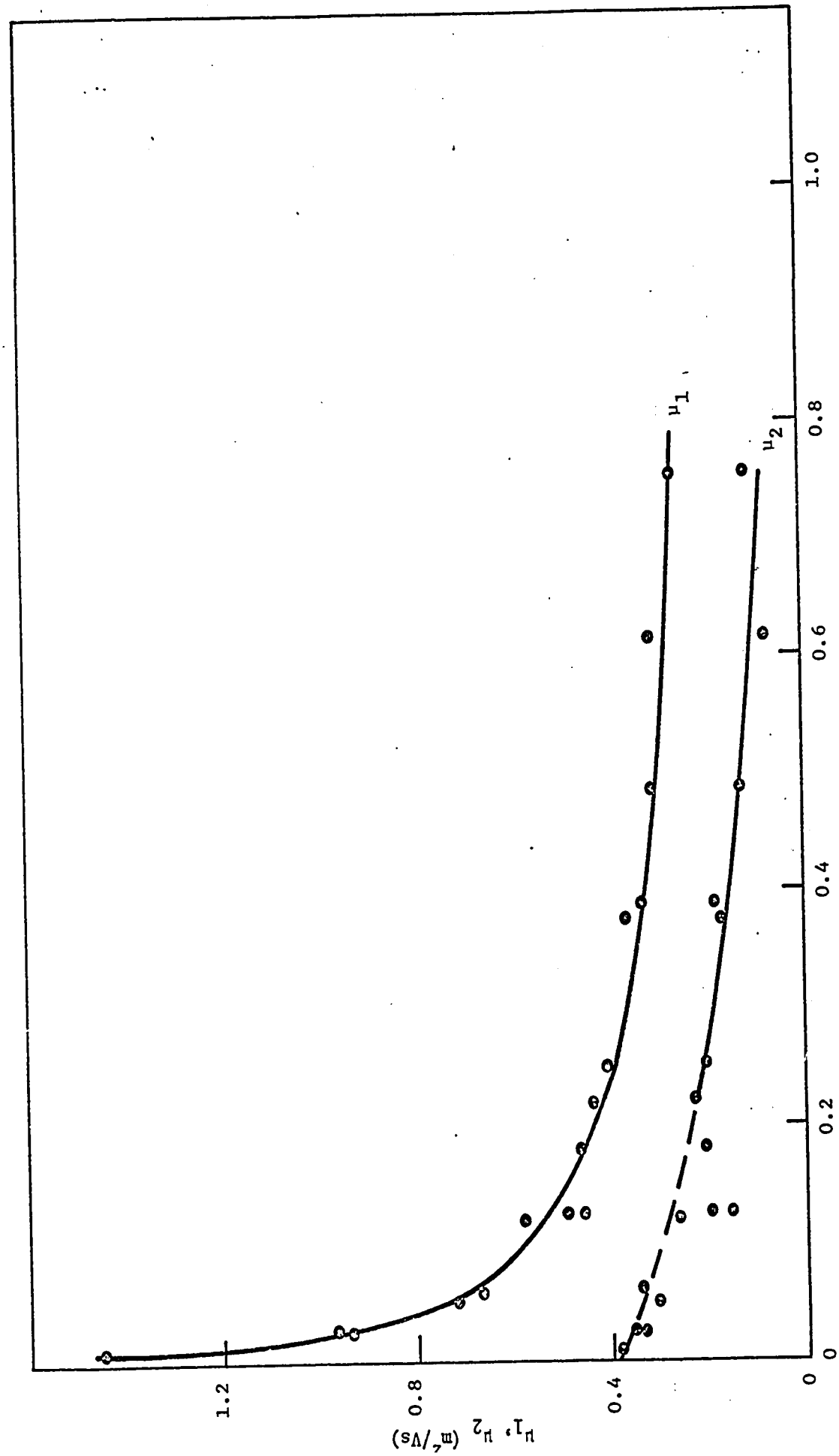

FIGURE (6,8) μ_1 AND μ_2 IN InSb VERSUS TELLURIUM CONTENT

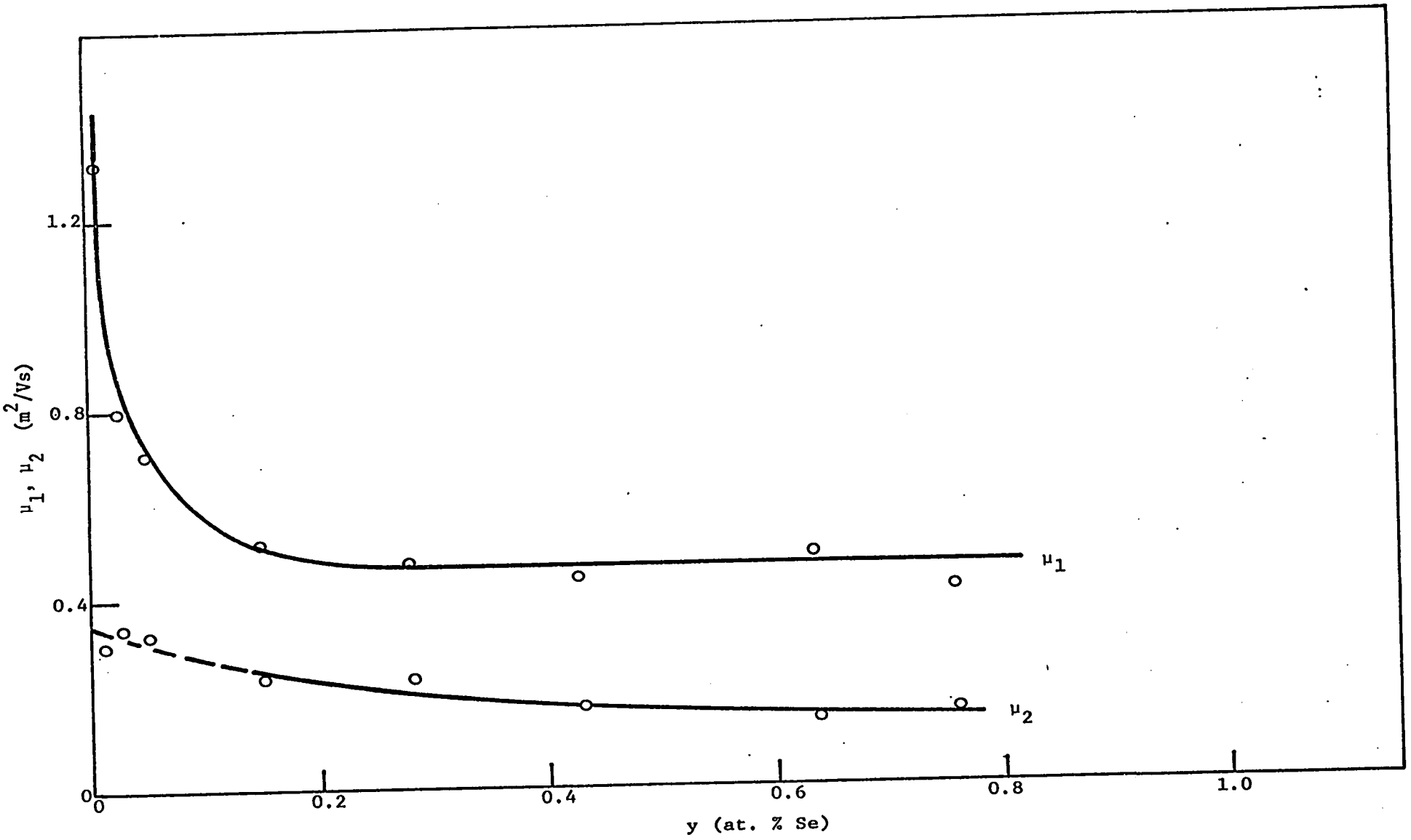

FIGURE (6,9) μ_1 AND μ_2 IN InSb VERSUS SELENIUM CONTENT

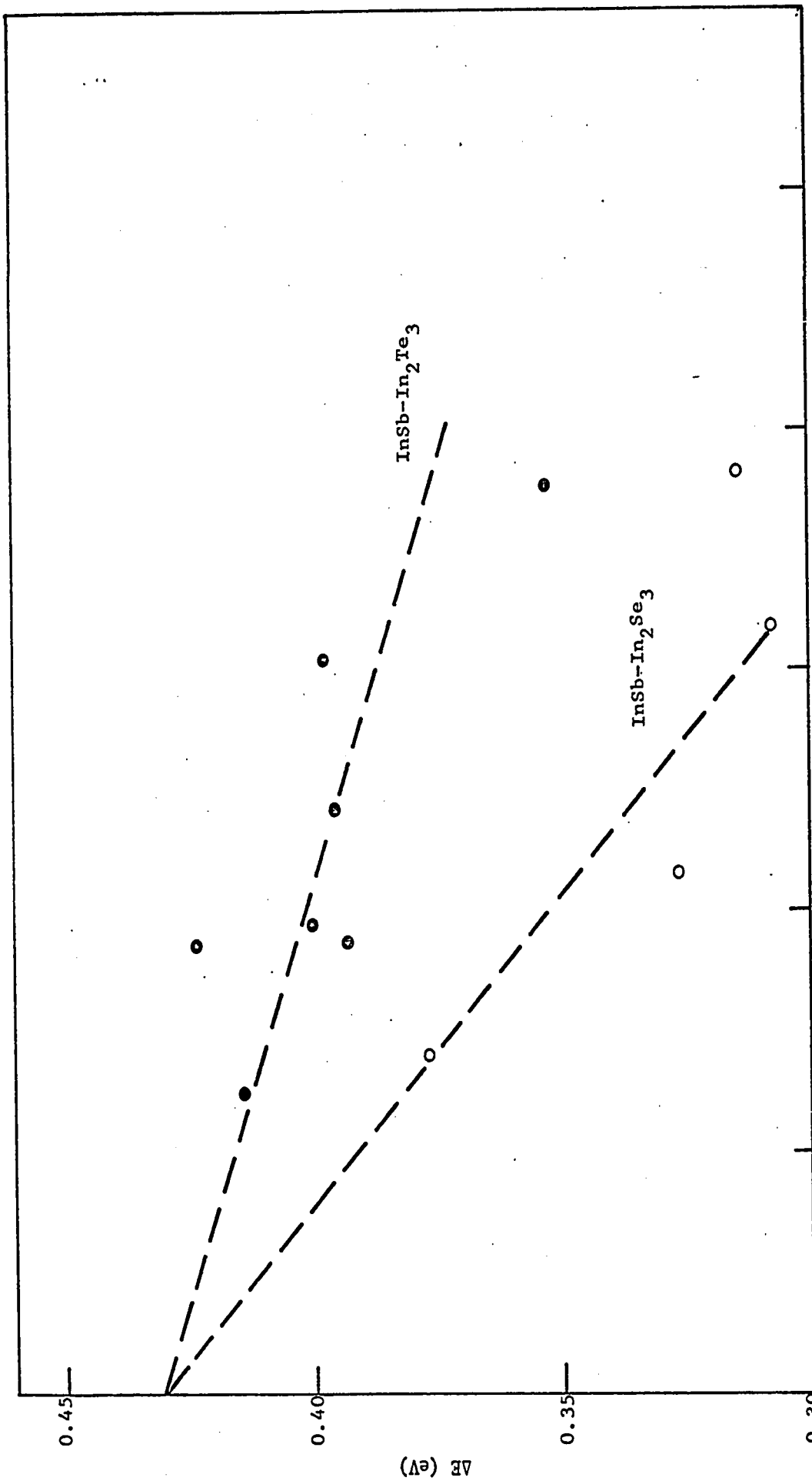

FIGURE (6,10) ΔE FOR InSb AS A FUNCTION OF DOPING

4. DISCUSSION

The two sets of results in the InSb project were fairly similar. In both cases, R_∞ initially decreases rapidly with increasing y but becomes constant and even rises slightly for y greater than .30% (Figure (6,1)). Woolley et al (60W, 61Wa, 61Wb) had observed a similar behavior in R_0 and had suggested two possible explanations for this phenomenon. As mentioned in Chapter III, In_2Te_3 and In_2Se_3 both have a defect zinc blende structure but at low percentages of these compounds in InSb, do not produce the expected large number of vacancies. The result is the same as that obtained by doping with Te or Se. The minimum value of R_0 may correspond to the limit of solid solution of Te or Se in InSb. Above this value, lattice vacancies are produced. The alternative explanation given by Woolley and Keating (61Wa) suggests that solid solution of Te or Se continues beyond the minimum in the Hall coefficient but that the electrons enter another conduction band with a much higher effective mass. Thus their contribution to the Hall coefficient would be very small.

The author's results indicate that both explanations are partially correct. The quantity $R_\infty = \frac{1}{e(n_1 + n_2)}$ which depends only upon the total carrier concentration was found to approach a minimum and even began to rise slightly for y greater then .30% thus substantiating the first explanation. This may also be seen from Figures (6,6) and (6,7) where n_1 rises rapidly with y initially, approaches a maximum and finally decreases. On the other hand, n_2 starts at zero at y = .15%

and increases at a rate which is much too low to match the initial increase of n_1. The second explanation is also correct in that the second conduction band becomes populated, although this is not the main reason for which the Hall coefficient saturates. Woolley and Keating had assumed that ΔE would be constant but Figure (6,10) shows that ΔE decreases with increasing y allowing some of the electrons in the (000) band to fall into the <111> band. The rate of change is approximately .07 eV/atomic percent Te and .20 eV/atomic percent Se. Both curves predict a ΔE for pure InSb of approximately 0.43 eV.

Woolley et al (60W, 61Wa, 61Wb) also measured the optical energy gap E_g of InSb and InAs alloyed with In_2Te_3 and In_2Se_3 at room temperature and found that it increased initially with y and reached a maximum of .44 eV at $y \sim .15\%$ for InSb-In_2Te_3 and .43 eV at $y \sim .30\%$ for InSb-In_2Se_3. Beyond the maximum a slight decrease was observed. The initial increase may be explained in terms of the Burstein shift while the maximum value of E_g may correspond to the point at which the Fermi level reaches the <111> band minimum. If this is so, one can calculate ΔE from these results. Since the height of the Fermi level above the conduction band minimum is given by $E_g - E_0 + 4kT$ and $E_0 = .18$ eV at room temperature, $\Delta E = .36$ eV for InSb-In_2Te_3 and $\Delta E = .35$ eV for InSb-In_2Se_3. These room temperature values could be too low (ignoring for the moment the fact that the author's measurements were performed at 4.2°K) according to the preceding paragraph which leads one to the conclusion that E_g ceases to increase because the total number of carriers also ceases to increase. It must be pointed out however,

that these ΔE values of Woolley and Keating are not those for pure InSb since ΔE varies with y as shown by the author. For example, in the case of InSb-In_2Se_3, $\Delta E = .35$ eV at $y \sim .3\%$. At this point, the author's result would indicate $\Delta E = .43 - .3 \times .20 = .37$ eV which agrees fairly well with Woolley and Keating. A discrepancy may arise because of temperature effects but this is expected to be small. The above difference of .02 eV between the room temperature and liquid helium temperature results would give ΔE a temperature coefficient of $< -8 \times 10^{-5}$ eV/°K. This is consistent with the corresponding Ge (58M) and GaSb (69V) values. It is therefore possible that the Fermi level did reach the <111> band minimum at room temperature for $y \sim .3\%$. The author's measurements at 4.2°K showed that at $y \sim .3\%$ the total number of carriers reached a maximum. Thus, regarding the two phenomena produced as y increases, the Fermi level reaching the <111> band minimum and the limit of solid solution of Se in InSb being reached, the author's results cannot resolve which occurs first.

In the case of InSb-In_2Te_3, at $y \sim .15\%$, the author obtains $\Delta E = .43 - .15 \times .07 = .42$ eV at 4.2°K while at room temperature, Woolley and Keating obtain $\Delta E = .36$ eV. Here the difference is too large to be attributed to temperature effects and it must be concluded that in the room temperature measurements, the Fermi level reached the <111> band minimum after and not before the limit of solid solution of Te in InSb had been reached.

It was mentioned above that Woolley et al found that E_g decreased slightly beyond the maximum. The largest rate of decrease occurred in the $InSb-In_2Te_3$ system and was approximately 0.018 eV/at % Te. This is much lower than the author's results for ΔE quoted above. One might then conclude that the rate of decrease of ΔE is mainly due to a rise of the (000) band minimum. In that case, the slight decrease of E_g with increasing y beyond the maximum could correspond to a lowering of the <111> band minimum as Te and Se impurity levels merge with that band. These conclusions are only tentative since one cannot be sure that the Kane model is still applicable at high doping levels and that parameters such as the effective mass at the (000) minimum m_0^* remains unchanged. It was shown that E_0 could in fact change considerably although this is not expected to cause significant changes in the results.

It was suggested above that Te and Se impurity levels associated with the <111> band are involved in the variation of ΔE. This is consistent with the pressure experiments of Kosicki and Paul (66Ka) who noted the existence of Se donor levels in GaSb associated with the <111> conduction band. Paul (69P) also reported the existence of Te levels associated with the <111> band of InSb.

Another interesting point involves the observation of Belle and Galavanov (66B) that the $L_3 \rightarrow L_1$ doublet in Se doped InSb shifts to lower energies for increasing electron concentration. Their reflectivity

studies indicated a maximum shift of 0.04 eV at $n \sim 7 \times 10^{18}$ cm^{-3}. This maximum value of n was presumably obtained with y at least 0.2% according to Figure (6,1). Thus the <111> minimum could move as rapidly as 0.04/0.2 = 0.20 eV/at % Se. This coincides with the author's results as long as the (000) band minimum remains fixed relative to the valence bands which is rather doubtful. Thus although it has been shown that ΔE decreases with increasing Te and Se content in InSb, it is impossible to say from these results which of the two bands moves relative to the valence band.

Molodyan et al (66M) determined the effective mass of electrons in $(InSb)_x$ $(InTe)_{1-x}$ crystals by thermal and electrical measurements. They found that solid solutions having $x > 0.99$ behave like InSb doped with Te and that samples containing an electron concentration $n > 2 \times 10^{24}$ m^{-3} show an $m^*(n)$ dependence which differs from that predicted by Kane. They attributed this to the influence of a second conduction band but did not pursue the matter any further.

Kwan and Woolley (68K), in experiments analogous to those of the author found that ΔE in InAs also decreased with increasing y. They also performed infrared absorption measurements and obtained optical energy gap values which they plotted versus $n_1 + n_2$. No maximum was reached for the InAs-In_2Te_3 specimens but those of InAs-In_2Se_3 reached a maximum value of $E_g \sim 1.0$ eV. Thus, of the four cases discussed here, two measured by Kwan and Woolley and two by the author, in only two cases, those of InAs-In_2Se_3 and InSb-In_2Te_3 was the minimum

in the Hall Coefficient caused by the filling of the (000) band up to the <111> band minimum. In the two other cases, the <111> band became populated only after the Hall coefficient minimum had been reached (due to the limit of solid solution of Te or Se) and ΔE had become low enough.

The following table summarizes the author's results as well as those of Kwan and Woolley concerning the variation of ΔE in InSb and InAs due to the presence of Te and Se

	InSb	InAs
Te	a) .07 eV / at %	b) .17 eV / at %
Se	c) .20 eV / at %	d) .13 eV / at %

The relative values of the numbers a, b, c, d should be consistent with the relative positions of the elements involved in the periodic table:

Ga	Ge	As	Se
In	Sn	Sb	Te

For example, one would expect that $a < b$ since Te should fit in substitutionally more easily in InSb than in InAs. In all, four relations would be expected to apply:

$$a < b, \quad d < c, \quad a < c, \quad d < b$$

A check of the above values shows all four conditions to be satisfied.

CHAPTER VII

SUMMARY AND CONCLUSIONS

Three projects were undertaken by the author and are reported in this thesis.

In the first project, the magnetothermoelectric power of $InAs_xSb_{1-x}$ and $In_{1-x}Ga_xSb$ alloys was measured at room temperature. Assuming that the conduction band in these alloys satisfies the Kane model, the electron effective mass m_0^* at the bottom of the (000) conduction band was calculated as well as the scattering parameter s. The variation of m_0^* with x exhibited a parabolic behavior for both alloy systems in agreement with the theoretical predictions of Woolley and Thompson (64W). These theoretical curves were slightly too low, however, because of an incorrect choice of the matrix element P. In the $InAs_xSb_{1-x}$ system, the effective mass dipped to a minimum of .010 m at $x \sim .3$.

The scattering parameter s varied from .4 to .7 with the higher values related to the more highly doped specimens. This indicates a greater degree of ionized impurity scattering as the carrier concentration is increased. The dominant scattering mechanism however is either piezoelectric or optical phonon scattering. The ambiguity arises because the same s value is associated with both mechanisms. Following Ehrenreich's results (57E, 59E) for several III-V compounds, it was concluded that optical phonon scattering dominates in the measured alloys as well as in InSb, InAs and GaSb. The results show clearly that alloy scattering is negligible in the measured alloys in agreement with the predictions of Tietjen and Weisberg (65T).

In the second project, formulae were derived to predict the variation of the Hall coefficient and resistivity with magnetic field due to an energy dependent relaxation time. These predictions were then tested at room temperature with 12 GaAs single crystals doped with Sn or Te. Good agreement was obtained with the Hall coefficient variation which gave a scattering parameter of $\sim .40$. This agreed very well with the values of .38 and .44 obtained from the magnetothermoelectric power of two of the specimens. It was concluded that optical phonons dominate the scattering in GaAs at room temperature in agreement with Ehrenreich (60E). The magnetoresistivity, however, exhibited small discrepancies for 10 specimens and much larger discrepancies for the two purest specimens. The small discrepancies, and possibly the larger ones (67Pa) are due to inhomogeneities. It is also possible that the larger discrepancies are due to Sn impurity levels associated with the (000) conduction band. Confirmation would require the study of a larger number of Sn and Te doped specimens.

Finally, the magnetoresistivity of InSb alloyed with In_2Te_3 and In_2Se_3 was studied at $4.2^{o}K$. A two conduction band analysis using a Kane model for the (000) band and a parabolic <111> band showed the subsidiary <111> band minimum to be .43 eV above the (000) band minimum in pure InSb. As the Te or Se content was increased, the band separation ΔE was found to decrease at a rate of .07 eV/at. % Te and .20 eV/at. % Se. These values are consistent with themselves and with those obtained by Kwan and Woolley (68K) for InAs alloyed with In_2Te_3 and In_2Se_3.

REFERENCES

31N Nordheim L., Ann. Physik (Leipzig) 9, 607 (1931)

31W Wilson A.H., Proc. Roy. Soc. (London) A133, 458 (1931)

31Wa Wilson A.H., Proc. Roy. Soc. (London) A134, 277 (1931)

37F Fröhlich H., Proc. Roy. Soc. (London) A160, 230 (1937)

40S Seitz F., Modern Theory of Solids, p. 352. McGraw-Hill (1940)

50E Erginsoy C., Phys. Rev. 79, 1013 (1950)

50S Shockley W. and Bardeen J., Phys. Rev. 77, 407 (1950)

50Sa Shockley W., Phys. Rev. 78, 173 (1950)

51P Pearson G.L. and Suhl H., Phys. Rev. 83, 768 (1951)

52W Welker H., Z. Naturforsch. 7a, 744 (1952)

53H Howarth D.J. and Sondheimer E.H., Proc. Roy. Soc. A219, 53 (1953)

53W Welker H., Z. Naturforsch. 8a, 248 (1953)

54R Read W.T., Phil. Mag. 45, 1119 (1954)

54W Welker H., Physica 20, 893 (1954)

55B Brooks H., Advan. Electron. Electron Phys. 7, 85 (1955)

55D Dresselhaus G., Kip A.F. and Kittel C., Phys. Rev. 98, 368 (1955)

55F Folberth O.G., Z. Naturforsch. 10a, 502 (1955)

55H Herring C., Bell Syst. Tech. J. 34, 237 (1955)

55Ha Hrostowski H.J., Morin F.J., Geballe T.H. and Wheatley G.H., Phys. Rev. 100, 1672 (1955)

55P Parmenter R.H., Phys. Rev. 97, 587 (1955)

55Pa Parmenter R.H., Phys. Rev. 99, 1759 (1955)

56A Antell, Chasmar, Champness and Cohen, Rugby Semiconductor Conference Report, Phys. Soc. (London) p. 99 (1956)

56B Barrie R., Proc. Phys. Soc. B69, 553 (1956)

56D Dexter R.N., Zeiger H.J. and Lax B., Phys. Rev. 104, 637 (1956)

56H Harrison W.A., Phys. Rev. 101, 903 (1956)

56W Weiss H., Z. Naturforsch. 11a, 430 (1956)

56Wa Woolley J.C., Smith B.A. and Lees D.G., Proc. Phys. Soc. B69, 1339 (1956)

56Wb Welker H. and Weiss H., Solid State Physics 3, edited by F. Seitz and D. Turnbull. Academic Press (1956)

57E Ehrenreich H., J. Phys. Chem. Solids 2, 131 (1957)

57K Kane E.O., J. Phys. Chem. Solids 1, 249 (1957)

57W Woolley J.C. and Smith B.A., Proc. Phys. Soc. B70, 153 (1957)

58G Glicksman M., Phys. Rev. 111, 125 (1958)

58M Macfarlane G.G., McLean T.P., Quarrington J.E. and Roberts V., Proc. Phys. Soc. 71, 863 (1958)

58R Reid F.J. and Willardson R.K., J. Electron. and Control 5, 54 (1958)

59A Abrahams M.S., Braunstein R. and Rosi F.D., J. Phys. Chem. Solids 10, 204 (1959)

59E Ehrenreich H., J. Phys. Chem. Solids 12, 97 (1959)

59F Fan H.Y. and Fisher P., J. Phys. Chem. Solids 8, 270 (1959)

59G Glicksman M., J. Phys. Chem. Solids 8, 511 (1959)

59M Mass T.S., Smith S.D. and Taylor K.W., J. Phys. Chem. Solids 8, 323 (1959)

59R Rodot M., J. Phys. Chem. Solids 8, 358 (1959)

59S Smith R.A., Semiconductors, p. 22. Cambridge University Press (1959)

59Sa Smith R.A., ibid, p. 119

59Sb Smith R.A., ibid, p. 107

59Sc Smith R.A., ibid, p. 156

59Sd Smith R.A., ibid, p. 131

59Se Smith R.A., ibid, p. 351

59W Woolley J.C., Evans J.A. and Gillett C.M., Proc. Phys. Soc. 74, 244 (1959)

60A Aukerman L.W. and Willardson R.K., J. Appl. Phys. 31 939 (1960)

60E Ehrenreich H., Phys. Rev. 120, 1951 (1960)

60F Furukawa Y., J. Phys. Soc. Japan 15, 730 (1960)

60I Ivanov-Omskii V.I. and Kolomiets B.T., Soviet Phys. Solid State 2, 363 (1960)

60S Sladek R.J., J. Phys. Chem. Solids 16, 1 (1960)

60W Woolley J.C., Gillett C.M. and Evans J.A., J. Phys. Chem. Solids 16, 138 (1960)

60Wa Willardson R.K. and Duga J.J., Proc. Phys. Soc. 75, 280 (1960)

61A Ansel'm A.I. and Askerov B.M., Soviet Phys. Solid State 3, 2665 (1961)

61C Cardona M., Phys. Rev. 121, 752 (1961)

61Ca Csavinsky P., J. Phys. Soc. Japan 16, 1865 (1961)

61E Ehrenreich H., J. Appl. Phys. 32, 2155 (1961)

61N Nasledov D.N., J. Appl. Phys. 32, 2140 (1961)

61W Woolley J.C., Gillett C.M. and Evans J.A., Proc. Phys. Soc. 77, 700 (1961)

61Wa Woolley J.C. and Keating P.N., Proc. Phys. Soc. 78, 1009 (1961)

61Wb Woolley J.C., Pamplin B.R. and Evans J.A., J. Phys. Chem. Solids 19, 147 (1961)

62S Shalyt S.S., Soviet Phys. Solid State 4, 1403 (1962)

62Sa Smith S.D., Pidgeon C.R. and Prosser V., Proc. Intern. Conf. on Semiconductor Physics, p. 301. Exeter (1962)

62Z Zawadzki W., Phys. Stat. Sol. 2, 385 (1962)

63C Cardona M., Phys. Rev. 129, 69 (1963)

63Ca Cardona M., J. Phys. Chem. Solids 24, 1543 (1963)

63W Warner J., Ph.D. thesis, University of Nottingham (1963)

64H Hilsum C., Proc. Intern. Conf. on Semiconductors, p. 297. Paris (1964)

64K Korenblit L.L. Mashovets D.V. and Shalyt S.S., Soviet Phys. Solid State 6, 438 (1964)

64M Madelung O., Phys. of III-V Compounds. Wiley, New-York (1964)

64P Potter R.F. and Kretschmar G.G., Infrared Phys. 4, 57 (1964)

64W Woolley J.C. and Thompson A.G., Can. J. Phys. 42, 2030 (1964)

64Wa Woolley J.C. and Warner J., Can. J. Phys. 42, 1879 (1964)

64Wb Woolley J.C. and Warner J., J. Electrochem. Soc. 111, 1142 (1964)

65H Harland H.B., Ph.D. thesis, University of Ottawa (1965)

65T Tietjen J.J. and Weisberg L.R., Appl. Phys. Let. 7, 261 (1965)

65W Williams F., J. Electrochem. Soc. 112, 8 (1965)

66B Belle M.L. and Galavanov V.V., Soviet Phys. Solid State 8, 122 (1966)

66Ba Basinski J., Can. J. Phys. 44, 941 (1966)

66C Cardona M., Shaklee K.L. and Pollak F.H., Phys. Let. 23, 37 (1966)

66F Filipchenko A.S., Molodyan I.P., Nasledov D.N., Sidorov V.G. and Emelyanenko O.V., Phys. Stat. Sol. 14, K195 (1966)

66H Harland H.B. and Woolley J.C., Can. J. Phys. 44, 2715 (1966)

66K Kolodziejczak J., Zukotynski S. and Stramska H., Phys. Stat. Sol. 14, 471 (1966)

66Ka Kosicki B.B. and Paul W., Phys. Rev. Let. 17, 246 (1966)

66M Molodyan I.P., Nasledov D.N., Radautsan S.I. and Sidorov V.G., Phys. Stat. Sol. 18, 677 (1966)

66S Seraphin B.O., J. Appl. Phys. 37, 721 (1966)

66T Thompson A.G., Cardona M. Shaklee K.L. and Woolley J.C., Phys. Rev. 146, 601 (1966)

66W Willardson R.K. and Beer A.C., Semiconductors and Semimetals. Academic Press (1966)

66Wa Woolley J.C., Can. J. Phys. 44, 2709 (1966)

67C Cardona M., Shaklee K.L. and Pollak F.H., Phys. Rev. 154, 696 (1967)

67H Hutson A.R., Jayaraman A. and Coriell A.S., Phys. Rev. 155, 786 (1967)

67K Kudman I, and Seidel T.E., J. Appl. Phys. 38, 4379 (1967)

67P Pidgeon C.R., Groves S.H. and Feinleib J., Solid State Comm. 5, 677 (1967)

67Pa Proshko G.P. and Shveikin V.I., Soviet Phys. Semiconductors 1, (1967)

67T Thompson A.G. and Woolley J.C., Can. J. Phys. 45, 255 (1967)

68A Aubin M.J. and Woolley J.C., Can. J. Phys. 46, 1191 (1968)

68C Coderre W.M. and Woolley J.C., Can. J. Phys. 46, 1207 (1968)

68Ca Craford M.G., Stillman G.E., Rossi J.A. and Holonyak N., Phys. Rev. 168, 867 (1968)

68K Kwan C.C.Y. and Woolley J.C., Can. J. Phys. 46, 1669 (1968)

68V van Tongerloo E.H. and Woolley J.C., Can. J. Phys. 46, 1199 (1968)

69A Aubin M.J., Thomas M.B., van Tongerloo E.H. and Woolley J.C., Can. J. Phys. 42, 631(1969)

69C Coderre W.M., Ph.D. thesis, University of Ottawa (1969)

69P Paul W. (to be published)

69V van Tongerloo E.H. and Woolley J.C., Can. J. Phys. 47, 241 (1969)

POST ORAL DISCUSSION

This section was written after the oral examination to summarise points made by the examiners during the oral. The examining board consisted of Dr. C. H. Champness of McGill University, Dr. Y. P. Varshni, Dr. A. Manoogian and Dr. R. G. Tross.

1) In Chapter IV, the contribution of holes to the magnetothermoelectric power was neglected. Although this approximation is entirely justified, a significant contribution could arise from the "cross" term i. e. terms involving both electrons and holes. Tsidil'kovskii (62T) calculated $\Delta\alpha_\infty$ in the case of mixed conduction but assumed parabolic bands along with non degenerate electrons and holes with the same scattering parameter so that only an approximate result can be obtained with his equation. Using the known values for electron and hole effective masses and mobilities for InSb and setting the Fermi level at the conduction band minimum, it is found that the contribution of the cross terms to $\Delta\alpha_\infty$ approaches that of the electrons. It is not clear in Tsidil'kovskii's results however, what magnetic field is necessary for the saturation of the cross term effect. One would expect it to be higher than that necessary for the saturation of the electron effect because the hole mobility is less than the electron mobility. This may explain the behaviour of curve 2 of Figure (4, 2) which had been explained in terms of quantum effects. If this is the case, the initial plateau was correctly taken as that corresponding to the electron effect and specimens which behaved in a manner shown by curve 1 were also correctly interpreted. Even if $\Delta\alpha_\infty$ were due mostly to the cross terms, however, the results for s and m_0^* would not be altered appreciably since $\Delta\alpha_\infty$ was always relatively small.

2) Most specimens in both alloy systems behaved in a manner illustrated by curve 1 of Figure (4, 2). In all only four or five specimens did not exhibit complete saturation (curves 2 and 3). These all had a high InSb content and a low carrier concentration.

3) Equation (2, 46) applies to crystals of cubic symmetry and to magnetic fields small enough for one to neglect terms higher than the second order.

4) In the GaAs project, the author measured the variation of the Hall coefficient R with magnetic field. Since one cannot back-off the Hall coefficient to zero field, however, the value R_0 had to be obtained by extrapolating the measured values of R to zero field. This makes the choice of R_0 quite critical if one wants reasonably accurate values of ΔR versus field. For this reason, these measurements were not attempted for the more highly doped specimens, whose Hall coefficients do not change sufficiently for accurate determinations of ΔR.

5) If specimens are not homogeneous, but contain concentration gradients, the interpretation of the magnetoresistance presents a serious problem. The larger the concentration gradient or discontinuity, the larger the resulting magnetoresistance. One then has to subtract this magnetoresistance from the observed one to obtain the normal effect. Hieronymus and Weiss (62H) performed experiments on an InSb specimen whose Hall coefficient varied 15% along the length. The magnetoresistance was anomalously large and depended on the position of the potential probes.

62H Hieronymus H. and Weiss H., Solid State Electron. 5, 71 (1962)

62T Tsidil'kovskii I. M., Thermomagnetic Effects in Semiconductors. Academic Press, New York (1962)

```
C     PROGRAMME 1
C
C
C
C     CALCULATES FERMI LEVEL AND EFFECTIVE MASS
C     FEED IN THERMOELECTRIC POWER AND HALL IN INFINITE FIELD
C     USES THE AUBIN FORMULA----EQUATION (2,12) IN THESIS
C     NDATA IS NUMBER OF SETS OF DATA
C     EG IS THE ENERGY GAP
C     DELTA IS SPIN ORBIT SPLITTING
      DIMENSION F(3000)
      READ (1,7) NDATA
    7 FORMAT (I2)
      DO 99 M=1,NDATA
      READ (1,5) ALY,RY,EG,DELTA
    5 FORMAT (4F6.3)
      RY=RY*1.0E-06
      GAM=.0254/EG
      L=1
      A=-2.0
      IJ=-1
      F(1)=0.0
   11 EVEN1=0.0
      EVEN2=0.0
      ODD1=0.0
      ODD2=0.0
      DELX=.04
      XE=.04
      XO=.06
      DO 100 I=1,1000
      AE=(1.+GAM*XE)
      AO=(1.+GAM*XO)
      BE=AE+DELTA/EG
      BO=AO+DELTA/EG
      CE=AE+(2*DELTA)/(3*EG)
      CO=AO+(2*DELTA)/(3*EG)
      DE=(XE*AE*BE/CE)**1.5
      DO=(XO*AO*BO/CO)**1.5
      PE=EXP(XE-A)
      PO=EXP(XO-A)
      F2E=(DE*PE)/((1+PE)*(1+PE))
      F1E=F2E*XE
      IF (IJ) 16,20,14
   16 IJ=0
      GO TO 14
   20 IF (F1E-F(I-1)) 12,12,14
   12 WRITE (3,13) I,F(I-1)
   13 FORMAT (2X,I4,E15.3)
      IJ=1
   14 F(I)=F1E
      F2O=(DO*PO)/((1+PO)*(1+PO))
      F1O=F2O*XO
      EVEN1=EVEN1+F1E
      EVEN2=EVEN2+F2E
      ODD1=ODD1+F1O
      ODD2=ODD2+F2O
      XE=XE+DELX
  100 XO=XO+DELX
      AI1=(DELX/6.)*(4.*EVEN1+2.*ODD1)
```

```
      AI2=(DELX/6.)*(4.*EVEN2+2.*ODD2)
      CALC=.8616E+02*(AI1/AI2-A)
      FUNC=CALC-ALY
      WRITE (3,101) CALC,FUNC
  101 FORMAT (2E15.4)
      GO TO %21,22,23,24,25,26,27,28,29<,L
   21 IF %FUNC< 32,30,31
   32 L#2
      GO TO 11
   22 IF %FUNC< 34,30,36
   34 A=A+10.
      GO TO 11
   36 L#4
   38 A=A-1.
      GO TO 11
   24 IF %FUNC< 40,30,38
   40 L#6
   42 A=A+.1
      GO TO 11
   26 IF %FUNC< 42,30,44
   44 L#8
   46 A=A-.01
      GO TO 11
   28 IF %FUNC< 30,30,46
   31 L#3
      GO TO 11
   23 IF %FUNC< 35,30,34
   35 L#5
      GO TO 38
   25 IF %FUNC< 38,30,37
   37 L#7
      GO TO 42
   27 IF %FUNC< 39,30,42
   39 L#9
      GO TO 46
   29 IF %FUNC< 46,30,30
   30 CONTINUE
      WRITE (3,15) F(1),F(3000)
   15 FORMAT (5X,2E15.3)
      WRITE (3,90) ALY,EG,A
   90 FORMAT (3F15.3)
      P2=EG*EG*GAM*(.05410E-19*AI2*RY)**.66666
      AMOS=(3.0*3.8098E-20*EG/P2)*(EG+DELTA)/(3*EG+2*DELTA)
      WRITE (3,95) P2,AMOS
   95 FORMAT (20X,2E15.4)
      WRITE (3,105)
  105 FORMAT (10H PLUS VITE///)
   99 CONTINUE
      STOP
      END
```

```
C     PROGRAMME 2
C
C
C
C     CALCULATES SCATTERING PARAMETER S
C     FEED IN THERMOELECTRIC POWER IN ZERO FIELD AND FERMI LEVEL
C     NDATA IS NUMBER OF SETS OF DATA
C     EG IS ENERGY GAP
C     DELTA IS SPIN ORBIT SPLITTING
C     "A" IS THE SCATTERING PARAMETER
      READ (1,7) NDATA
    7 FORMAT (I2)
      DO 99 M=1,NDATA
      READ (1,6) ALO,AMUS,EG,DELTA
    6 FORMAT (4F6.3)
      GAM=.0254/EG
      L#1
      A=-2.0
   11 CONTINUE
      EVEN1=0.0
      EVEN2=0.0
      ODD1=0.0
      ODD2=0.0
      DELX=.04
      XE=.04
      XO=.06
      DO 100 I=1,1000
      AE=1+GAM*XE
      AO=1+GAM*XO
      BE=AE+DELTA/EG
      BO=AO+DELTA/EG
      CE=AE+(2*DELTA)/(3*EG)
      CO=AO+(2*DELTA)/(3*EG)
      DE=(XE*AE*BE/CE)
      DO=(XO*AO*BO/CO)
      PE=EXP(XE-AMUS)
      PO=EXP(XO-AMUS)
      F2E=(DE**(A+1.5))*PE/(((AE*BE/CE+XE*BE*GAM/CE+XE*AE*GAM/CE-
     1DE*GAM/CE)*(1+PE))**2)
      F1E=F2E*XE
      F2O=(DO**(A+1.5))*PO/(((AO*BO/CO+XO*BO*GAM/CO+XO*AO*GAM/CO-
     1DO*GAM/CO)*(1+PO))**2)
      F1O=F2O*XO
      EVEN1=EVEN1+F1E
      EVEN2=EVEN2+F2E
      ODD1=ODD1+F1O
      ODD2=ODD2+F2O
      XE=XE+DELX
  100 XO=XO+DELX
      AI1=(DELX/6.)*(4.*EVEN1+2.*ODD1)
      AI2=(DELX/6.)*(4.*EVEN2+2.*ODD2)
      CALC=.8616E+02*(AI1/AI2-AMUS)
      FUNC=CALC-ALO
      GO TO %21,22,23,24,25,26,27,28,29<,L
   21 IF %FUNC< 32,30,31
   32 L#2
      GO TO 11
   22 IF %FUNC< 34,30,36
   34 A=A+1.
```

```
      GO TO 11
   36 L#4
   38 A=A-.1
      GO TO 11
   24 IF %FUNC< 40,30,38
   40 L#6
   42 A=A+.01
      GO TO 11
   26 IF %FUNC< 42,30,44
   44 L#8
   46 A=A-.001
      GO TO 11
   28 IF %FUNC< 30,30,46
   31 L#3
      GO TO 11
   23 IF %FUNC< 35,30,34
   35 L#5
      GO TO 38
   25 IF %FUNC< 38,30,37
   37 L#7
      GO TO 42
   27 IF %FUNC< 39,30,42
   39 L#9
      GO TO 46
   29 IF %FUNC< 46,30,30
   30 CONTINUE
   17 WRITE (3,18) ALG,EG,A
   18 FORMAT (3F15.3)
      WRITE (3,105)
  105 FORMAT (18H METTEZ-Y DU TIGRE///)
   99 CONTINUE
      STOP
      END
```

****

```
C     PROGRAMME 3 ------      CALCULATES FERMI LEVEL
C
C
C
C     USES SIMPLIFIED KANE MODEL   --- EQUATION (2,9) IN THESIS
C     NDATA IS NUMBER OF SETS OF DATA
C     RY IS HALL COEFFICIENT IN INFINITE MAGNETIC FIELD
C     EG IS THE ENERGY GAP
C     TMOS IS EFFECTIVE MASS AT BAND MINIMUM
C     ALPHA IS HBAR OVER 2*M
C     THE FERMI LEVEL "A" IS SET INITIALLY AT -5
      DOUBLE PRECISION  RY,EG,AMOS,ALPHA,GAM,CI2,A,EVEN2,ODD2,DELX
      DOUBLE PRECISION  XE,XO,AE,AO,BE,BO,DE,DO,PE,PO,F2E,F2O,F1E
      DOUBLE PRECISION  AI2,FUNC,F(1200),TMOS
      READ (1,7) NDATA
    7 FORMAT (I2)
      DO 99 M=1,NDATA
      READ (1,5) RY,EG,TMOS
    5 FORMAT (3D10.4)
      AMOS=TMOS*(1 -TMOS)
      ALPHA=3.8098D-20
      GAM=.0254D+00/EG
      CI2=(18.482D+19/RY)*(TMOS*2*ALPHA/EG)**1.5
      L#1
      A=-5.00+00
   11 EVEN2=0.0D+00
      ODD2=0.0D+00
      IJ=-1
      F(1)=0.0D+00
      DELX=.02D+00
      XE=.02D+00
      XO=.03D+00
      DO 100 I=1,1200
      AE=1+2*GAM*TMOS*XE
      AO=1+2*GAM*TMOS*XO
      BE=DSQRT(1+4*GAM*AMOS*XE)
      BO=DSQRT(1+4*GAM*AMOS*XO)
      DE=(AE-BE)**1.5
      DO=(AO-BO)**1.5
      PE=DEXP(XE-A)
      PO=DEXP(XO-A)
      F2E=(DE*PE)/((1+PE)*(1+PE))
      F2O=(DO*PO)/((1+PO)*(1+PO))
      IF (IJ) 16,20,14
   16 IJ=0
      GO TO 14
   20 IF (F2E-F(I-1)) 12,12,14
   12 WRITE (3,13) I,F(I-1)
   13 FORMAT (2X,I4,E15.3)
      IJ=1
   14 F(I)=F2E
      EVEN2=EVEN2+F2E
      ODD2=ODD2+F2O
      XE=XE+DELX
  100 XO=XO+DELX
      WRITE (3,15) F(1),F(1200)
   15 FORMAT (5X,2E15.3)
      AI2=(DELX/6 )*(4 *EVEN2+2 *ODD2)
      FUNC=AI2-CI2
```

```
      GO TO %21,22,23,24,25,26,27,28,29<,L
   21 IF %FUNC< 32,30,31
   32 L#2
      GO TO 11
   22 IF %FUNC< 34,30,36
   34 A=A+1
      GO TO 11
   36 L#4
   38 A=A-.1D+00
      GO TO 11
   24 IF %FUNC< 40,30,38
   40 L#6
   42 A=A+.01D+00
      GO TO 11
   26 IF %FUNC< 42,30,44
   44 L#S
   46 A=A-.001D+00
      GO TO 11
   28 IF %FUNC< 30,30,46
   31 L#3
      GO TO 11
   23 IF %FUNC< 35,30,34
   35 L#5
      GO TO 38
   25 IF %FUNC< 38,30,37
   37 L#7
      GO TO 42
   27 IF %FUNC< 39,30,42
   39 L#9
      GO TO 46
   29 IF %FUNC< 46,30,30
   30 CONTINUE
      WRITE (3,90) RY,EG,A
   90 FORMAT (E15.3,2F15.3)
      WRITE (3,105)
  105 FORMAT (10H PLUS VITE///)
   99 CONTINUE
      STOP
      END
```

```
C      PROGRAMME 4
C
C
C
C      CALCULATES (DELTA RHO)/RHO AND (DELTA R)/R
C      DOES CALCULATION FOR 11 MAGNETIC FIELDS THAT ARE FED IN
C      USES SIMPLIFIED KANE MODEL   --- EQUATION (2,9) IN THESIS
C      NDATA IS NUMBER OF SETS OF DATA
C      RHOO IS RESISTIVITY IN ZERO MAGNETIC FIELD
C      EG IS ENERGY GAP
C      MOS IS EFFECTIVE MASS AT BAND MINIMUM
C      MUS IS THE REDUCED FERMI LEVEL
C      S IS THE SCATTERING PARAMETER
       REAL*8 N,MOS,I1,I2,I3,I4,I5,MUS,KT
       DOUBLE PRECISION  RHOO,EG,    AO,E,   DELX,ALPHA,C1,C2,C3,C4,S
       DOUBLE PRECISION  EVEN2,EVEN3,ODD2,ODD3,XE,XO,AE,BE,BO,CE,CO,AO
       DOUBLE PRECISION  DE,DO,EE,EO,FE,FO,GE,GO,HE,HO,      DBO,B,EVEN4
       DOUBLE PRECISION  EVEN5,ODD4,ODD5,C9,OE,OO,QE,QO,      A,B,DELRO
       DOUBLE PRECISION  DELPO,C5,C6,C7,AEE,  AOO,Y(11)
       READ(1,1)(Y(J),J=1,11)
       READ(1,71)NDATA
    71 FORMAT(I2)
       DO 70 NN=1,NDATA
       READ (1,1) RHOO,EG,MOS,MUS,S
     1 FORMAT(5D16.6)
       WRITE(3,2)RHOO,EG,MOS,MUS
     2 FORMAT(////,5X,4D17.6)
       AO=1/RHOO
       E=1.602D-19
       KT=.0254D+00
       DELX=.01D+00
       ALPHA=3.8098D-20
       C1=MOS*(1-MOS)
       C2=DSQRT(EG/(MOS*2*ALPHA))
       C3=(1/MOS)-1
       C5=4*KT*C1/EG
       C6=2*KT*MOS/EG
       C7=4*ALPHA*C3/EG
       C4=2*ALPHA/KT
     3 EVEN2=0.0D+00
       EVEN3=0.0D+00
       ODD2=0.0D+00
       ODD3=0.0D+00
       DO 23 J=1,11
       B=Y(J)
     5 EVEN4=0.0D+00
       EVEN5=0.0D+00
       ODD4=0.0D+00
       ODD5=0.0D+00
       XE=.01D+00
       XO=.015D+00
       C9=((29.609D+00*B)/(E*RHOO*I2))**2
       DO 6 I=1,5000
       AEE=DEXP(XE-MUS)
       AOO=DEXP(XO-MUS)
       AE=AEE/((1+AEE)*(1+AEE))
       AO=AOO/((1+AOO)*(1+AOO))
       BE=DSQRT(1+C5*XE)
       BO=DSQRT(1+C5*XO)
```

```
      CE=C6*XE
      CO=C6*XO
      DE=DSQRT(1+CE-BE)*C2
      DO=DSQRT(1+CO-BO)*C2
      EE=DE**(2*S+1 )
      EO=DO**(2*S+1 )
      IF (S-.25D+00) 30,31,32
   30 FE=1 /DE**(1 -4*S)
      FO=1 /DO**(1 -4*S)
      GO TO 33
   31 FE=1.0D+00
      FO=1.0D+00
      GO TO 33
   32 FE=DE**(4*S-1 )
      FO=DO**(4*S-1 )
   33 GE=1+C7*DE*DE
      GO=1+C7*DO*DO
      HE=C4*DE*(1+C3/DSQRT(GE))
      HO=C4*DO*(1+C3/DSQRT(GO))
      IF (8-2.25D+00) 21,20,20
   21 EVEN2=EVEN2+AE*EE*HE*HE
      ODD2=ODD2+AO*EO*HO*HO
      EVEN3=EVEN3+AE*FE*(HE**4)
      ODD3=ODD3+AO*FO*(HO**4)
   20 IF(S-1 )40,41,42
   40 OE=(HE/DE**(1 -S))**4
      OO=(HO/DO**(1 -S))**4
      GO TO 43
   41 OE=HE**4
      OO=HO**4
      GO TO 43
   42 OE=(DE**(S-1 )*HE)**4
      OO=(DO**(S-1 )*HE)**4
   43 QE=1+C9*OE
      QO=1+C9*OO
      EVEN4=EVEN4+AE*EE*HE*HE/QE
      ODD4=ODD4+AO*EO*HO*HO/QO
      EVEN5=EVEN5+AE*FE*(HE**4)/QE
      ODD5=ODD5+AO*FO*(HO**4)/QO
   51 XE=XE+DELX
    6 XO=XO+DELX
      I2=(DELX/6)*(4*EVEN2+2*ODD2)
      I3=(DELX/6)*(4*EVEN3+2*ODD3)
      DBO=(29.609D+00*I3)/(E*RHOO*RHOO*I2*I2)
      I4=(DELX/6)*(4*EVEN4+2*ODD4)
      I5=(DELX/6)*(4*EVEN5+2*ODD5)
      WRITE(3,7)I2,I3,DBO,I4,I5
    7 FORMAT(/,10X,5D16.7)
      A=I4/(RHOO*I2)
      B=(29.609D+00*B*I5)/(E*RHOO*RHOO*I2*I2)
      DELRO=1 -AO**2*D/(B*DBO*(A**2+D**2))
      DELPO=AO/(A+D*D/A)-1.0
      WRITE(3,7)B,A,D,DELPO,DELRO
   23 CONTINUE
      RETURN
      END
```

```
C     PROGRAMME 5
C
C
C
C     CALCULATES SCATTERING PARAMETER S
C     FEED IN DELINF=(DELTA RHO)/RHO IN INFINITE MAGNETIC FIELD
C     USES SIMPLIFIED KANE MODEL   --- EQUATION (2,9) IN THESIS
C     NDATA IS NUMBER OF SETS OF DATA
C     EG IS THE ENERGY GAP
C     MOS IS EFFECTIVE MASS AT BAND MINIMUM
C     MUS IS REDUCED FERMI LEVEL
      REAL*8 N,MOS,I1,I2,I3,I4,I5,MUS,KT
      DOUBLE PRECISION  RHOO,EG,     AO,E,    DELX,ALPHA,C1,C2,C3,C4,S
      DOUBLE PRECISION  EVEN2,EVEN3,ODD2,ODD3,XE,XO,AE,BE,BO,CE,CO,AO
      DOUBLE PRECISION  DE,DO,EE,EO,FE,FO,GE,GO,HE,HO,       DBO,B,EVEN4
      DOUBLE PRECISION  EVEN5,ODD4,ODD5,C9,OE,OO,QE,QO,       A,B,DELRO
      DOUBLE PRECISION  DELPO,C5,C6,C7,AEE,  AOO,Y(11),DELINF
      READ(1,71)NDATA
   71 FORMAT(I2)
      DO 70 NN=1,NDATA
      READ (1,1) RHOO,EG,MOS,MUS,DELINF
    1 FORMAT(5D16.6)
      WRITE(3,2)RHOO,EG,MOS,MUS
      WRITE(3,2)RHOO,EG,MOS,MUS,DELINF
    2 FORMAT(////,5X,4D17.6)
      AO=1/RHOO
      M=1
      E=1.602D-19
      KT=.0254D+00
      DELX=.01D+00
      ALPHA=3.8098D-20
      C1=MOS*(1-MOS)
      C2=DSQRT(EG/(MOS*2*ALPHA))
      C3=(1/MOS)-1
      C5=4*KT*C1/EG
      C6=2*KT*MOS/EG
      C7=4*ALPHA*C3/EG
      C4=2*ALPHA/KT
      S=.10D+00
    3 EVEN2=0.0D+00
      EVEN3=0.0D+00
      ODD2=0.0D+00
      ODD3=0.0D+00
    5 EVEN4=0.0D+00
      EVEN5=0.0D+00
      ODD4=0.0D+00
      ODD5=0.0D+00
      XE=.01D+00
      XO=.015D+00
      DO 6 I=1,5000
      AEE=DEXP(XE-MUS)
      AOO=DEXP(XO-MUS)
      AE=AEE/((1+AEE)*(1+AEE))
      AO=AOO/((1+AOO)*(1+AOO))
      BE=DSQRT(1+C5*XE)
      BO=DSQRT(1+C5*XO)
      CE=C6*XE
      CO=C6*XO
      DE=DSQRT(2+CE-BE)*C2
```

```
      DO=DSQRT(1+CO-BO)*C2
      IF(S+.5D+00)60,61,62
   60 EE=1/DE**(-2*S-1)
      EO=1/DO**(-2*S-1)
      GO TO 63
   61 EE=DE
      EO=DO
      GO TO 63
   62 EE=DE**(2*S+1 )
      EO=DO**(2*S+1 )
   63 IF (S-.25D+00) 30,31,32
   30 FE=1 /DE**(1 -4*S)
      FO=1 /DO**(1 -4*S)
      GO TO 33
   31 FE=1.0D+00
      FO=1.0D+00
      GO TO 33
   32 FE=DE**(4*S-1 )
      FO=DO**(4*S-1 )
   33 GE=1+C7*DE*DE
      GO=1+C7*DO*DO
      HE=C4*DE*(1+C3/DSQRT(GE))
      HO=C4*DO*(1+C3/DSQRT(GO))
   21 EVEN2=EVEN2+AE*HE*EE*HE
      ODD2=ODD2+AO*HO*EO*HO
      EVEN3=EVEN3+HE*(HE*AE*HE*FE*HE)
      ODD3=ODD3+HO*(HO*AO*HO*FO*HO)
   20 IF(S-1 )40,41,42
   40 OE=(HE/DE**(1 -S))**4
      OO=(HO/DO**(1 -S))**4
      GO TO 43
   41 OE=HE**4
      CO=HO**4
      GO TO 43
   42 OE=(DE**(S-1 )*HE)**4
      OO=(DO**(S-1 )*HE)**4
   43 EVEN4=EVEN4+AE*HE*EE*HE/GE
      ODD4=ODD4+AO*HO*EO*HO/OO
      EVEN5=EVEN5+HE*AE*HE*FE*HE/OE*HE
      ODD5=ODD5+HO*AO*HO*FO*HO/OO*HO
   51 XE=XE+DELX
    6 XO=XO+DELX
      I2=(DELX/6)*(4*EVEN2+2*ODD2)
      I3=(DELX/6)*(4*EVEN3+2*ODD3)
      DBO=(29.6O9D+00*I3)/(E*RHOO*RHOO*I2*I2)
      C9=(29.6O9D+00/(E*RHOO*I2))**2
      I4=(DELX/6)*(4*EVEN4+2*ODD4)/C9
      I5=(DELX/6)*(4*EVEN5+2*ODD5)/C9
      A=I4/(RHOO*I2)
      D=(29.6O9D+00*  I5)/(E*RHOO*RHOO*I2*I2)
      DELRO=AO**2/(DBO*D)-1
      DELPO=AO*A/(D*D)-1
      WRITE(3,8)  A,D,DELPO,DELRO,S
    8 FORMAT(/,15X,5D14.7)
      FUNC=DELINF-DELPO
      GO TO (100,200),M
  100 IF(FUNC)9,70,23
   23 S=S+.1D+00
      GO TO 3
```

```
    9 S=S-.1D-01
      M=2
      GO TO 3
  200 IF(FUNC)9,70,70
   70 CONTINUE
      RETURN
      END
```

****

```
C     PROGRAMME 6
C
C
C
C     CALCULATES CONCENTRATIONS AND MOBILITIES FROM TWO BAND MAGNETORES
C     NDATA IS NUMBER OF SETS OF DATA
C     RHOO IS RESISTIVITY IN ZERO MAGNETIC FIELD
C     RINF IS HALL COEFFICIENT IN INFINITE MAGNETIC FIELD
C     S AND A ARE SLOPE AND INTERCEPT FROM RHOO/(DELTA RHO) VERSUS B**(-
C     MEN IS SPECIMEN NUMBER
C     FNO AND FN1 ARE CONCENTRATIONS IN THE TWO BANDS
C     UO AND U1 ARE MOBILITIES IN THE TWO BANDS
      READ(1,2)NDATA
    2 FORMAT(I2)
      K=1
      EC=1.602E-19
 2056 READ(1,1)RHOO,RINF,S,A,MEN
    1 FORMAT(4E14.6,I3)
      SIGMAO=1./RHOO
      II=0
   49 L=1
      C=.55/RHOO
 1011 IF(C-10.**9)1500,250,250
  250 WRITE(3,251)
  251 FORMAT(14H C IS TOO HIGH)
      GO TO 55
 1500 SIGMA2=SIGMAO-C
      A1=4.0*A*RINF**2*SIGMAO**2
      A2=SIGMAO-C-A*C
      BB=+2.0*A*RINF*SIGMAO
      AA=SQRT(A*A1+A1*A2/C)
      CC=2.0*A2
      R1POS=(AA-BB)/CC
      R1NEG=(-AA-BB)/CC
      IF(II)51,50,51
   50 R1=R1POS
      GO TO 52
   51 R1#R1NEG
   52 IF%R1<53,53,5500
 5500 WRITE(3,5400 )
 5400 FORMAT%8H R1#POS <
      GO TO 55
   53 R2=R1*RINF/(R1-RINF)
      IF (R2) 65,65,5501
 5501 WRITE (3,5401)
 5401 FORMAT (8H R2=POS )
      GO TO 55
   65 CONTINUE
      FF=(SIGMAO*(R1-RINF)/(R1*(RINF*SIGMAO-R1*C)))**2
      FINK=S-FF/(C*(SIGMAO-C))
      WRITE(3,61) C,FINK
   61 FORMAT(5X,E15.4,5X,E15.4)
      GO TO %1021,1022,1023,1024,1025,1026,1027,1028,1029,1030,1031<,L
 1021 IF%FINK<1032,1100,1310
 1032 L#2
 1034 C=C+5000.
      GO TO 1011
 1022 IF%FINK<1034,1100,1036
 1036 L#4
```

```
C      PROGRAMME 6
C
C
C
C      CALCULATES CONCENTRATIONS AND MOBILITIES FROM TWO BAND MAGNETORES
C      NDATA IS NUMBER OF SETS OF DATA
C      RHOO IS RESISTIVITY IN ZERO MAGNETIC FIELD
C      RINF IS HALL COEFFICIENT IN INFINITE MAGNETIC FIELD                (-2)
C      S AND A ARE SLOPE AND INTERCEPT FROM RHOO/(DELTA RHO) VERSUS B**(-
C      MEN IS SPECIMEN NUMBER
C      FNO AND FN1 ARE CONCENTRATIONS IN THE TWO BANDS
C      UO AND U1 ARE MOBILITIES IN THE TWO BANDS
       READ(1,2)NDATA
     2 FORMAT(I2)
       K=1
       EC=1.602E-19
  2056 READ(1,1)RHOO,RINF,S,A,MEN
     1 FORMAT(4E14.6,I3)
       SIGMAO=1./RHOO
       II=0
    49 L=1
       C=.55/RHOO
  1011 IF(C-10.**9)1500,250,250
   250 WRITE(3,251)
   251 FORMAT(14H C IS TOO HIGH)
       GO TO 55
  1500 SIGMA2=SIGMAO-C
       A1=4.0*A*RINF**2*SIGMAO**2
       A2=SIGMAO-C-A*C
       BB=+2.0*A*RINF*SIGMAO
       AA=SQRT(A*A1+A1*A2/C)
       CC=2.0*A2
       R1POS=(AA-BB)/CC
       R1NEG=(-AA-BB)/CC
       IF(II)51,50,51
    50 R1=R1POS
       GO TO 52
    51 R1=R1NEG
    52 IF%R1<53,53,5500
  5500 WRITE(3,5400 )
  5400 FORMAT%8H R1#POS <
       GO TO 55
    53 R2=R1*RINF/(R1-RINF)
       IF (R2) 65,65,5501
  5501 WRITE (3,5401)
  5401 FORMAT (8H R2=POS )
       GO TO 55
    65 CONTINUE
       FF=(SIGMAO*(R1-RINF)/(R1*(RINF*SIGMAO-R1*C)))**2
       FINK=S-FF/(C*(SIGMAO-C))
       WRITE(3,61) C,FINK
    61 FORMAT(5X,E15.4,5X,E15.4)
       GO TO %1021,1022,1023,1024,1025,1026,1027,1028,1029,1030,1031<,L
  1021 IF%FINK<1032,1100,1310
  1032 L=2
  1034 C=C+5000.
       GO TO 1011
  1022 IF%FINK<1034,1100,1036
  1036 L=4
```

```
1038 C=C-10.**3
     GO TO 1011
1024 IF%FINK<1040,1100,1038
1040 L#6
1042 C=C+10.**2
     GO TO 1011
1026 IF%FINK<1042,1100,1044
1044 L#8
1046 C=C-10.
     GO TO 1011
1028 IF%FINK<1048,1100,1046
1048 L#10
1050 C=C+1.
     GO TO 1011
1030 IF%FINK<1050,1100,1100
1310 L#3
     GO TO 1011
1023 IF%FINK<1035,1100,1034
1035 L#5
     GO TO 1038
1025 IF%FINK<1038,1100,1037
1037 L#7
     GO TO 1042
1027 IF%FINK<1039,1100,1042
1039 L#9
     GO TO 1046
1029 IF%FINK<1046,1100,1045
1045 L#11
     GO TO 1050
1031 IF%FINK<1100,1100,1050
1100 CONTINUE
     FN0#1.0/%R1*EC<
     FN1#1.0/%R2*EC<
     U0#C/%FN0*EC<
     U1#SIGMA2/%FN1*EC<
     FN023#%ABS%FN0<<**0.66667
     FN123#%ABS%FN1<<**0.66667
     WRITE (3,7) S,A
   7 FORMAT (5X,2E15.4)
     WRITE(3,215  )
 215 FORMAT(7H  SPEC.,5X,3HN1=,12X,3HN2=,12X,3HU1=,12X,3HU2=,11X,5HN123
    1=,12X,5HN223=/)
     WRITE(3,16   )MEN,FN0,FN1,U0,U1,FN023,FN123
  16 FORMAT(2X,I3,6E15.4)
  55 IF%II-1<56,54,54
  56 II#II&1
     GO TO 49
  54 CONTINUE
     WRITE(3,999  )
 999 FORMAT%29H SO MUCH FOR THIS SPECIMEN.../////<
  25 K#K&1
     IF%K-NDATA<2056,2056,57
  57 STOP
     END
```

```
C     PROGRAMME 7
C
C
C
C     CALCULATES ENERGY SEPARATION BETWEEN TWO BANDS GIVEN CARRIER DENSI
C     LOWER BAND USES THE AUBIN APPROXIMATION--EQUATION (2,12)
C     UPPER BAND IS PARABOLIC
C     NDATA IS NUMBER OF SETS OF DATA
C     EG IS ENERGY GAP
C     DELTA IS SPIN ORBIT SPLITTING
C     P2 IS SQUARE OF MATRIX ELEMENT
C     INSB AT 4.2 DEGREES
C     DELE IS SEPARATION OF MINIMA OF TWO BANDS IN EV
      DIMENSION F(1200)
      READ (1,7) NDATA
    7 FORMAT (I2)
      READ (1,5) EG,DELTA,P2
    5 FORMAT (2F6.3,E10.2)
      GAM=3.628E-04/EG
      ALPHA=3.8098E-20
      AM1S=.2
      DO 99 M=1,NDATA
      READ (1,6) AN1,AN2,AM1S
    6 FORMAT (2E12.4,E4.2)
      AN2=.25*AN2
      JBAND=1
      CI2=29.609*AN1*(P2/(EG*EG*GAM))**1.5
      A=500.
      AF=100.
      DELX=.05
      L=1
   11 XE=A-25.
      XO=XE+.025
      IF (JBAND-1) 81,81,86
   82 JBAND=2
      AF=1.0
      A=-5.0
      L=1
      CI2=29.609*AN2*(ALPHA/(3.628E-04*AM1S))**1.5
      DELX=.04
   86 XE=.04
      XO=.06
   81 EVEN2=0.0
      ODD2=0.0
      IJ=-1
      F(1)=0.0
      DO 100 I=1,1000
      IF (JBAND-1) 83,83,84
   83 AE=(1.+GAM*XE)
      AO=(1.+GAM*XO)
      BE=AE+DELTA/EG
      BO=AO+DELTA/EG
      CE=AE+(2*DELTA)/(3*EG)
      CO=AO+(2*DELTA)/(3*EG)
      DE=(XE*AE*BE/CE)**1.5
      DO=(XO*AO*BO/CO)**1.5
      GO TO 85
   84 DE=XE**1.5
      DO=XO**1.5
```

```
C     PROGRAMME 7
C
C
C
C     CALCULATES ENERGY SEPARATION BETWEEN TWO BANDS GIVEN CARRIER DENSI
C     LOWER BAND USES THE AUBIN APPROXIMATION--EQUATION (2,12)
C     UPPER BAND IS PARABOLIC
C     NDATA IS NUMBER OF SETS OF DATA
C     EG IS ENERGY GAP
C     DELTA IS SPIN ORBIT SPLITTING
C     P2 IS SQUARE OF MATRIX ELEMENT
C     INSB AT 4.2 DEGREES
C     DELE IS SEPARATION OF MINIMA OF TWO BANDS IN EV
      DIMENSION F(1200)
      READ (1,7) NDATA
    7 FORMAT (I2)
      READ (1,5) EG,DELTA,P2
    5 FORMAT (2F6.3,E10.2)
      GAM=3.628E-04/EG
      ALPHA=3.8098E-20
      AM1S=.2
      DO 99 M=1,NDATA
      READ (1,6) AN1,AN2,AM1S
    6 FORMAT (2E12.4,E4.2)
      AN2=.25*AN2
      JBAND=1
      CI2=29.609*AN1*(P2/(EG*EG*GAM))**1.5
      A=500.
      AF=100.
      DELX=.05
      L=1
   11 XE=A-25.
      XO=XE+.025
      IF (JBAND-1) 81,81,86
   82 JBAND=2
      AF=1.0
      A=-5.0
      L=1
      CI2=29.609*AN2*(ALPHA/(3.628E-04*AM1S))**1.5
      DELX=.04
   86 XE=.04
      XO=.06
   81 EVEN2=0.0
      ODD2=0.0
      IJ=-1
      F(1)=0.0
      DO 100 I=1,1000
      IF (JBAND-1) 83,83,84
   83 AE=(1.+GAM*XE)
      AO=(1.+GAM*XO)
      BE=AE+DELTA/EG
      BO=AO+DELTA/EG
      CE=AE+(2*DELTA)/(3*EG)
      CO=AO+(2*DELTA)/(3*EG)
      DE=(XE*AE*BE/CE)**1.5
      DO=(XO*AO*BO/CO)**1.5
      GO TO 85
   84 DE=XE**1.5
      DO=XO**1.5
```

```
 85 SE=XE-A
    SO=XO-A
    IF (ABS(SE)-174.0) 8,8,9
  8 IF (ABS(SO)-174.0) 10,10,9
  9 WRITE (3,111)
111 FORMAT (9HTOO LARGE)
    GO TO 99
 10 F2E=DE/(2+EXP(SE)+EXP(-SE))
    F2O=DO/(2+EXP(SO)+EXP(-SO))
    IF (IJ) 16,20,14
 16 IJ=0
    GO TO 14
 20 IF (F2E-F(I-1)) 12,12,14
 12 WRITE (3,13) I,F(I-1)
 13 FORMAT (2X,I4,E15.3)
    IJ=1
 14 F(I)=F2E
    EVEN2=EVEN2+F2E
    ODD2=ODD2+F2O
    XE=XE+DELX
100 XO=XO+DELX
    WRITE (3,15) F(1),F(1000)
 15 FORMAT (5X,2E15.3)
    AI2=(DELX/6.)*(4.*EVEN2+2.*ODD2)
    FUNC=AI2-CI2
    GO TO %21,22,23,24,25,26,27,28,29<,L
 21 IF %FUNC< 32,30,31
 32 L#2
    GO TO 11
 22 IF %FUNC< 34,30,36
 34 A=A+1.*AF
    GO TO 11
 36 L#4
 38 A=A-.1*AF
    GO TO 11
 24 IF %FUNC< 40,30,38
 40 L#6
 42 A=A+.01*AF
    GO TO 11
 26 IF %FUNC< 42,30,44
 44 L#8
 46 A=A-.001*AF
    GO TO 11
 28 IF %FUNC< 30,30,46
 31 L#3
    GO TO 11
 23 IF %FUNC< 35,30,34
 35 L#5
    GO TO 38
 25 IF %FUNC< 38,30,37
 37 L#7
    GO TO 42
 27 IF %FUNC< 39,30,42
 39 L#9
    GO TO 46
 29 IF %FUNC< 46,30,30
 30 CONTINUE
    WRITE (3,90) AN1,AN2,A
 90 FORMAT (3E15.5)
```

```
   85 SE=XE-A
      SO=XO-A
      IF (ABS(SE)-174.0) 8,8,9
    8 IF (ABS(SO)-174.0) 10,10,9
    9 WRITE (3,111)
  111 FORMAT (9HTOO LARGE)
      GO TO 99
   10 F2E=DE/(2+EXP(SE)+EXP(-SE))
      F2O=DO/(2+EXP(SO)+EXP(-SO))
      IF (IJ) 16,20,14
   16 IJ=0
      GO TO 14
   20 IF (F2E-F(I-1)) 12,12,14
   12 WRITE (3,13) I,F(I-1)
   13 FORMAT (2X,I4,E15.3)
      IJ=1
   14 F(I)=F2E
      EVEN2=EVEN2+F2E
      ODD2=ODD2+F2O
      XE=XE+DELX
  100 XO=XO+DELX
      WRITE (3,15) F(1),F(1000)
   15 FORMAT (5X,2E15.3)
      AI2=(DELX/6.)*(4.*EVEN2+2.*ODD2)
      FUNC=AI2-CI2
      GO TO %21,22,23,24,25,26,27,28,29<,L
   21 IF %FUNC< 32,30,31
   32 L#2
      GO TO 11
   22 IF %FUNC< 34,30,36
   34 A=A+1.*AF
      GO TO 11
   36 L#4
   38 A=A-.1*AF
      GO TO 11
   24 IF %FUNC< 40,30,38
   40 L#6
   42 A=A+.01*AF
      GO TO 11
   26 IF %FUNC< 42,30,44
   44 L#8
   46 A=A-.001*AF
      GO TO 11
   28 IF %FUNC< 30,30,46
   31 L#3
      GO TO 11
   23 IF %FUNC< 35,30,34
   35 L#5
      GO TO 38
   25 IF %FUNC< 38,30,37
   37 L#7
      GO TO 42
   27 IF %FUNC< 39,30,42
   39 L#9
      GO TO 46
   29 IF %FUNC< 46,30,30
   30 CONTINUE
      WRITE (3,90) AN1,AN2,A
   90 FORMAT (3E15.5)
```

```
      IF (JBAND-1) 71,71,72
   71 A1=A
      GO TO 82
   72 DELE=(A1-A)*3.628E-04
      WRITE (3,91) DELE
   91 FORMAT (2X,E15.5)
      WRITE (3,105)
  105 FORMAT (10H PLUS VITE///)
   99 CONTINUE
      STOP
      END
```

****

CURRICULUM VITAE

NOM: Marcel Joseph Aubin

LIEU ET DATE DE NAISSANCE: Kirkland Lake, Ontario, 1941

ETUDES:

Primaire: Ecole St.Jérôme, Kirkland Lake, 1947-1952

Ecole Assomption, Kirkland Lake, 1952-1955

Secondaire: Kirkland Lake Collegiate, 1955-1957

Ecole Secondaire d'Eastview, 1957-1960

Université: Université d'Ottawa, 1960-1969

Cours: Physique

Diplôme: B.Sc. (Honours), 1964

POSTE: Chargé d'enseignement, Université de Sherbrooke, 1968-